Aus dem Fachbereich Medizin
der Johann Wolfgang Goethe-Universität
Frankfurt am Main

betreut am
Gustav Embden-Zentrum der Biochemie
Institut für Biochemie II
Direktor: Prof. Dr. Ivan Dikic

Deciphering regulation and substrate-specificity of SUMO-specific isopeptidases

Dissertation
zur Erlangung des Doktorgrades der theoretischen Medizin
des Fachbereichs Medizin
der Johann Wolfgang Goethe-Universität
Frankfurt am Main

vorgelegt von
Kathrin Schunck, geb. Kunz

aus Zweibrücken

Frankfurt am Main, 2019

Dekan:	Prof. Dr. Josef Pfeilschifter
Referent:	Prof. Dr. Stefan Müller
1. Korreferentin:	Prof. Dr. Liliana Schaefer
2. Korreferent:	Prof. Dr. Michael Rieger
Tag der mündlichen Prüfung:	19.12.2019

Contents

1 Abbreviations 6

2 Summary 11

3 Zusammenfassung 13

4 Introduction 15

4.1 Control of protein function by post-translational modifications 15

4.2 Ubiquitin and ubiquitin-like proteins 16

4.3 The SUMO system 20

4.3.1 Mechanisms of protein SUMOylation 20

4.3.2 Cellular consequences of SUMO modification 24

4.4 The SENP family of SUMO-specific isopeptidases 26

4.4.1 Characteristics and functions of SENPs 26

4.4.2 Selected pathways under the control of SENPs 28

4.5 The SUMO system under stress: Regulation by PTMs 31

5 Aims of this study 35

6 Results 36

6.1 Investigation of SUMO signalling under hypoxia 36

6.1.1 Effects of hypoxia on the activity of individual SUMO proteases 36

6.1.2 Identification of SUMO1 conjugates under hypoxia 44

6.1.3 The role of BHLHE40 as SENP1-regulated hypoxic SUMO target 48

6.2 Identification of SENP3-regulated SUMO2/3 targets 53

6.2.1 Validation of a U-2 OS SENP3 knockout cell line and experimental conditions for endogenous SUMO2/3 IP 53

6.2.2 LC-MS/MS analysis of endogenous SUMO2/3 targets in SENP3 KO and WT cells 55

6.2.3 Comparison of SENP3 interactors and targets 60

6.2.4 Investigating the role of SENP5 under loss of SENP3 63

6.3 Identification of SENP6-regulated SUMO2/3 targets 64

6.3.1 Comparative analysis of SUMO2/3 targets in control HeLa cells and cells upon SENP6 knockdown 64

6.3.2 Comparison of SENP6-regulated SUMO2/3 targets and SENP6 interactome analysis 68
6.3.3 SENP6 regulates functions in mammalian cohesin complex and DNA damage repair 71

7 Discussion 78

7.1 Regulation of SENP activity by hypoxia 78
7.2 SENP3 function is tightly linked to mammalian ribosome biogenesis 83
7.3 Identification of SENP6-controlled SUMO2/3 targets 85
7.4 Conclusion 91

8 Materials and Methods 93

8.1 Reagents and Chemicals 93
8.2 Microbiological methods 93
8.2.1 *E. coli (Escherichia coli)* strain used 93
8.2.2 Generation of competent *E. coli* 94
8.2.3 Storage and cultivation of *E. coli* 94
8.2.4 Transformation of plasmid DNA in *E. coli* 94
8.3 Cell-biological methods 95
8.3.1 Cell lines used 95
8.3.2 Mammalian expression vectors used 95
8.3.3 Cultivation and treatment of mammalian cell lines 95
8.3.4 Storage of cell lines 96
8.3.5 Transfection of cells with siRNA 97
8.3.6 Transfection of cells with plasmid DNA 98
8.3.7 Generation of knockout cell line with CRISPR-Cas9 99
8.4 Molecular biological methods 100
8.4.1 PCR (polymerase chain reaction) 100
8.4.2 Agarose gel electrophoresis 101
8.4.3 Purification of DNA from agarose gels 101
8.4.4 Restriction and ligation 102
8.4.5 Ligation of DNA 102
8.4.6 Mutagenesis 102
8.4.7 Used plasmids 102

8.4.8 Isolation of plasmid DNA from *E. coli* 103
8.4.9 Isolation of RNA from cells 104
8.4.10 Reverse transcription of RNA in cDNA 104
8.4.11 Quantitative real-time PCR 104
8.5 Protein biochemistry methods 106
8.5.1 SDS-Polyacrylamide gel electrophoresis 106
8.5.2 Western blot 107
8.5.3 Immunofluorescence 110
8.5.4 SUMO-AMC measurements 110
8.5.5 SUMO-VS assays 112
8.5.6 Dual-Luciferase Reporter Assays 112
8.5.7 Ni-NTA pulldown 113
8.5.8 Flag-IP 114
8.5.9 Endogenous PRP19 IP 115
8.5.10 Fractionation of cells 115
8.5.11 Endogenous SUMO1 and SUMO2/3 IPs 117
8.6 Liquid chromatography and mass spectrometry 117
8.6.1 Sample preparation for LC-MS/MS analysis 117
8.6.2 Instrument settings 120
8.6.3 Downstream data analysis 122
8.7 Functional protein network and enrichment analysis 123

9 Supplement 124
9.1 Supplemental Figures 124
9.2 Supplemental Table 133

10 References 137

11 Acknowledgement 145

12 Conferences and Posters 147

13 Schriftliche Erklärung 148

1 Abbreviations

%	Percent
°C	Degree Celsius
3D	Three-dimensional
ABC	Ammonium bicarbonate
ACN	Acetonitrile
AMC	7-Amido-4-methylcoumarin
APS	Ammonium persulphate
ATP	Adenosine triphosphate
BSA	Bovine serum albumin
C18	Octadecylsilane
CAA	Chloroacetamide
cDNA	Complementary DNA
cm	Centimetre
CO_2	Carbondioxide
CRISPR-Cas9	Clustered regularly interspaced short palindromic repeats-Cas9
Cys	Cysteine, C
D	Aspartic acid, Asp
DAPI	4',6-Diamidino-2-phenylindole
ddH_2O	Double-distilled water
DDR	DNA damage response
DMEM	Dulbecco's Modified Eagle Medium
DMSO	Dimethyl sulfoxide
DNA	Deoxyribonucleic acid
dNTPs	Deoxyribonucleotides (N = A, C, G, T)
Dox	Doxycycline
DSB	Double-strand break
DTT	Dithiothreitol
dTTP	Deoxythymidine triphosphate

DUBs	Deubiquitinating enzymes
dUTP	Deoxyuridine triphosphate
E	Glutamate, Glu
E. coli	*Escherichia coli*
E1	Ubiquitin-activating enzyme
E2	Ubiquitin-conjugating enzyme
E3	Ubiquitin-ligating enzyme
ECL	Enhanced chemiluminescence
EDTA	Ethylenediaminetetraacetate
EGTA	Ethylene glycol-bis(2-aminoethylether)-N,N,N',N'-tetraacetic acid
et al.	*et alii*
FA	1. Fanconi anemia, 2. Formic acid
FB	Freezing buffer
FCS	Fetal calf serum
FDR	False discovery rate
g	1. Gram, 2. centrifugal force
Gly	Glycine, G
GO BP	Gene ontology biological process
GSH	Glutathione
GTP	Guanosine triphosphate
h	Hour
H_2O_2	Hydrogen peroxide
H3K9	Histone 3 lysine 9
HBS	HEPES-buffered saline
HCD	Higher-energy collisional dissociation
HeLa	Henrietta Lacks
HR	Homologous recombination
ICL	Interstrand crosslink
IgG	Immunoglobulin G
Ile	Isoleucine, I
IP	Immunoprecipitation

JAMMs	JAMM/MPN domain-associated metallopeptidases
K	Lysine
kb	Kilobase
kDa	Kilodalton
l	Liter
LB	Lysogeny broth
LC-MS/MS	Liquid chromatography-tandem mass spectrometry
Leu	Leucine, L
LFQ	Label-free quantification
M	Molar, mol/l
m/z	Mass/charge
mA	Milliampere
MCL	Markov clustering
Met	Methionine, M
mg	Milligram
min	Minutes
MJDs	Machado-Joseph disease protein domain proteases
ml	Milliliter
mM	Millimol/liter
mRNA	Messenger RNA
ms	Millisecond
NEM	N-Ethylmaleimide
ng	Nanogram
Ni-NTA	Nickel-nitrilotriacetic acid
O_2	Oxygen
OD_{600}	Optical density at 600 nm
OTUs	Ovarian-tumour proteases
PBS	Phosphate-buffered saline
PCR	Polymerase chain reaction
PFA	Paraformaldehyde
Phe	Phenylalanine, F
PML NBs	Promyelocytic leukemia nuclear bodies

pmol	Pikomole
PMSF	Phenylmethylsulfonyl fluoride
PS	Penicillin/Streptomycin
PTMs	Post-translational modifications
q-RT-PCR	Quantitative real-time PCR
RAR	Retinoic acid receptor
RIPA	Radioimmunoprecipitation assay
RLU	Relative light units
ROS	Reactive oxygen species
rpm	Revolutions per minute
rRNA	Ribosomal ribonucleic acid
RT	Room temperature
S	Svedberg unit
S. cerevisiae	*Saccharomyces cerevisiae*
S. pombe	*Schizosaccharomyces pombe*
SD	Standard deviation
SDS-PAGE	Sodium dodecylsulphate polyacrylamide gel electrophoresis
sec	Seconds
SEM	1. Standard error of the mean, 2. sucrose-EDTA-MOPS
SIM	SUMO-interacting motif
siRNA	Small interfering RNA
StUbL	SUMO-targeted ubiquitin ligase
TAE	Tris-acetate-EDTA
TCA	Trichloroacetic acid
TEMED	Tetraethylmethylenediamine
TFA	Trifluoroacetic acid
Th	Thomson
U/ml	Units per milliliter
Ub	Ubiquitin
UbLs	Ubiquitin-like proteins

UCHs	Ubiquitin carboxy-terminal hydrolases
UHPLC	Ultra high performance liquid chromatography
UPS	Ubiquitin-proteasome system
USPs	Ubiquitin-specific proteases
UV	Ultraviolet
V	1. Valine, 2. Volt
Val	Valine, V
VS	Vinyl sulfone
Zn	Zinc
λ_{Em}	Emission wavelength
λ_{Ex}	Excitation wavelength
*µ*g	Microgram
*µ*l	Microliter
*µ*m	Micrometre
γH2AX	Histone γH2AX

2 Summary

The ubiquitin-related SUMO system represents a versatile post-translational modification pathway controlling a variety of cellular signalling networks. In mammalian cells, lysine residues of target proteins can be covalently modified with three SUMO isoforms (SUMO1, SUMO2 and SUMO3) resulting in conjugation of either single SUMO moieties or formation of poly-SUMO chains. Importantly, SUMO modification is a reversible process, where the deconjugation of SUMO from its substrates is mediated by SUMO proteases. In humans, the best-characterized subfamily is the SENP family of SUMO-specific isopeptidases comprised of SENP1-3 and SENP5-7. For undisturbed cellular signalling events, a proper balance of SUMO conjugation and deconjugation is crucial. SENPs fulfil the important function of counteracting SUMOylation. A key question is how the relatively low number of SENPs specifically controls the SUMOylation status of hundreds of cellular proteins.

The aim of this thesis was to uncover the regulation and substrate specificity of distinct SUMO isopeptidases in order to better understand their role in cellular signalling pathways.

In the first part of this work, we investigated the influence of hypoxia on SUMO signalling, in particular on the activity of SENPs. Importantly, we found that the catalytic activity of distinct SENPs (especially SENP1 and SENP3) is strongly but reversibly diminished under low oxygen. As a consequence, the SUMO modification of a specific subset of proteins is changed under hypoxia. We specifically identified proteins being hyperSUMOylated after 24 hours of hypoxia by SUMO1 immunoprecipitation followed by mass spectrometry. We further validated the transcriptional co-repressor BHLHE40 as hypoxic SUMO target and confirmed SENP1 as responsible isopeptidase for deconjugation of SUMOylated BHLHE40. We provide evidence that SUMO conjugation to BHLHE40 enhances its repressive functions on the expression of the metabolic master regulator PGC-1α. Therefore we propose a model where inactivation of

SENP1 under hypoxia results in SUMOylated BHLHE40, possibly contributing to metabolic reprogramming under hypoxia.

To get insight into substrate selectivity of SENP family members, in particular SENP3 and SENP6, we choose a proteomic profiling strategy. For the identification of specific SUMO substrates controlled by SENP3, we applied a large-scale IP-MS approach in SENP3 KO and WT cells. The most strongly induced SUMO targets in the absence of SENP3 were key regulators of ribosome maturation. We identified factors involved in the remodelling of both 90S and 60S pre-ribosomes. SENP3 has already been described as being critically involved in maturation of the pre-60S subunit and 28S rRNA processing. Previously described SENP3-regulated master targets in this process are the ribosome maturation factors PELP1 and Las1L. Importantly, both were also identified as the most significantly regulated SENP3 targets in our unbiased proteomic approach. Importantly, however, enhanced SUMOylation was also detected on 90S-associated regulators, such as BMS1. Altogether, these data strengthen the functional link between SENP3 and ribosome biogenesis and point to a role of SENP3 beyond 60S maturation.

In addition to SENP3, we explored the substrate specificity of SENP6, which mainly acts on polymeric SUMO2/3 chains. Applying a proteomic profiling strategy, we were able to identify SENP6-controlled SUMO networks functioning in DNA damage response as well as chromatin organization. We demonstrated that SENP6 reverses polySUMOylation of several subunits of the cohesin complex, thereby regulating the SUMOylation status and chromatin association of this complex. Furthermore, we found a tight interaction of SENP6 with the hPSO4/PRP19 complex, involved in DNA damage response by activation of the ATR-CHK1 signalling cascade. In cells depleted of SENP6, we observe deficient recruitment of the co-activator ATRIP to chromatin which results in diminished CHK1 activation. We therefore illustrate a general role of SENP6 in the control of chromatin-associated protein networks involved in genome integrity and chromatin organization.

3 Zusammenfassung

Das Ubiquitin-verwandte SUMO System ist eine vielseitige post-translationale Modifikation, die etliche zelluläre Signalnetzwerke kontrolliert. In humanen Zellen können Lysinreste von Zielproteinen kovalent mit einer der drei SUMO Isoformen (SUMO1, SUMO2 und SUMO3) verknüpft werden, was entweder in Konjugation mit einer einzelnen SUMO Einheit resultiert oder zur poly-SUMO Kettenbildung führt. Die SUMO Modifikation ist zudem ein reversibler Prozess, bei dem die Dekonjugation von SUMO durch spezielle Proteasen durchgeführt wird. Die am besten charakterisierte Untergruppe von SUMO-spezifischen Isopeptidasen ist die SENP Familie, bestehend aus SENP1-3 und SENP5-7. Um fehlerlose zelluläre Kommunikation zu gewährleisten, ist ein fein eingestelltes Gleichgewicht von SUMO Konjugation und Dekonjugation nötig. Die SENPs sind dabei wichtige Gegenspieler der SUMO Konjugation. Eine Schlüsselfrage dabei ist, wie eine kleine Anzahl von SENPs die SUMOylierung hunderter zellulärer Proteine spezifisch kontrolliert. Das Ziel dieser Dissertation war es daher, die Regulation und Substratspezifität bestimmter SUMO Isopeptidasen zu erforschen, um deren Rolle in zellulären Signalwegen besser verstehen zu können.

Im ersten Teil dieser Arbeit wurde der Einfluss der Hypoxie auf das SUMO System und im Speziellen auf die Aktivität der SENPs untersucht. Interessanterweise wurde ein erheblicher, aber reversibler Aktivitätsverlust einiger SENPs (vor allem SENP1 und SENP3) unter Sauerstoffmangel beobachtet. Daraus resultiert ein verändertes SUMO-Konjugationsmuster bestimmter Proteine unter Hypoxie. Mittels SUMO1-Immunpräzipitation gefolgt von Massenspektrometrie konnten gezielt diejenigen Proteine identifiziert werden, die nach 24 Stunden unter Hypoxie eine vermehrte SUMOylierung aufwiesen. Weiterhin haben wir den transkriptionellen Regulator BHLHE40 als hypoxisches SUMO Substrat identifiziert und bestätigt, dass SENP1 für die Dekonjugation von SUMOyliertem BHLHE40 zuständig ist. Dies deutet darauf hin, dass die SUMOylierung von BHLHE40 dessen Repression auf die Aktivität

des metabolischen Regulators PGC-1α erhöht. Wir schlagen deshalb ein Modell vor, bei dem die Inaktivierung von SENP1 unter Hypoxie und die daraus resultierende SUMOylierung von BHLHE40 zur Anpassung des Metabolismus unter Hypoxie beitragen könnte.

Um Einblick in die Substratselektivität insbesondere von SENP3 und SENP6 zu erhalten, wurden IP-MS Experimente in Zellen in Abwesenheit dieser SENPs durchgeführt. Die am stärksten SUMO-modifizierten Substrate beim Fehlen von SENP3 sind Regulatoren der Ribosomenbiogenese. SENP3 ist bekanntlich in die Bildung der 28S rRNA und die Reifung der pre-60S Untereinheit involviert. Schon beschriebene und SENP3-regulierte Schlüsselproteine in diesem Prozess sind PELP1 und Las1L, die beide als höchst signifikante SENP3-regulierte SUMO Substrate in unserem Experiment identifiziert werden konnten. Des Weiteren wurden auch Regulatoren der 90S Untereinheit, wie BMS1, als verstärkt SUMO-modifiziert gefunden. Zusammengefasst unterstreichen diese Daten die Rolle von SENP3 in der Ribosomenbiogenese, deuten aber auch auf SENP3-gesteuerte Prozesse über die Reifung der 60S Untereinheit hinaus.

Zusätzlich zu SENP3 untersuchten wir die Substratspezifität von SENP6, das hauptsächlich an SUMO2/3-Ketten agiert. Hier konnten wir SENP6-kontrollierte Proteinnetzwerke identifizieren, die eine Rolle in der DNA Schadensantwort und der Chromatindynamik spielen. Wir konnten zeigen, dass SENP6 die poly-SUMOylierung einiger Cohesinkomplex Komponenten kontrolliert und somit die SUMOylierung und Chromatinassoziierung des Komplexes steuert. Weiterhin konnten wir eine starke Interaktion von SENP6 mit dem hPSO4/PRP19 Komplex nachweisen, welcher in die Aktivierung des ATR-CHK1 Signalweges der DNA Schadensantwort involviert ist. Fehlt SENP6, kommt es zur mangelhaften Rekrutierung des Co-Aktivators ATRIP an Chromatin was eine verminderte CHK1 Aktivierung zur Folge hat. Diese Ergebnisse belegen eine Rolle von SENP6 in der Kontrolle der Chromatinassoziierung von Proteinnetzwerken, die zur Integrität des Genoms und der Chromatinordnung beitragen.

4 Introduction

4.1 Control of protein function by post-translational modifications

Post-translational modifications of proteins are rapid and direct ways for a cell to react to internal and external stimuli. One or more amino acids of a given protein can be modified during the whole life cycle of a protein. For example, starting right after protein synthesis with the cleavage of precursor forms into mature proteins and ending with modifications leading to degradation. PTMs (post-translational modifications) involve various alterations, which can be classified into reversible and irreversible modifications. Cleavage of proteins leading to proteolytic degradation and elimination of single amino acids are for example permanent changes whereas addition of diverse chemical groups or molecules can be reversed by the action of specified enzymes. The variety of reversible PTMs is depicted in Figure 1. This includes addition of small chemical groups with phosphorylation as most prominent example, the attachment of complex molecules like fatty acids or sugars or even the conjugation of small proteins like ubiquitin or ubiquitin-like proteins. Modifications of histones with small molecules like acetyl- or phospho-residues have already been discovered in the early 1960s[1] and have been proposed to regulate gene expression. Today, using advanced mass spectrometry-based methods, more than 200 different PTMs are known and also complex PTM crosstalk is studied more intensively[2,3]. Modification with one or more of these PTMs often results in altered conformation or binding behaviour or influences localization, activity or turnover of the modified protein. Thus, post-translational protein modification represents one way to rapidly and dynamically control cellular protein functions.

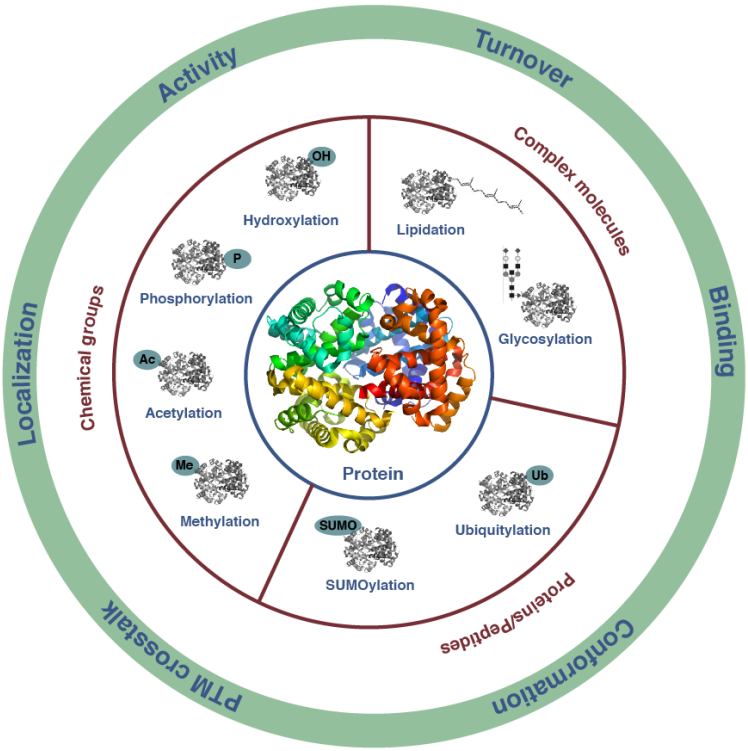

Figure 1: Variety of post-translational modifications. Possible cellular consequences for proteins being modified with different chemical groups, complex molecules or whole proteins.

4.2 Ubiquitin and ubiquitin-like proteins

Ubiquitin is the prototype of small proteins being attached to other proteins thereby executing a multitude of cellular functions. Ubiquitin itself is an 8.6 kDa protein, evolutionary highly conserved and ubiquitously expressed in eukaryotic cells. In the human genome, four genes encode for an ubiquitin precursor protein that needs further maturation to obtain the processed and conjugatable C-terminal GlyGly (glycine-glycine) motif[4,5]. Ubiquitin, like many other proteins, belongs to the superfamily of β-grasp folded proteins adopting an extremely stable conformation[6]. Its hydrophobic core is composed of a mixed parallel-anti-parallel β-sheet, consisting of five β-strands, and an α-helix (Figure 2 B). Through this secondary structure, ubiquitin possesses a compact architecture that is further stabilized by hydrophobic interactions. Thus the Ub (ubiquitin) molecule is highly stable regarding changes in pH or temperature[7].

The process of conjugating ubiquitin to target proteins it termed ubiquitination. Canonical ubiquitination relies on E1- (Ub-activating), E2- (Ub-conjugating) and E3 (Ub-ligating) enzymes. In this ATP- (adenosine triphosphate) dependent pathway, an isopeptide linkage is formed between the amino group of lysine residues of the target protein and the C-terminal glycine of mature ubiquitin. The modification cycle starts with E1-mediated ATP activation of ubiquitin leading to formation of an ubiquitin-adenylate. This in turn is transferred to the E1, forming a thioester-linkage between ubiquitin and a conserved cysteine residue in the active site of the E1 enzyme[8]. Ubiquitin is subsequently transferred to the active cysteine residue in the E2 enzyme[9]. The resulting thioester-linked Ub-E2 intermediate is then finally coupled to the substrate protein with the help of E3 ligases. Thereby it is either directly transferred from the E2 to the E3-bound substrate protein or via a thioester-linked Ub-E3-intermediate (Figure 2 A).

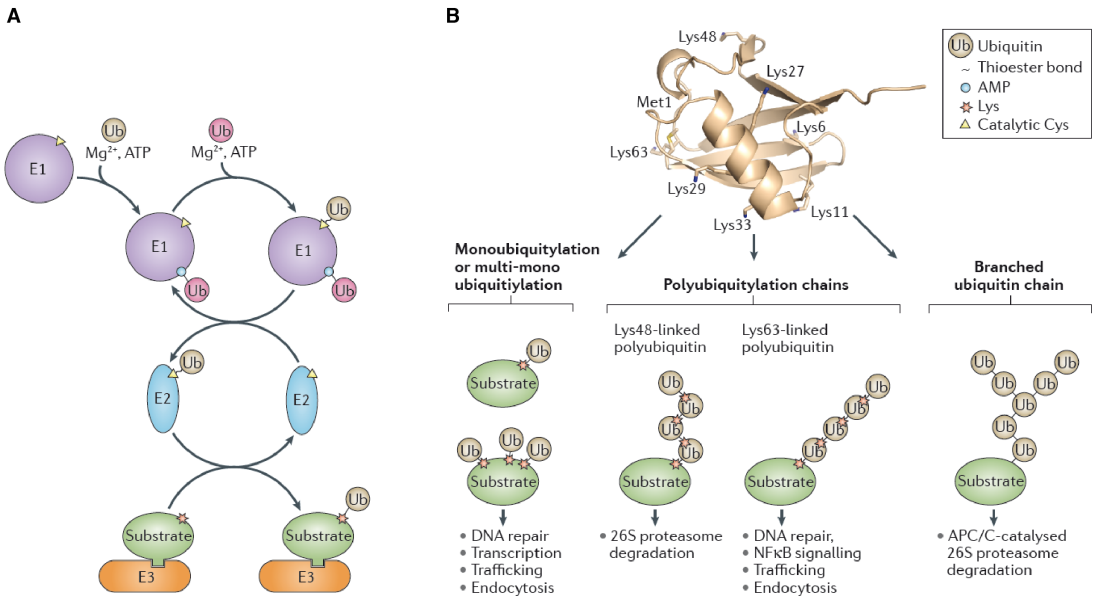

Figure 2: Ubiquitin conjugation/deconjugation cycle and different outcomes of ubiquitination and Ub chain formation. (A) Ubiquitin activation involves the formation of a thioester bond with the activating enzyme E1 in an ATP-dependent process. Ub is then further transferred to the conjugating enzyme E2 and finally transferred to a lysine residue of a substrate protein with the help of Ub E3 ligases. **(B)** Cellular consequences of ubiquitination are determined by different modes of Ub modification. Ub can be conjugated to one or more single acceptor lysine residues, termed monoubiquitination or multi-monoubiquitination. Furthermore, Ub harbours seven lysine residues on its surface, enabling it to form polyubiquitin chain. These Ub-Ub linkages result in either homogenous or branched chains, triggering different downstream effects. From Buetow and Huang[10].

Protein ubiquitination occurs in various manners. Conjugation of one ubiquitin moiety to a target protein is called monoubiquitination, whereas attachment of several ubiquitin molecules to different lysine residues of the substrate is termed multi-monoubiquitination. Besides this, ubiquitin itself possesses seven lysine residues as well as a free N-terminal amino group at methionine 1 (Met1), which all can be used to form diverse polyubiquitin chains (Figure 2 B). The different chain types are specifically involved in numerous cellular pathways. For example, K11- (lysine 11) and K48-linked polyubiquitin chains are a signal for proteasomal degradation[11,12]. Other chain types, like K63-linked chains exert non-degradative functions in endocytosis or DNA (deoxyribonucleic acid) repair. Furthermore, an unconventional chain type, Met1-linked linear ubiquitin chains control inflammatory signalling and apoptotic cell death[13]. In addition to homogenous ubiquitin chains, also branched chains can be formed, acting as potent proteolytic degradation signal[14]. In contrast to the canonical ubiquitination at lysine residues, also non-canonical types of Ub modification for example at serine or cysteine residues have been identified[15].

The ubiquitin conjugating machinery is a giant family of enzymes regulating the specific modification of target proteins. In humans, there are two E1 enzymes, roughly 40 E2 enzymes and around 700 E3 ligases, including proteins with predicted ligase activity. The ubiquitin ligases provide specificity for a subset of proteins and can be divided into two major subfamilies. One class, comprised of approximately 30 members in humans, are HECT ligases, which catalyse transfer of ubiquitin to the substrate via a thioester intermediate. A second, larger group consists of more than 600 RING finger E3 ligases encoded in the human genome. These are characterized by a cysteine-histidine-rich Zn^{2+} (zinc)-coordinating domain and in contrast to HECT E3s do not form a catalytic intermediate with Ub. Rather they act as scaffold molecules to bring the Ub-charged E2 in close contact to their substrates. RING-type E3 ligases can act as monomeric, dimeric or multi subunit complexes. RNF4 is one example for a homodimeric E3 Ub ligase, where dimerization is mediated by the RING finger domain. The prototypical multimeric RING-type E3 ligases are the Cullin-RING ligases that are build on a cullin scaffold and bind a RING-box containing

protein at its N-terminus. Additionally, an adaptor protein and a substrate receptor are bound via their C-terminus.

Protein ubiquitination is a reversible process. In humans, there are around 100 DUBs (deubiquitinating enzymes) involved in deconjugation of Ub from its substrates or the processing of Ub precursors into their mature forms. The DUBs are classified into five subfamilies (Figure 3): the UCHs (ubiquitin carboxy-terminal hydrolases), USPs (ubiquitin-specific proteases), OTUs (ovarian-tumour proteases), MJDs (Machado-Joseph disease protein domain proteases) and the JAMMs (JAMM/MPN domain-associated metallopeptidases). The UCH, USP, OTU and MJD proteases are all cysteine proteases, containing cysteine and histidine boxes with the catalytic triad cysteine, histidine and aspartate. The JAMMs, however, exhibit a papain-like fold and possess two histidines and an aspartate residue that together coordinate a zinc ion and so they exert their proteolytic activity.

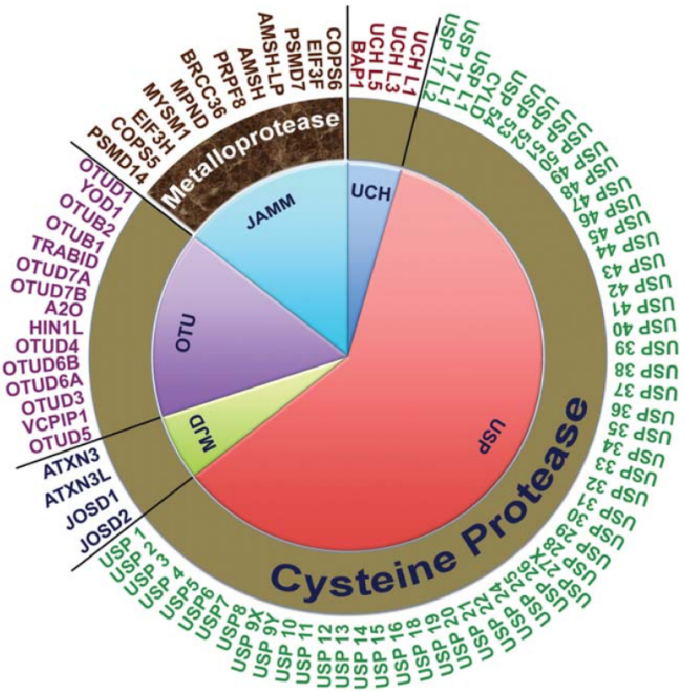

Figure 3: Classification of human deubiquitinating enzymes. Different colours represent the five diverse mammalian DUB classes. The UCHs, USPs, OTUs and MJDs belong to the cysteine proteases whereas the JAMMs are metallopeptidases. From Hanpude *et al.*[16] (*et alii).*

Apart from ubiquitin, there are several proteins sharing a common 3D (three-dimensional) structure and folding. They mostly exhibit a C-terminal Gly motif in the mature form and get conjugated and deconjugated via similar enzymatic cascades in an Ub-like fashion. Examples for such proteins are NEDD8, ISG15, FAT10 or SUMO, being named UbLs (ubiquitin-like proteins).

4.3 The SUMO system

4.3.1 Mechanisms of protein SUMOylation

Post-translational protein modification with the small-ubiquitin related modifier SUMO is termed SUMOylation. Members of the SUMO family are small proteins, around 10 kDa, which are structurally highly similar to ubiquitin (Figure 4 A). In humans, there are four genes encoding for SUMO1, SUMO2, SUMO3 or SUMO4, whereas insects, yeast or nematodes harbour only one SUMO gene, also known as smt3. Like ubiquitin, SUMO isoforms are expressed as precursors that need to be edited for maturation by SUMO-specific isopeptidases. To exhibit the conjugatable GlyGly residues, two, four or 11 residues are cleaved off from the C-terminus of SUMO2, SUMO1 or SUMO3, respectively. SUMO4, however, differs from SUMO1-3 such that maturation by SUMO-specific isopeptidases is prevented and a covalent conjugation of SUMO4 to other proteins is unlikely[17]. Therefore, only modification with the isoforms SUMO1, 2 and 3 will be taken into consideration whenever SUMO conjugation is mentioned in the following. The mature SUMO2 and 3 isoforms are almost identical and differ only in three amino acids after processing, whereas SUMO1 and SUMO2/3 only share around 50% sequence similarity (Figure 4 B).

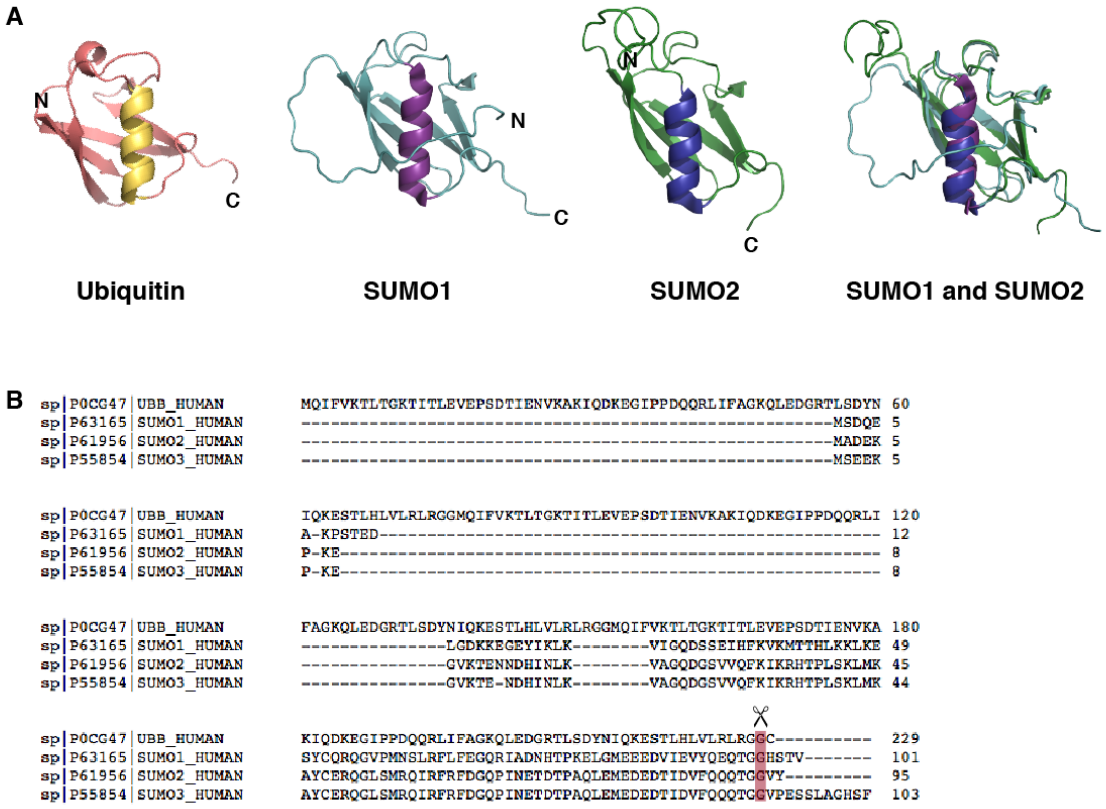

Figure 4: Structure and sequence comparison of mammalian ubiquitin and SUMO isoforms. (A) Ubiquitin adopts a β-grasp folding with a hydrophobic core consisting of several β-sheets and one α-helix, whereas SUMO exhibits a common Ub-fold with an extended and flexible N-terminus. The highly similar secondary structure of all three SUMO isoforms is represented by an overlay of SUMO1 and SUMO2 (PDBs: SUMO1 2N1V, SUMO2 2N1W, Ub 1UBQ). **(B)** Comparison of sequence similarities of ubiquitin with all three SUMO isoforms by sequence alignment. SUMO1 and SUMO2/3 exhibit about 50% sequence identity whereas SUMO2 and SUMO3 differ in only three amino acids after processing. Both, SUMO and Ub display a C-terminal GlyGly motif after maturation.

The mammalian SUMO conjugation-deconjugation cycle is mechanistically similar to the ubiquitin pathway but the enzymatic machinery is less complex. The enzymatic cascade of SUMO E1, E2 and E3 enzymes is comprised of the heterodimeric SUMO-activating enzyme SAE1-SAE2, the sole SUMO-conjugating enzyme Ubc9 and a limited number of SUMO E3 ligases like RanBP2, ZNF451 or the PIAS family. The formation of a covalent isopeptide bond between the C-terminal glycine residue of SUMO and an acceptor lysine residue of the target protein proceeds via thioester intermediates that are formed between SUMO and the active cysteine residues in the E1 subunit SAE1 and E2 Ubc9. Deconjugation of SUMO from its substrates is ensured by

SUMO-specific isopeptidases with six members of the SENP family (SENP1, 2, 3, 5, 6 and SENP7) as most prominent proteases (Figure 5).

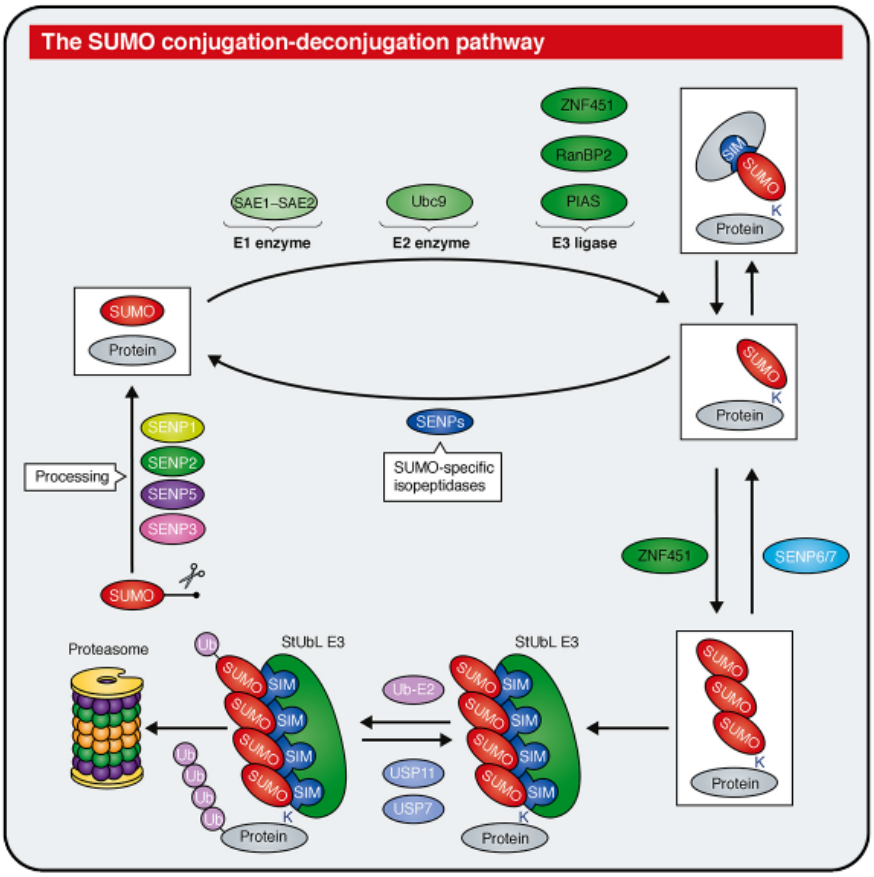

Figure 5: The SUMO conjugation and deconjugation pathway. Prior to SUMO conjugation, the immature SUMO isoforms obligatory undergo processing by SUMO-specific isopeptidases to exhibit their C-terminal GlyGly motif. Similar to Ub, SUMO is first activated by the single E1 heterodimer SAE1-SAE2 and then transferred to the E2 conjugating enzyme Ubc9. Few SUMO E3 ligases can facilitate the final conjugation of SUMO to an acceptor lysine residue of the target protein. SUMO modification can happen as mono- or multiple-monoSUMOylation at one or more target lysines. Furthermore, poly-SUMO chains can build up through modification of internal SUMO2/3 lysine residues. Reversibility of the whole cycle is gained through the action of SENPs. One consequence of poly-SUMO chain formation is the recruitment of Ub E3 ligases (StUbLs), recognizing SUMO chains and the subsequent proteolytic degradation of target proteins. From Kunz *et al.*[18].

Conjugation of SUMO to target proteins can occur in different ways. Attachment of only one SUMO moiety is termed mono-SUMOylation whereas addition of several SUMO proteins can result in either multiple-mono-SUMOylation or poly-SUMO chains.

The majority of SUMOylated proteins is conjugated at one or more lysine residues within a so called SUMO consensus motif. The most commonly used motif has the sequence ψKxE/D, where ψ is a large, hydrophobic residue

(mostly Val, Ile, Leu, Met or Phe), K is the modified lysine, x can be any amino acid and E/D (glutamate/aspartic acid) stands for acidic residues[19,20].

Apart from the canonical KxE motif, lysine residues surrounded by related sequences can also be targeted by SUMOylation. These include the inverted motif (D/ExKψ), the hydrophobic motif (ψψψKxE), the phospho-dependent motif (ψKxExxS^{P}P), the negatively charged amino acid dependent motif (ψKxExxEEEE) and the phosphorylated motif (ψKxS^{P}P) (Figure 6 A). SUMO2/3 itself each harbour a surface exposed SUMO consensus motif surrounding K11, which is preferentially used to build up poly-SUMO2/3 chains.

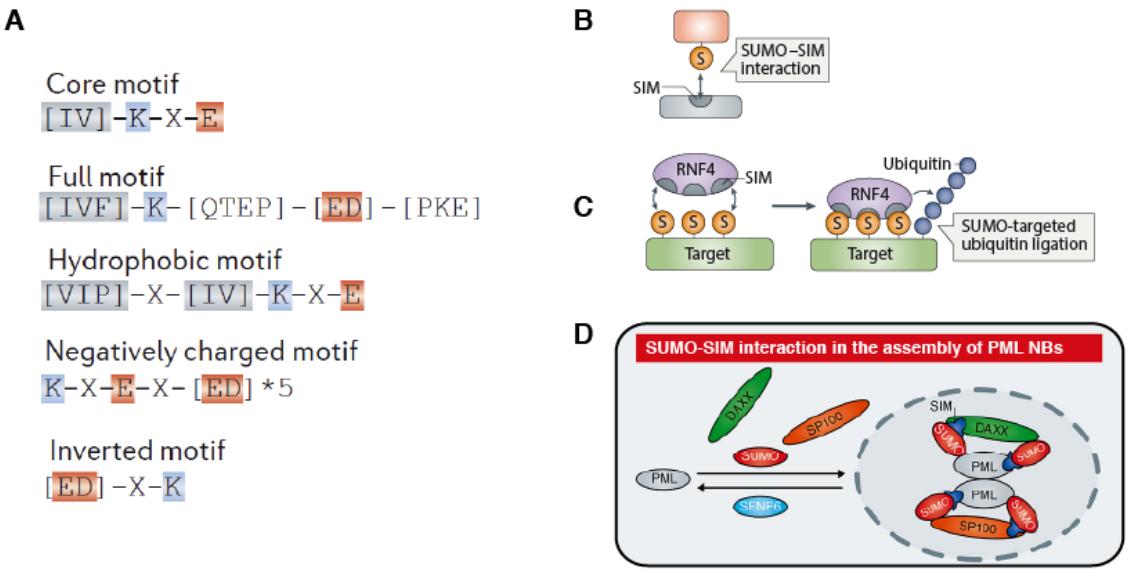

Figure 6: The SUMO consensus motif and SUMO-SIM-driven protein interactions. (A) Depicted are the sequences of different SUMO consensus motifs. Typically, SUMO is covalently bound to lysine residues lying within such a motif. In the canonical consensus motif, the lysine is flanked by large hydrophobic residues (isoleucine, valine) and acidic residues like glutamate, X stands for any amino acid. **(B)** SUMO-interacting motifs enable the non-covalent interaction of SUMO with target proteins. They exhibit a hydrophobic core region stabilizing the interaction with SUMO. **(C)** The StUbL RNF4 as prominent example of SIM-harbouring proteins, enabling them to recognize their poly-SUMOylated substrates. **(D)** Formation of PML NBs through SUMO-SIM-mediated association of SUMO, PML and other recruited interaction partners. Adapted from Hendriks *et al.*[21] and Kunz *et al.*[18].

A typical consequence of SUMO conjugation is the recruitment of binding partners that harbour distinct SUMO recognition motifs. The best-characterized motif so far consists of a short peptide motif, so-called SIM (SUMO-interacting motif), which enables non-covalent interactions of SUMO and target proteins (Figure 6 B). There is a large number of proteins exhibiting SIMs that recognize

either SUMO1 or SUMO2/3. Structural studies, for example on the SIM of PIAS family members, showed that the short hydrophobic core sequence of this motif is essential for the recognition of SUMO isoforms. The canonical SIM consists of a V/I-x-V/I-V/I hydrophobic core, which forms a β-strand aligning in parallel or antiparallel to the β2-strand of SUMO. This core region contacts specific amino acid residues in a hydrophobic pocket lying between the β2-strand and the α1-helix of SUMO. In addition to these hydrophobic interactions, electrostatic interactions frequently contribute to SUMO-SIM binding. Negative charges adjacent to the hydrophobic core of SIMs are either provided by glutamate/aspartate or phosphoserine/threonine residues. These negatively charged residues are in contact with positively charged basic regions of the SUMO molecule. Phospho-dependent SIMs (phospho-SIMs) exemplify how PTM's on SIMs or SUMO can additionally modulate these electrostatic interactions and thereby alter the specificity and dynamics of binding. On the one hand, SUMO-SIM interactions can be strongly enhanced by phosphorylated serine/threonine residues. On the other hand, the neutralization of basic charges in the SUMO molecule by the addition of acetyl groups prevents SIM binding. This again shows that PTMs can act as versatile switches that regulate protein-protein interactions and determine their specificity.

4.3.2 Cellular consequences of SUMO modification

SUMO-SIM mediated protein interactions regulate a wide variety of cellular pathways. The first described target for mono-SUMOylation was the small GTPase-activating protein for Ran, RanGAP1. Ran is a small ras-like GTPase involved in the regulation of nucleocytoplasmic transport. In mammalians, RanGAP1 exists in two forms: one subpopulation is cytoplasmic, while a SUMO1-conjugated fraction is targeted to the nuclear pore complex[22,23]. RanGAP1 is the most prominent target of SUMO1 and almost exclusively detectable in its SUMO1-conjugated version. At the nuclear pore complex, RanGAP1 is part of a multisubunit complex consisting of SUMOylated RanGAP1, Ubc9 and RanBP2. RanBP2 itself has a canonical SIM domain and

functions as SUMO E3 ligase. Together these three proteins build a docking site for nucleocytoplasmic transport and represent one important complex where SUMOylation in its monomeric form exerts an important regulatory role.

The second paradigm of SUMO-dependent assembly of a multisubunit protein complex is the formation of PML NBs (promyelocytic leukemia nuclear bodies). This process represents a good example for SIM-regulated protein-protein networks and SUMO acting as modifier of whole protein groups. Hereby, PML NBs act as scaffold for multivalent protein interactions, whose dynamics are regulated by numerous SUMO-SIM connections. PML itself contains a SIM motif and is SUMO-modified at at least three distinct lysine residues. This allows SUMO-SIM-dependent oligomerization of PML and recruitment of other SIM-containing binding partners such as Daxx or SP100. SUMO-SIM interactions thus function as molecular glue for the formation of PML NBs (Figure 6 D). SUMOylation of one or more interaction partners in NBs represents an adaptable way to react to internal or external stimuli by recruiting or releasing proteins from NBs or modulating their interactions.

A specialized pathway, where poly-SUMOylation acts in concert with poly-SIMs is the StUbL pathway, which is primarily a stress-induced processes involving poly-SUMOylated targets. Here, the poly-modified proteins are specifically recognized by mammalian E3 ubiquitin ligases such as RNF111 or RNF4 possessing three or four SIMs to bind to poly-SUMO2/3. Subsequent ubiquitination events lead to proteolytic or non-proteolytic consequences for the modified proteins (Figure 5 and 6 C). In this example, SIMs fulfil the important function of binding modules for poly-SUMO2/3-modified proteins.

The consequences of poly-SUMO chain formation on target proteins are exemplified on the arsenic-dependent degradation of PML and the oncogenic fusion protein PML-RARα (retinoic acid receptor alpha), which provides a key example of RNF4-mediated degradation of poly-SUMOylated proteins in disease context. Acute promyelocytic leukaemia is characterized by the

expression of a fusion protein between the retinoic acid receptor alpha and the PML protein. This leads to disturbed myeloid differentiation and also impairs PML NB formation. The disease can be effectively treated by administration of arsenic trioxide that induces poly-SUMOylation of the PML-RAR fusion and induces degradation via RNF4-mediated ubiquitination.

More SUMO-controlled pathways relevant for this work will be explained in chapter 4.4.2 below.

4.4 The SENP family of SUMO-specific isopeptidases

4.4.1 Characteristics and functions of SENPs

Conjugation of SUMO to target proteins is a reversible, fine-tuned mechanism involved in many cellular key processes like gene expression, ribosome biogenesis or DNA repair. To assure the functionality of these pathways a precisely balanced SUMO modification/demodification homeostasis is needed. Specialized proteases cleave SUMO from its substrates and thus enable a rapid and dynamic deconjugation process. These SUMO-specific isopeptidases have first been discovered in the yeast *S. cerevisiae (Saccharomyces cerevisiae)*, where they are called Ulp1 and Ulp2[24,25]. The mammalian SENP family is comprised of six members (SENP1-3, SENP5-7), whereas SENP8 is acting on the ubiquitin-like protein NEDD8. Additionally, there are also other classes of SUMO proteases, like the DeSI-1/DeSI-2 and USPL1 isopeptidases, which act on different substrates than SENPs. However, in this work the focus is set on SUMO proteases of the SENP family.

All human SENPs belong to the family of cysteine proteases and exhibit a papain-like fold. Their conserved active centre is classically located in the C-terminal region comprising the catalytic triad histidine, aspartate and cysteine. The N-terminal region of SENPs is typically involved in substrate selection or in the control of their subcellular localization. SENP3 for instance is targeted to the

nucleolus via interaction of its N-terminal part with NPM1[26]. The domain structure of SENPs is depicted in Figure 7. This figure also illustrates the pairwise evolutionary relationship of SENP family members. SENP1, SENP2, SENP3 and SENP5 originate from the Ulp1 branch, whereas SENP6 and SENP7 emanate from the Ulp2 branch. The pairwise evolutionary relationship is also reflected by the preference of SENP family members for distinct SUMO paralogs or SUMO chains. SENP6/SENP7 are predominantly acting on poly-SUMO2/3 chains whereas SENP3/SENP5 are primarily deconjugating single SUMO2/3 moieties from its substrates and SENP1/SENP2 are acting on all three SUMO isoforms. Another important function, like already mentioned earlier, is the processing of SUMO precursors to mature SUMO isoforms. In this step, SENPs hydrolyse a peptide bond at the very C-terminus of pre-SUMO and thus eliminate a few amino acids to expose the GlyGly motif, enabling SUMO to be conjugated to target proteins. Also in this maturation procedure the different SENP isoforms show preferences towards SUMO1, 2 or SUMO3. Their cleaving activity of pre-SUMO is shown in Figure 7, where for example SENP1 preferentially acts on SUMO1, SENP2 is most active on SUMO2 but SENP6 and SENP7 show no detectable cleavage activity.

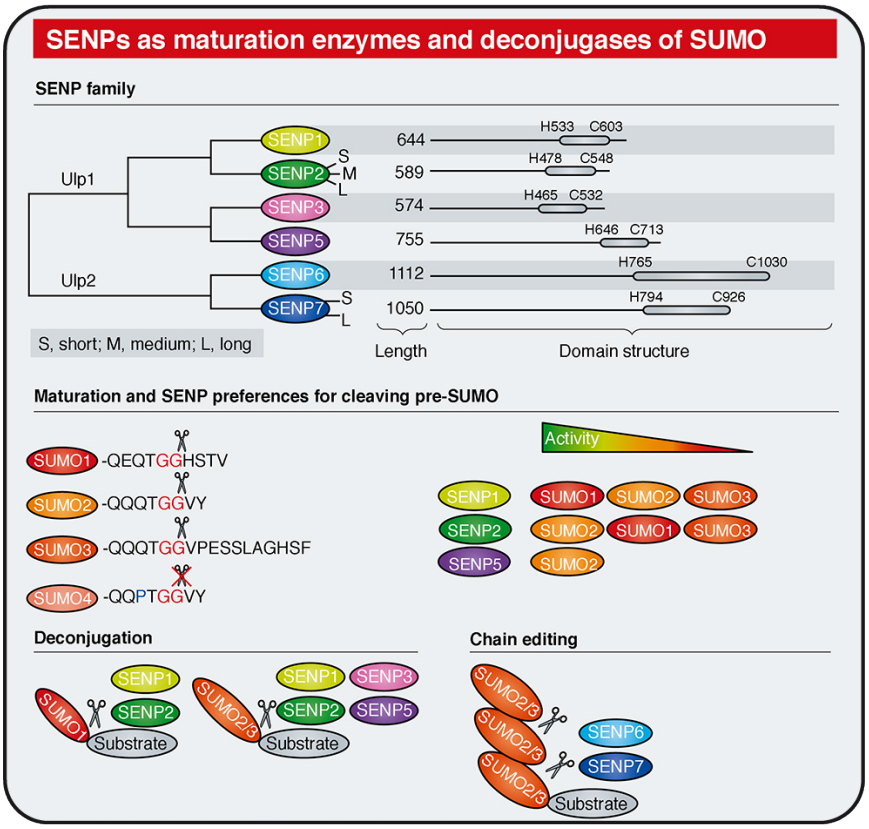

Figure 7: The mammalian SENP family of SUMO-specific isopeptidases and their preferences for SUMO maturation and deconjugation. Depicted are the six human SENPs including their catalytic core and domain structure. SENP1, SENP2, SENP3 and SENP5 evolutionary originate from the same branch (Ulp1), whereas SENP6 and SENP7 emanate from the Ulp2 branch (sequences of SENP family members were compared and a phylogenetic analysis considering their catalytic domain was carried out). Experimentally validated preferences for cleaving pre-SUMO are shown as well as the inability of SENPs to process SUMO4. SENP1-SENP5 are acting on single SUMO moieties while SENP6 and SENP7 are modifying poly-SUMO chains. From Kunz *et al.*[18].

4.4.2 Selected pathways under the control of SENPs

Like introduced earlier, SUMOylation plays an important regulatory role in many cellular signalling pathways. SUMO proteases are counteracting the conjugation of SUMO to target proteins and thus ensuring the equilibrium of modification. In the following, several cellular components or pathways will be shortly introduced where SUMO-specific isopeptidases exert direct regulatory effects by counteracting SUMOylation. Regarding the action of SENPs in these processes one has to differentiate between removal of mono-SUMO modifications like SENP3 does in steps of ribosomal maturation and deconjugation of poly-SUMO

chains which will be explained on the example of SENP6 and the StUbL (SUMO-targeted ubiquitin ligase) pathway.

One important cellular target of direct SENP regulation are PML nuclear bodies. They act as nuclear hub for the recruitment of proteins affecting and regulating diverse pathways. As outlined above, the dynamics in the PML NBs are driven by SUMO-SIM interactions. Importantly, SENP6 and SENP7 are critical for deconjugation of modified proteins within NBs. Both have been shown to act on nuclear bodies[27] and also PML itself is a known poly-SUMO2/3 modified target.

Another cellular pathway where the action of SUMO proteases is critically involved is rRNA (ribosomal ribonucleic acid) processing and pre-ribosomal maturation. Here, SENP3 has been shown to be critical for 60S ribosome biogenesis and 28S rRNA maturation[28,29]. As example the mammalian PELP1 complex, at least comprised of PELP1, Las1L, TEX10, WDR18 and SENP3, was shown to be controlled by SENP3. This complex is needed for proper nuclear maturation of pre-60S ribosomes[30]. Hereby, PELP1 is the core of the complex and its SUMOylation enables the association of MDN1, a AAA ATPase responsible for 60S remodelling. SENP3 is deconjugating SUMO from PELP1 and thereby releases the PELP1-MDN1 complex from pre-60S ribosomes enabling their subsequent maturation.

Also gene activation or silencing can be influenced by SUMO modification. Occasionally, SUMOylation can activate gene expression but in most of the known cases, SUMO exerts a repressive function by modifying transcription factors. In these cases, SUMO proteases deconjugate SUMO from its substrates to trigger gene expression processes. One example is the SUMO-regulated gene expression by the nuclear co-repressor TRIM28, also known as KAP1 or TIF1β. SUMOylation of TRIM28 facilitates gene silencing by recruitment of the chromatin remodeler CHD3 and the histone methyltransferase SETDB1 through their canonical SIMs. Transcriptional repression is achieved by increasing methylation of H3K9 (histone 3 lysine 9),

thus facilitating a repressive heterochromatin environment[31]. The SUMO-specific proteases SENP1 and SENP7 have been found to reverse this gene repression by deconjugating SUMO from its target TRIM28. Besides the transcriptional control, further important roles of SUMO proteases can be demonstrated on the process of TRIM28 deSUMOylation. Especially deleting poly-SUMO2/3 chains from TRIM28 seems to be crucial for DNA damage repair. Hereby, the deSUMOylation of TRIM28 by SENP7 hinders the association with CHD3 and thus facilitates chromatin relaxation and fosters homologous recombination in response to DNA damage[32].

Worth mentioning is also the crucial role of SENP6 in controlling poly-SUMO chain formation and thereby countering the RNF4-mediated StUbL pathway. As described above, RNF4 acts as SUMO-targeted ubiquitin ligase, recognizing poly-SUMOylated proteins via its internal SIMs. Subsequently, RNF4 triggers the formation of K48- or K63-polyubiquitin chains, depending on the cooperating E2. This induces proteasomal degradation or exerts non-degradative functions for instance in DSB (double-strand break) repair. SENP6 can antagonize this process as exemplified in the control of the FA (Fanconi anemia) repair pathway. In the FA pathway upon damaged DNA and stalling replication fork, the FA core complex is translocating to the nucleus, where the monoubiquitination of FANCD2 and its heterodimeric partner FANCI takes place. They then dissociate, bind to sites of damaged chromatin and form so called DNA repair foci together with BRCA2, RAD51, PCNA and others[33]. Subsequent polySUMOylation of FANCD2/FANCI recruits RNF4, which is able to polyubiquitinate the FANCI/D2 dimer. As a consequence the complex can be extracted from chromatin lesions through the action of the ubiquitin-selective segregase VCP/p97. This process is counteracted by SENP6, limiting SUMO chain formation on FANCI and thus contributing to maintain genome stability[34] (Figure 8).

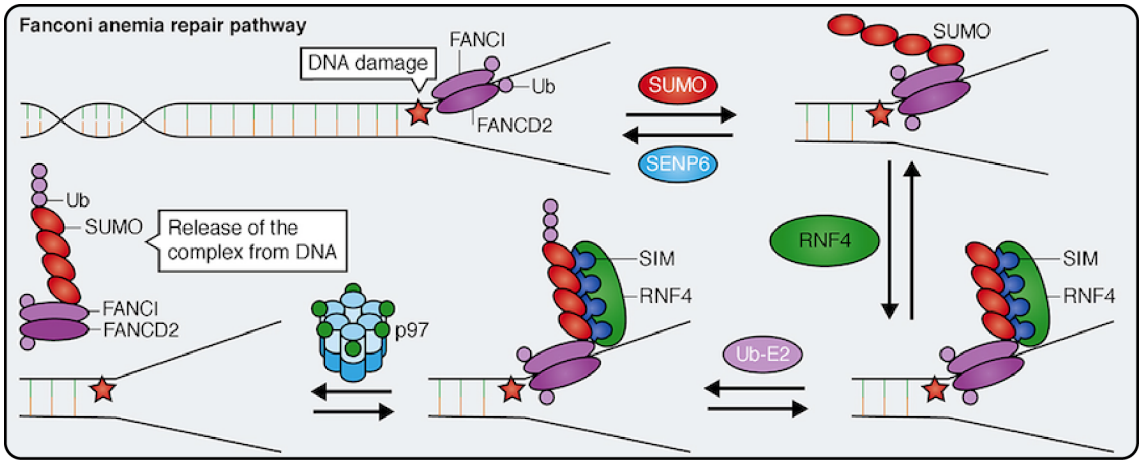

Figure 8: The Fanconi anemia repair pathway under control of SENP6. SENP6 counteracts the polySUMOylation of FANCI, a member of the FA repair complex that is localizing to sites of DNA lesions upon DNA damage. SENP6 thereby limits the RNF4-mediated polyubiquitination and the subsequent extraction of the complex by the p97 segregase. From Kunz *et al.*[18].

Another important process under the control of SENP6 is the stabilization of centromere proteins. Several members of the kinetochore have been shown to be degraded via the StUbL pathway. In particular, SENP6 protects inner kinetochore proteins of the CENP-H/I/K complex from being targeted by RNF4 and thereby prevents their proteasomal degradation[35]. Cells depleted of SENP6 are characterized by prolonged mitotic arrest, chromosome misalignments and missegregation due to defective inner kinetochore assembly. Thus, SENP6 ensures proper mitotic progression by antagonizing RNF4-mediated proteolytic degradation of inner kinetochore proteins.

4.5 The SUMO system under stress: Regulation by PTMs

As described earlier in this work, SUMOylation is a very dynamic process involved in the regulation of various pathways. To ensure reliability and functionality, a tight way to control the conjugation and deconjugation machinery is needed. One way to control SENP activity are post-translational modifications. Large-scale proteomic approaches for instance identified phosphorylation sites on SENP1, SENP3, SENP6 and SENP7 in dividing cells[36]. Furthermore, SENP3 has been shown to be phosphorylated in its N-terminal region by the mTOR kinase, thereby facilitating its nucleolar targeting

by enhancing its interaction with NPM1[26]. Not only are SENPs regulated by PTMs to control their subcellular localization, also their gene expression and turnover may be influenced[37–40]. SENP7 for instance is known to get degraded by the UPS (ubiquitin-proteasome system), whereas SENP3 gets phosphorylated under ischemic conditions. This leads to its lysosomal degradation and results in elevated global SUMO2/3 levels[38]. This mechanism may explain the cytoprotective consequences of elevated SUMOylation in ischemia.

Generally, increased SUMOylation, mostly by SUMO2/3, is seen as a major cellular response to cellular or environmental stress. These may be extracellular factors like heat stress, pH changes, osmotic stress or changes in oxygen supply[41]. Oxidative stress is a typical challenge to the cell and can be caused by all before mentioned insults[42]. Usually, intracellular reactive oxygen species, especially the superoxide radical anion arise as normal by-products from the electron transport chain (complex I, II and III) of the mitochondria. The cell has multiple safeguard systems to cope with these reactive molecules. To name only one, the superoxiddismutase is capable to catalyse the reaction of harmful superoxide radical anions to less reactive H_2O_2 (hydrogen peroxide). H_2O_2 in turn is converted into water by the enzymes catalase or glutathione peroxidase. If the cell is still able to cope with the amount of reactive species, the system is in equilibrium. Under normal conditions, ROS (reactive oxygen species) also play an important role as signalling molecules involved for instance in inflammatory signalling. When the system is in a redox imbalance, the duration and extent of this state determine the cell's fate. Insufficient oxygen supply, called hypoxia, is known to cause ROS by its own despite the lack of oxygen[43]. Initially, it was thought that ROS decrease under hypoxia because the level of free radicals would be directly proportional to the availability of cellular oxygen. This thesis was challenged over the past years by more and more data demonstrating increasing ROS levels under hypoxia. Meanwhile we know that the paradoxically increased formation of ROS under low oxygen is necessary for HIF1-mediated transcriptional response to hypoxia which is mediated by functional mitochondria, being the major sources of hypoxic ROS[44]. Severe

hypoxia leads to senescence and cell death while only mild oxidative stress was shown to even increase cellular survival. In this latter situation, global changes in PTM and gene expression pattern take place[45]. SUMOylation is seen as one major response to cellular redox stress[37,46,47]. Especially susceptible for modifications by reactive species, not only in the SUMO system, are cysteine residues. They are able to transduce changes in redox state and thereby act as molecular switches. This requires the reversibility of the redox modification. Irreversible changes of cysteine residues may lead to non-functional proteins.

Several observations link the SUMO system to redox stress or redox signalling, highly depending on the ROS concentration. One example where ROS influences the SUMO system already at low concentration of H_2O_2 is the reversible inhibition of SUMO conjugation. At low concentrations, H_2O_2 has been shown to trigger reduced SUMOylation of several tested substrates. This effect was reversible by DTT (dithiothreitol) or GSH (glutathione) treatment. Not only exogenously added H_2O_2 shows this phenomenon, also an oxidative burst in macrophages leads to the same results. Mechanistically, in these cases, the Ubc9-SUMO thioester formation is inhibited due to a cross-link forming between the catalytic cysteines of SAE2 and Ubc9, making SUMO conjugation to target proteins impossible[48]. At high doses however, an increase in global SUMOylation was observed. This can be explained by the inhibition of SUMO isopeptidases since the catalytic activity of SENP1 has been shown to be inhibited by high levels of H_2O_2.

Concerning the mechanism, SENP1 dimerizes via two oxidized cysteine residues forming a disulphide linkage upon H_2O_2 treatment. This inhibition is reversed by the addition of DTT. It has been proposed that this intermolecular dimerization protects SENP1 from irreversible oxidation and inhibition[49].

Also the activity and stability of SENP3 is influenced by changes in redox state. Under basal conditions, SENP3 levels are kept low by CHIP-mediated ubiquitination and subsequent degradation. Under mild oxidative stress however, two cysteine residues in SENP3 undergo oxidative modification. This in turn recruits HSP90, which binds to SENP3 and thereby abrogates CHIP-

dependent ubiquitination[40]. Also the subcellular distribution of SENP3 is influenced by oxidative stress. ROS causes shuttling of SENP3 from the nucleolus to the nucleoplasm, where it is able to control also nuclear events[39]. The stabilization of SENP3 under mildly increased ROS stands in correlation with an increased transcriptional activity of HIF-1α.

Altogether, these data demonstrate the important influence of redox regulation on the SUMO system. Still further investigations are needed finally leading to an improved understanding of PTMs as sensors for changes in redox-state.

5 Aims of this study

As outlined in detail above, post-translational protein modification by SUMO is an important regulatory mechanism to control various cellular pathways. A fine balanced equilibrium between SUMO conjugation and deconjugation is essential for proper function of the system. SUMO-specific deconjugases fulfil the critical task to release SUMO from target proteins, thereby counteracting SUMO conjugation. However, the fine-tuned regulation of SUMO proteases and their specific targets is not well understood. Unlike in the ubiquitin system, where around 100 deubiquitinases are responsible for deconjugation of target proteins, the SUMO system relies on six SENP family members deconjugating hundreds of SUMO targets. The model of SUMO group modification wherein a subset of proteins is regulated by one distinct SUMO protease may help to explain this challenging physiological situation. However, the regulation and specificity of distinct family members has remained largely unclear.

The aim of this thesis was therefore to uncover the regulation and substrate specificity of distinct SUMO isopeptidases in order to better understand their role in cellular signalling pathways.

In particular we aimed to

- Investigate SUMO signalling and SENP regulation under hypoxia
- Define substrate selectivity of SENP3 and SENP6 by a comprehensive proteomic profiling approach
- Dissect signalling pathways controlled by SENP3 and SENP6.

6 Results

6.1 Investigation of SUMO signalling under hypoxia

As introduced earlier, SUMO-specific isopeptidases fulfil versatile functions regulating different pathways. In addition, their action is controlled by various layers of regulation or influenced by cellular stressors, like heat stress, DNA damage or low oxygen supply. In the case of hypoxia it was already known, that modification of proteins with SUMO1 is increased[41], however, the exact mechanism has remained elusive. Studies on the hypoxic effects on SUMOylation are available but they were mostly done using overexpressed SUMO[50]. In our work we wanted to address the regulation of SUMOylation under hypoxia at endogenous expression levels of SUMO.

6.1.1 Effects of hypoxia on the activity of individual SUMO proteases

To monitor the endogenous SUMOylation status under hypoxic conditions, we cultured HeLa (Henrietta Lacks) cells under low oxygen (1% O_2) in a hypoxia chamber for 1, 2, 4 or 24 h or under control conditions (5% CO_2). Subsequently, cells were lysed under denaturing conditions using Laemmli buffer and samples were separated by SDS-PAGE (sodium dodecylsulphate polyacrylamide gel electrophoresis). The cellular SUMOylation pattern was monitored by immunoblotting against SUMO1 and SUMO2/3. HIF1α was included to control for a proper cellular response to hypoxia and β-tubulin served as loading control (Figure 10 A). In comparison to control conditions, samples from hypoxic cells showed elevated levels for high molecular weight SUMO1-conjugates (longer exposure, second panel from top) with the maximal increase visible after 24 h of hypoxia (short exposure, first panel). The most prominent band around 90 kDa is SUMO1-modified RanGAP1, representing the most strongly SUMO1-modified protein. This increase in global SUMO1-modification is specific for SUMO1

since immunoblotting against SUMO2/3 revealed only a slight increase in SUMO2/3-conjugates under hypoxia when compared to normoxic conditions. Steadily increasing HIF1α protein levels can be observed with prolonged time under hypoxia, which confirmed proper hypoxic environment, whereas β-tubulin as loading control remained unchanged.

Next we investigated total SUMO protein levels and mRNA (messenger RNA) expression (Supplemental Figure 1), to explore whether increased SUMOylation is simply caused by elevated cellular SUMO levels in response to hypoxia. Therefore, HeLa cells were cultured under normoxia or hypoxia for 24 h and samples in triplicates were prepared for LC-MS/MS analysis. Label-free quantification of protein intensities revealed no major changes of SUMO1, 2 and 3 levels when comparing normoxic and hypoxic proteomes (Supplemental Figure 1 A). Also mRNA levels of SUMO1, 2 and 3 remained stable under normoxia or hypoxia for 4 h, 24 h and 24 h including a reoxygenation period of 30 min (Supplemental Figure 1 B). Furthermore, levels of the SUMO-conjugating enzyme Ubc9 and E3 ligases of the PIAS family remained unchanged in the proteome data of hypoxic and normoxic HeLa cells.

To further test whether increased SUMOylation under hypoxia is caused by reduced SENP protein levels (Supplemental Figure 2 A), HeLa cells were cultured under normoxia or hypoxia for indicated time points followed by denaturing lysis and immunoblotting against SUMO1, SUMO2/3, HIF1α, individual SENPs and β-tubulin. Again, increased SUMOylation pattern for SUMO1-conjugates could be observed, whereas SUMO2/3 conjugates showed only minor changes. For the individual tested SUMO isopeptidases (SENP1, 2, 3 and 6) no changes in protein level were detected under hypoxia or normoxia. Altogether, this suggests that enhanced SUMOylation under hypoxia is not due to altered expression of SUMO paralogs or the SUMO-conjugation machinery.

Another possible reason for increased SUMOylation of target proteins under hypoxia could be changes in the activity of SUMO isopeptidases. To test this hypothesis, we performed activity measurements of SUMO proteases utilizing a fluorogenic dye, named AMC (7-amido-4-methylcoumarin), which is covalently

linked via a reactive amino group to the C-terminal GlyGly residue of mature SUMO (SUMO1 or SUMO2). This ligation quenches the autofluorescence of the AMC molecule. Active SUMO proteases cleave the covalent linkage between SUMO and AMC and the fluorescence, emitted by AMC, can be recorded. The fluorescence intensity is nearly proportional to protease activity (see Figure 9 for reaction mechanism). This sensitive assay was used to generate quantitative data on SENP activity and to analyze steady state kinetics.

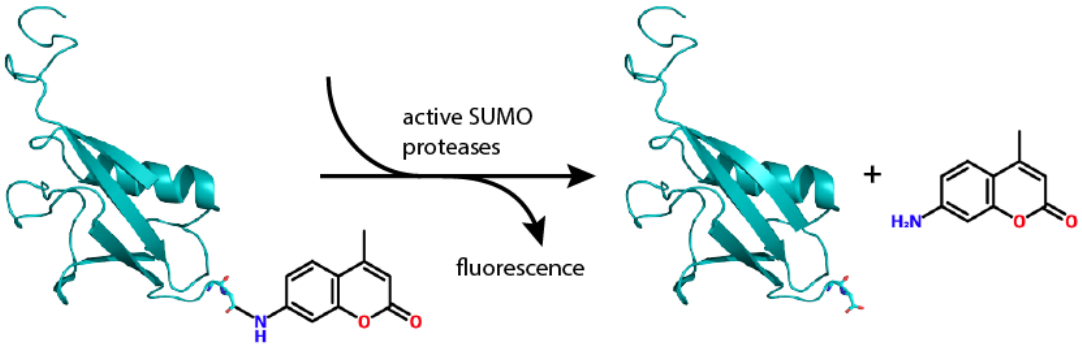

Figure 9: SUMO-AMC assay to determine SUMO protease activity. The fluorescent molecule 7-amido-4-methylcoumarin is coupled to mature SUMO isoforms, quenching its autoflourescence. Active SUMO proteases cleave the covalent linkage between SUMO and AMC and the following increase in fluorescence intensity can be monitored to determine protease activity. Adapted from Kunz *et al.*[51].

We applied this method to HeLa cells incubated under normoxia or under hypoxia for 2, 4, or 24 h. Additionally, cells kept for 4 h or 24 h under hypoxia were subjected to a reoxygenation period of 30 min. Cells were lysed after indicated time points and lysates were incubated with SUMO1-AMC or SUMO2-AMC for activity measurements. As negative control, the alkylating agent NEM (N-ethylmaleimide) (10 mM) was added to irreversibly inactivate cysteine proteases, including SENPs. As shown in Figure 10 B and C, when adding SUMO1-AMC or SUMO2-AMC to cell extracts from normoxic cells, fluorescence intensity is rapidly increasing over time, indicating cleavage activity of SUMO proteases on the SUMO-AMC substrate. In general, a faster increase of emitted fluorescence can be observed with SUMO2-AMC as substrate, presumably due to the preference of several SENPs to cleave SUMO2-AMC over SUMO1-AMC. Measurements show highest activity for HeLa cells in normoxic environment. Importantly, a reduced SENP activity was visible in cell lysates from cells kept

2 h and 24 h under hypoxia (Figure 10 B). This effect was observed on the SUMO1-AMC substrate but was even more pronounced on cleaving SUMO2-AMC after 4 h and 24 h of low oxygen (Figure 10 C). The activity of SUMO proteases was diminished about 40-50% after 2-4 h under hypoxia and an even more drastic decrease to 30% for SUMO1-AMC and less than 20% for SUMO2-AMC was observed after 24 h in hypoxia. By contrast, a reoxygenation period of 30 min was sufficient to restore activity of SUMO isopeptidases near normoxic control levels. NEM was able to abolish an increase in fluorescence signal over time, meaning no SUMO-AMC substrate was cleaved since SUMO isopeptidases were inactivated. These observations strengthen the hypothesis that SUMO isopeptidases can be inactivated under prolonged time in hypoxic environment but regain their ability after reoxygenation.

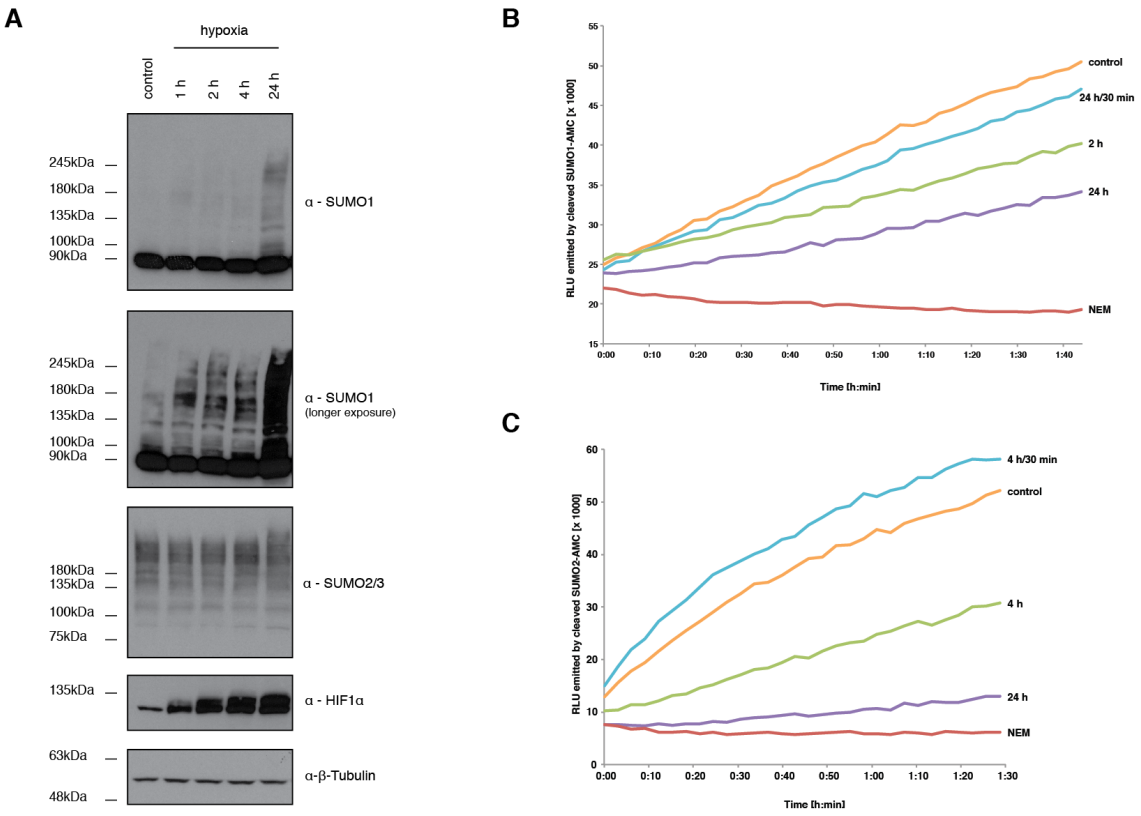

Figure 10: Hypoxia results in increased SUMOylation caused by reduced activity of SUMO proteases. (A) HeLa cells were kept under normoxic or hypoxic (1% O_2) conditions for indicated time points. Afterwards, lysis was performed in Laemmli buffer and separation of proteins was achieved by SDS-PAGE. Immunostaining was done with antibodies against SUMO1, SUMO2/3, HIF1α and β-tubulin. **(B)** SUMO1-AMC assay performed in HeLa cell extracts from normoxic, hypoxic or reoxygenated samples (24 h hypoxia/30 min reoxygenation). Collective SUMO protease activity was measured over time by recording fluorescence intensity in RLU (relative light units) produced by liberated AMC molecules. NEM (10 mM) was used as negative control to abolish SUMO protease activity. **(C)** SUMO2-AMC assay

performed in HeLa cell extracts as in (B) but with SUMO2-AMC as substrate to determine cleavage activity on SUMO2. Reoxygenation (30 min) of one sample was performed after 4 h of hypoxia. From Kunz *et al.*[52].

The AMC assay measures the overall activity of all cellular SUMO proteases. Only when this method is combined with knockout or knockdown of individual isopeptidases, the contribution of a distinct protease to cellular SENP activity can be deduced. To further elucidate which SENP family members are affected by low oxygen content, we therefore established an additional activity assay. In this assay, a commercially available active site probe is used. In this probe a VS-(vinyl sulfone) group is covalently linked to the C-terminus of SUMO paralogs. The VS-group attacks the catalytic cysteine of the SUMO protease and thereby forms a non-cleavable thioether bond. Thus the VS-group acts as a suicide trap for functional SUMO proteases. Through separation of the reaction products by Western blot analysis and staining against individual SENPs, the activity of individual SUMO proteases can be monitored by visualizing the SUMO-VS-SENP conjugates (see Figure 11 for reaction mechanism).

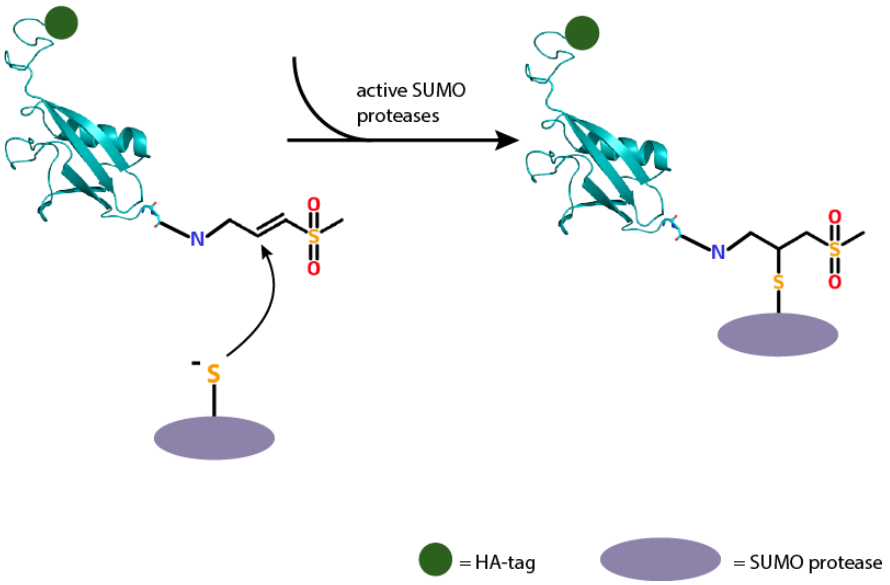

Figure 11: **SUMO-VS substrate acting as substrate trap to determine SENP activity.** Mature SUMO moieties with an N-terminal HA-tag are chemically ligated to a vinyl sulfone group. The active cysteine of SUMO proteases attacks the vinyl double bond and is trapped irreversibly. Separation by SDS-PAGE and following staining against individual SUMO proteases allows the analysis of the active proportion of reacting enzyme by detecting the SUMO-VS-SENP adduct. Adapted from Kunz *et al.*[51].

To test the activity of distinct SENP family members HeLa cell extracts were prepared and lysates were incubated with either SUMO1-VS or SUMO2-VS. Control reactions were performed without substrate or 10 mM NEM was used as negative control. The reaction was stopped by the addition of Laemmli buffer and samples were subjected to SDS-PAGE following immunoblotting. Samples were probed with anti-SENP1, anti-SENP3 or anti-SENP6 antibody (Figure 12 A, B, C). In the absence of SUMO-VS, SENP1 appears as 75 kDa protein in SDS-PAGE. However, the addition of SUMO1-VS or SUMO2-VS in Figure 12 A leads to the appearance of SUMO-VS-SENP1 adducts migrating at around 100 kDa. This observation is consistent with the idea that SENP1 acts on both, SUMO1 and SUMO2 conjugates. NEM is able to fully block the reaction (last lane) and prevents the formation of the SUMO-VS-SENP1 adduct. When lysates were stained against SENP3, the preference of SENP3 for SUMO2/3 over SUMO1 became obvious and was represented by a faint band for the SUMO1-VS-SENP adduct (100 kDa, upper panel) whereas almost the entire fraction of free SENP3, migrating at 75 kDa, in the lysate was reacting with SUMO2-VS, visible by a prominent band around 100 kDa (lower panel). In case of SENP6, NEM-sensitive SUMO1/2-VS adducts around 180 kDa could be detected. Due to lack of specific antibodies or low activity in HeLa cells, SUMO-VS adducts of other SENP family members could not be detected (Supplemental Figure 2 B). Probing against the HA-tag of SUMO-VS substrates we could detect bands migrating around 75, 100 and 180 kDa, representing SUMO-VS-SENP adducts formed in HeLa lysate after incubation with SUMO1-VS or SUMO2-VS (Supplemental Figure 3 A). These bands fully disappeared under NEM treatment and likely correspond to SENP1, SENP3 and SENP6 adducts as seen in Figure 12 A, B, C.

Having established this assay under normoxic conditions, we then monitored SENP adduct formation under hypoxia. Therefore, HeLa cells were cultured under normoxic conditions or under hypoxia for 2 or 24 h including a reoxygenated sample for the 24 h time point. NEM treatment served as negative control. HeLa cells were lysed and separated by SDS-PAGE following incubation with anti-SENP1, anti-SENP3 or anti-SENP6 antibodies (Figure 12

D, E, F). SENP1 was reacting with both, SUMO1-VS and SUMO2-VS to the same extent in control conditions but lost its activity already after 2 h of hypoxia. A short reoxygenation period of 30 min was sufficient to restore enzymatic activity of SENP1 towards SUMO1-VS and SUMO2-VS. Similar observations were made for SENP3 adduct formation (Figure 12 E). Under normoxia only a small fraction of SENP3 was reacting with SUMO1-VS, while under hypoxia SENP3 activity was completely lost. Also here reoxygenation for 30 min could restore the small part of SENP3 reacting with SUMO1-VS (left panel). In the right panel, a large proportion of SENP3 is reacting with SUMO2-VS under normoxia visible by a SUMO2-VS-SENP3 adduct at 100 kDa. This band is getting reduced after 2 h of hypoxia, reflecting reduced SENP3 activity. Complete loss of enzymatic activity is observed after 24 h low oxygen where absolutely no SUMO-VS-SENP3 adducts can be detected anymore. Remarkably also here a reoxygenation of 30 min is sufficient to restore initial activity like under normoxia. Different from SENP1 and SENP3 activity, SENP6 activity under hypoxia seems not to be severely influenced (Figure 12 F). Only after 24 h there is a small decrease in adduct formation with both, SUMO1-VS and SUMO2-VS. This decrease was also accompanied by a slight reduction in SENP6 protein level under hypoxia, which was even more pronounced after reoxygenation. However, SENP6 is still enzymatically active after 24 h of low oxygen supply. NEM abolished the reaction of all tested SENPs with SUMO1/2-VS in this experiment.

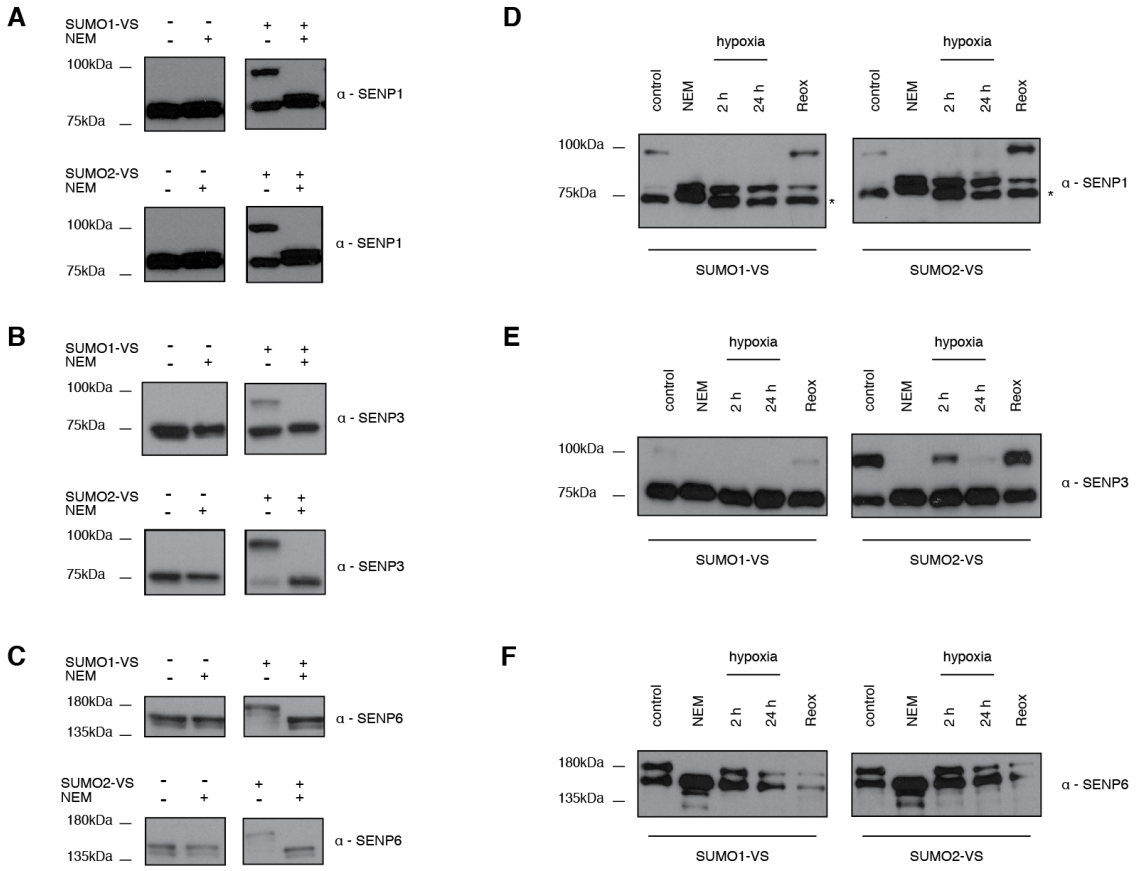

Figure 12: SUMO-VS assay reveals reversible inactivation of SENP1 and SENP3 under hypoxia. (A) HeLa cells were lysed in SEM buffer with or without addition of NEM as negative control. SUMO1-VS or SUMO2-VS was added as substrate where indicated and incubated at 25 °C for 15 min. Proteins were size-separated by SDS-PAGE and probed against SENP1. **(B)** As in (A) but samples were stained against SENP3. **(C)** As in (A) but an antibody against SENP6 was used. **(D, E, F)** HeLa cells were kept under normoxia or incubated at hypoxia for indicated time points. One sample was reoxygenated for 30 min after 24 h of hypoxia. Cell extracts were prepared as described for (A) and incubated with SUMO1-VS or SUMO2-VS. Addition of NEM served as negative control. Samples were separated by SDS-PAGE and transferred proteins were stained using antibodies against SENP1 (D), SENP3 (E) or SENP6 (F). Asterisk marks an unspecific band of the SENP1 antibody. From Kunz *et al.*[52].

Taken all together, these findings show that SENP1 and SENP3 are inactivated under hypoxia whereas SENP6 is not sensitive to changes in oxygen supply. This hypothesis is also supported by immunostaining of the HeLa lysates from Figure 12 D, E, F against HA-tag to monitor global adduct formation (Supplemental Figure 3 B). Here we could also observe an almost complete loss of SENP1 and SENP3 activity represented by vanishing bands at 100 kDa. SENP6 activity remains more or less stable under hypoxia reflected by bands at 180 kDa.

6.1.2 Identification of SUMO1 conjugates under hypoxia

Given the fact, that SENP1 acts on both, SUMO1 and SUMO2, whereas SENP3 prefers SUMO2 conjugates, we hypothesized that the increased amount of SUMO1 conjugates is primarily due to inactivation of SENP1 rather than SENP3. To confirm this, we performed siRNA- (small interfering RNA) mediated knockdown of SENP1, SENP3 or both in combination (Figure 13 A). Lysates were prepared in Laemmli buffer, separated by SDS-PAGE and stained against SENP1, SENP3, SUMO1 and β-tubulin as loading control. Compared to control conditions we observed increasing SUMO1-conjugates under siSENP1 (lower panel). Knockdown of SENP3 only slightly induced conjugation with SUMO1. Combined knockdown of SENP1 and SENP3 showed only a mild increase in SUMO1-conjugates when compared to siSENP1 alone. We therefore reasoned, that effect of elevated SUMO1 conjugation under hypoxia is mediated predominantly by loss of enzymatic activity of SENP1.

To further investigate cellular consequences of hypoxic inactivation of SENP1 and to define targets differentially regulated under hypoxia, we performed endogenous SUMO1 IPs followed by LC-MS/MS analysis of HeLa cells grown under normoxic and hypoxic conditions. Based on the published protocol from Barysch *et al.*[53] we generated HeLa cell lysates from normoxic cells or cells kept under hypoxia for 24 h. For each condition, 13 mg HeLa cell lysate were incubated with SUMO1- or IgG- (immunoglobulin G) coupled beads for immunoprecipitation overnight. To assure accurate quantification and statistical analysis, the experiment was performed in triplicates for each condition. IP samples were processed according to the given protocol, eluted from the affinity matrix by peptide elution and TCA- (trichloroacetic acid) precipitates were used for further analysis. A small volume of the IP samples was used to check for efficient enrichment (Supplemental Figure 4 A). Together with 30 μg input material for proteomic analysis, remaining TCA samples were separated by SDS-PAGE, proteins were stained and subjected to in-gel digestion to prepare samples for subsequent MS-analysis (see Figure 14 for IP-MS workflow).

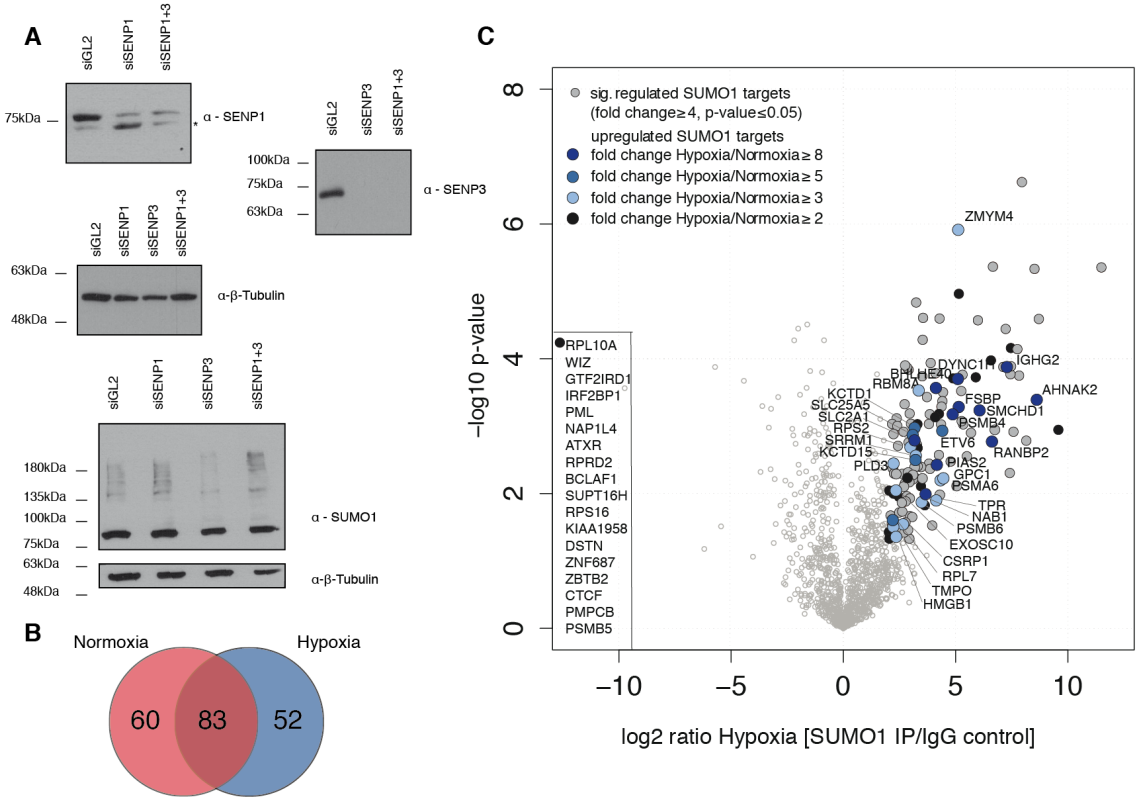

Figure 13: SUMO1-conjugation of distinct proteins caused by hypoxic inactivation of SENP1. (A) SENP1, SENP3 or both proteins were depleted from HeLa cells using siRNA-mediated knockdown. Cells were harvested in Laemmli buffer, separated by SDS-PAGE and probed against SENP1 or SENP3 to control for proper knockdown or against β-tubulin to ensure equal loading. Asterisk marks an unspecific band detected with the SENP1 antibody. Effect on the general SUMO1 pattern caused by depletion of the respective SENP was detected by staining against SUMO1, β-tubulin served as loading control. **(B)** Venn diagram depicting the overlap (83 proteins) of significantly enriched SUMO1 targets over the IgG control under normoxia (143 proteins) or hypoxia (135 proteins). As high-confident candidates considered were proteins with a p-value < 0.05 and being enriched more than 4-fold over the IgG control. **(C)** Results of quantitative LC-MS/MS analysis of endogenous SUMO1 IPs from hypoxic cells summarized in a volcano plot. HeLa cells were kept under hypoxia for 24 h, then SUMO1 conjugated were enriched by endogenous, denaturing IP. Depicted are significantly enriched hypoxic SUMO1 targets with a fold-change ≥ 4 and a p-value < 0.05. Proteins at least 2-fold more enriched in SUMO1 IP from hypoxic cells compared to normoxic cells are represented by colour-coded dots. From Kunz *et al.*[52].

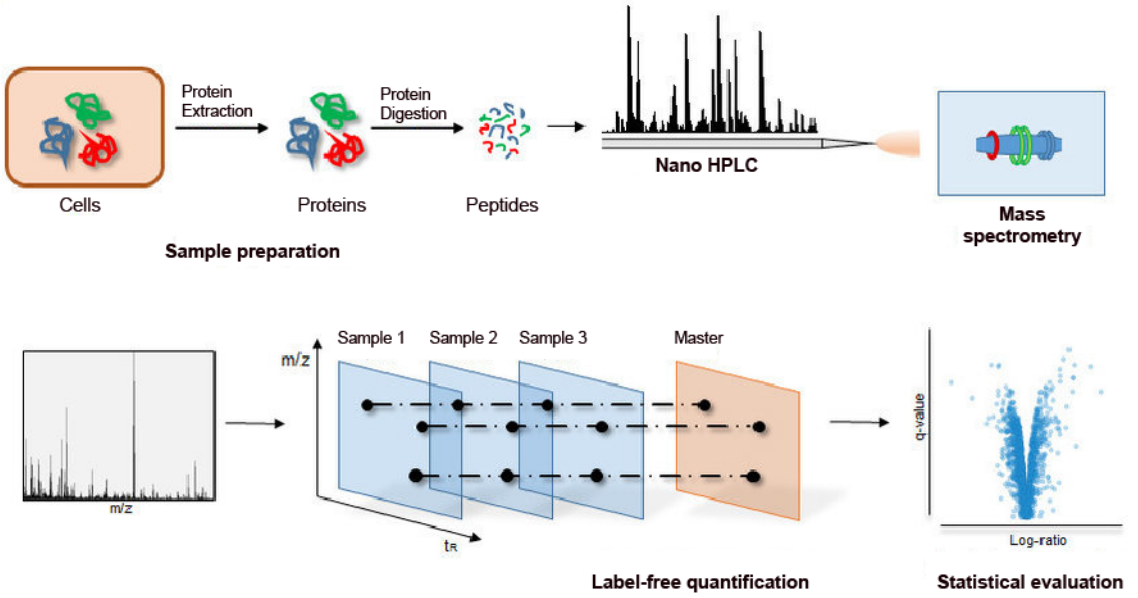

Figure 14: Overview of the endogenous SUMO IP-MS workflow. To analyse endogenous SUMO targets, SUMO-modified proteins were enriched by denaturing immunoprecipitation. Retained proteins were prepared for mass spectrometric analysis by in-gel digestion. Resulting peptides were desalted and concentrated using Stage tips, then separated according to their hydrophobicity by HPLC. Subsequent mass spectrometric analysis was performed and label-free quantification was applied using the MaxLFQ algorithm. Statistical evaluation, downstream analysis and graphical representation of the results were performed using Perseus, RStudio and Excel. Adapted from MPI for Terrestrial Microbiology, Marburg (https://www.mpi-marburg.mpg.de/353915/Mass-spectrometry_Proteomics).

Using the Perseus software, corresponding triplicates were assigned as one sample and their mean value was used for further calculations. Missing values were imputed like described in chapter 8.6.3. Pearson correlation coefficient revealed almost linear correlation (> 0.9) between the LFQ (label-free quantification) values of SUMO1 IPs in normoxia and hypoxia (data not shown). Visual histogram analysis was done to control for normal distribution of LFQ intensities among the samples (data not shown). Additionally, a principal component analysis proved high similarity among the experimental replicates (Supplemental Figure 4 B). These tests validated the quality of our analysis and proved its suitability for further interpretation.

For subsequent analysis, we first checked for enriched SUMO1 targets over IgG control in hypoxia and normoxia. As shown in the Venn diagram (Figure 13 B) we identified 143 targets that were enriched more than 4-fold in SUMO1 IP over IgG IP under normoxic conditions and 135 proteins meeting the same criteria under hypoxia. Volcano plots visualizing individual proteins enriched in SUMO1 IP over IgG control under hypoxic and normoxic conditions can be found in the

supplemental section of this work (Supplemental Figure 4 C, D). Among those significantly enriched proteins, 83 were detected in both conditions. When compared to targets identified by Barysch *et al.*[53] we see a good overlap with our data. Since we were primarily interested in proteins being differentially regulated under hypoxia compared to normoxia, we generated another Volcano plot to better visualize this subpopulation of proteins (Figure 13 C). Depicted on the y-axis is the negative log10 p-value indicating the significance of the hits. We considered targets being significantly regulated with a p-value < 0.05. The x-axis represents the log2 ratio of hypoxic SUMO1 targets compared to IgG control. Here we included only targets in our further analysis, that were at least 4-fold enriched over the IgG control. An additional subset of proteins, highlighted by a colour-code, shows the hyperSUMOylation under hypoxia. The most interesting candidates are the ones that exhibit strong differential regulation in hypoxia compared to control conditions. We found 48 proteins being enriched at least 2-fold under low oxygen compared to control conditions. Within this group, 30 hits are enriched at least 3-fold. RanBP2 and PIAS2 as SUMO E3 ligases are found under the most highly regulated proteins with an > 8-fold stronger SUMOylation under hypoxia. Both are part of the SUMO conjugation machinery and can undergo autoSUMOylation. Under normal conditions, this process is possibly limited by SENPs and the reason why we find those proteins hyperSUMOylated when distinct SENPs are inactivated under low oxygen. Another subgroup of heavily SUMO1-modified proteins under hypoxia (> 5-fold enriched compared to normoxia) is comprised of transcriptional repressors like for example ETV6, KCTD1, KCTD15, FSBP, NAB1 or BHLHE40. Mildly induced SUMOylation under hypoxia (2-3-fold enriched) show several proteins with functions in chromatin or transcriptional regulation. Among those are NAP1L, SUPT16H, ATRX, Wiz, CTCF, BCLAF1, IRF2BP1 or GTF2IRD1). For above-mentioned targets of hyperSUMOylation under hypoxia we additionally controlled for changes in expression levels in hypoxia compared to normoxia. Analysis of the dataset, generated by whole proteome analysis of normoxic and hypoxic samples, demonstrates that increased conjugation with SUMO1 is not due to elevated proteins levels under

hypoxia but likely mediated by hypoxic inactivation of SENP1. In contrast to these examples, we also identified subset of proteins whose increased SUMOylation correlates with higher protein levels under hypoxia (e.g. proteasomal subunits PSMB4/5/6 and PSMA6). Although not in the focus for our further analysis, we identified 30 proteins with at least 4-fold reduction in SUMO1-modification under low oxygen. Nearly half of them (13 of 30) exhibits also reduced protein amount (at least 2-fold) in hypoxic HeLa cell extracts. Altogether, the MS-based analysis of hypoxia-regulated SUMO1 targets reveals a distinct set of proteins, which exhibit enhanced SUMOylation under hypoxia. This subset of proteins is enriched for transcriptional regulators indicating that hypoxia-induced SUMOylation is involved in the control of gene expression programs.

6.1.3 The role of BHLHE40 as SENP1-regulated hypoxic SUMO target

To get insight into the functional consequences of hypoxic hyperSUMOylation, we selected BHLHE40 for further investigation. This transcriptional co-repressor has been described to play a role in adaption to low oxygen[54] and was revealed in our MS-analysis as one of the most strongly regulated SUMO targets under hypoxia compared to normoxia (8-fold enrichment). First, we wanted to validate this result by immunoblotting. To this end, SUMO1 IP from normoxic and hypoxic HeLa cells was performed like described for LC-MS/MS analysis. SUMO1-enriched proteins were eluted from the beads and subjected to TCA precipitation. Concentrated proteins were separated by SDS-PAGE following Western blotting and staining against endogenous BHLHE40 (Figure 15 A). In input samples of normoxic and hypoxic lysates endogenous BHLHE40 migrating at around 55 kDa is detected by anti-BHLHE40 immunoblotting. This band is slightly induced under hypoxic conditions, which is in line with our proteomic data (1.3-fold upregulated in hypoxia compared to normoxia). In the SUMO1-enriched sample from hypoxic cell extracts a single band at around

70 kDa corresponding to SUMO1-modified BHLHE40 is detectable by anti-BHLHE40 immunoblotting (lower panel). This band is exclusive for hypoxic SUMO1 IP since it is not found in the normoxic SUMO1-enriched sample (upper panel). Also after longer exposure no band is detected under normoxia (Supplemental Figure 5). This confirmed our MS data and indicates that BHLHE40 is exclusively SUMO1-modified in response to hypoxia. To strengthen this observation, we performed Ni-NTA- (nickel-nitrilotriacetic acid) pulldown experiments from hypoxic or normoxic cell lysates of His-SUMO1 expressing cells. Therefore, HeLa cells, harbouring a single copy of His-SUMO1 expressed from a tetracycline-inducible promoter, were cultured under hypoxia or normoxia for 24 h. Induction of His-SUMO1 by Dox (doxycycline) was done 14 h before cell lysis. Subsequently, denaturing cell lysis was performed, His-SUMO1 conjugates were enriched on Ni-NTA beads and subjected to SDS-PAGE and immunoblotting (Figure 15 B). Staining of input and pulldown samples against His-tag ensured equal expression and enrichment of His-SUMO1 (lower panel). Already in the input samples SUMO1-modified BHLHE40 appears as band at around 70 kDa in hypoxic samples. This BHLHE40-SUMO1 form is already visible in lysates from non-Dox-induced cells, which is in line with endogenous SUMO1 being conjugated to BHLHE40. The modification was further increased by induction of His-SUMO1 expression with Dox. At around 55 kDa we could observe endogenous, unconjugated BHLHE40, which is again slightly more expressed under hypoxia compared to normoxia. In the His-pulldown samples stained against BHLHE40 (upper right panel) there is only one band visible around 70 kDa in hypoxic lysates from induced cells. This band corresponds to SUMO1-conjugated BHLHE40 since it can only be enriched after induction of SUMO1 expression. This observation is in agreement with our previous data showing that BHLHE40 is only conjugated with SUMO1 under lack of oxygen. Taken together, these results confirm BHLHE40 as hypoxic SUMO1 target.

To directly prove the idea that BHLHE40 is a SENP1-regulated SUMO target, we expressed Flag-BHLHE40^{WT} or the SUMO-deficient variant Flag-BHLHE40^{K159R,K279R} in inducible His-SUMO1 expressing HeLa cells. This lysine

to arginine mutant serves as negative control since it can no longer be modified by SUMO[55]. To investigate the regulation by SENP1, we additionally performed siRNA-mediated knockdown of SENP1 or a non-targeting control siRNA. Unlike preceding experiments, this time Dox-stimulated HeLa cells were exclusively kept under normoxic conditions. Subsequently, His-pulldown was performed using Ni-NTA beads as described above. Proteins bound to beads were recovered by boiling in Laemmli buffer, separated by SDS-PAGE and analysed by immunoblotting (Figure 15 C). Staining of input and pulldown samples with anti-Flag antibodies (upper panel) revealed the presence of unmodified BHLHE40, migrating around 55 kDa in all input samples. In contrast, the 70 kDa SUMO1-modified BHLHE40 version was only visible in Ni-NTA enriched samples from cells expressing WT BHLHE40 under depletion of SENP1. These findings prove our hypothesis of BHLHE40 being a SENP1-regulated SUMO1 target. Additionally, K159 and K279 could be confirmed as major SUMOylation sites.

After validation of the initial mass spectrometry results on BHLHE40, we wanted to further trace down the cellular consequences of hyperSUMOylation of BHLHE40 under hypoxia. Since BHLHE40 was already described in the literature to negatively regulate PGC-1α expression[56], we followed up on this observation and performed a reporter gene assay on a luciferase reporter containing the promoter region of the PGC-1α gene (2 kb region from +78 to -2533). With this method, we wanted to assess the involvement of SUMOylation in BHLHE40-mediated gene repression. HeLa cells were transfected with the firefly luciferase PGC-1α reporter construct together with either $BHLHE40^{WT}$ or $BHLHE40^{K159R,K279R}$. A Renilla luciferase control plasmid was included for proper normalization of transfection. 48 h after transfection, cells were lysed and dual-luciferase reporter assay (Promega) was performed. Relative luciferase activity was used to monitor the activating or repressive functions of BHLHE40 versions on the PGC-1α reporter (Figure 15 D). As shown in the bar diagram, $BHLHE40^{WT}$ was able to inhibit PGC-1α activation to a greater extent than the SUMO-deficient mutant. The transfection of 200 ng $BHLHE40^{WT}$ caused a decrease in PGC-1α activity to 40%. Only moderate differences of

wild-type or SUMO-mutant BHLHE40 could be observed when using 200 ng of corresponding constructs. These differences could be slightly enhanced when transfecting 400 ng of Flag-BHLHE40 plasmids. Additionally, we noticed that the stability of the SUMO-mutant version of BHLHE40 was compromised since we needed to transfect double the amount compared to wild-type version to achieve similar expression levels (anti-Flag Western blot, lower panel). This fact might also contribute to the reduced repressive function on the PGC-1α promoter. These data imply that SUMOylation of BHLHE40 under hypoxia might enhance its stability and contribute to its repressive function.

Taken altogether, with the endogenous SUMO1 IP under hypoxic and normoxic conditions followed by LC-MS/MS analysis we could define a subset of proteins being differentially SUMO-modified under lack of oxygen. With further experiments we proved that this is caused by inactivation of distinct SUMO-specific isopeptidases under hypoxia. Finally, we identified and validated BHLHE40 as SENP1-regulated hypoxic SUMO target, possessing repressive functions on PGC-1α in its SUMOylated form.

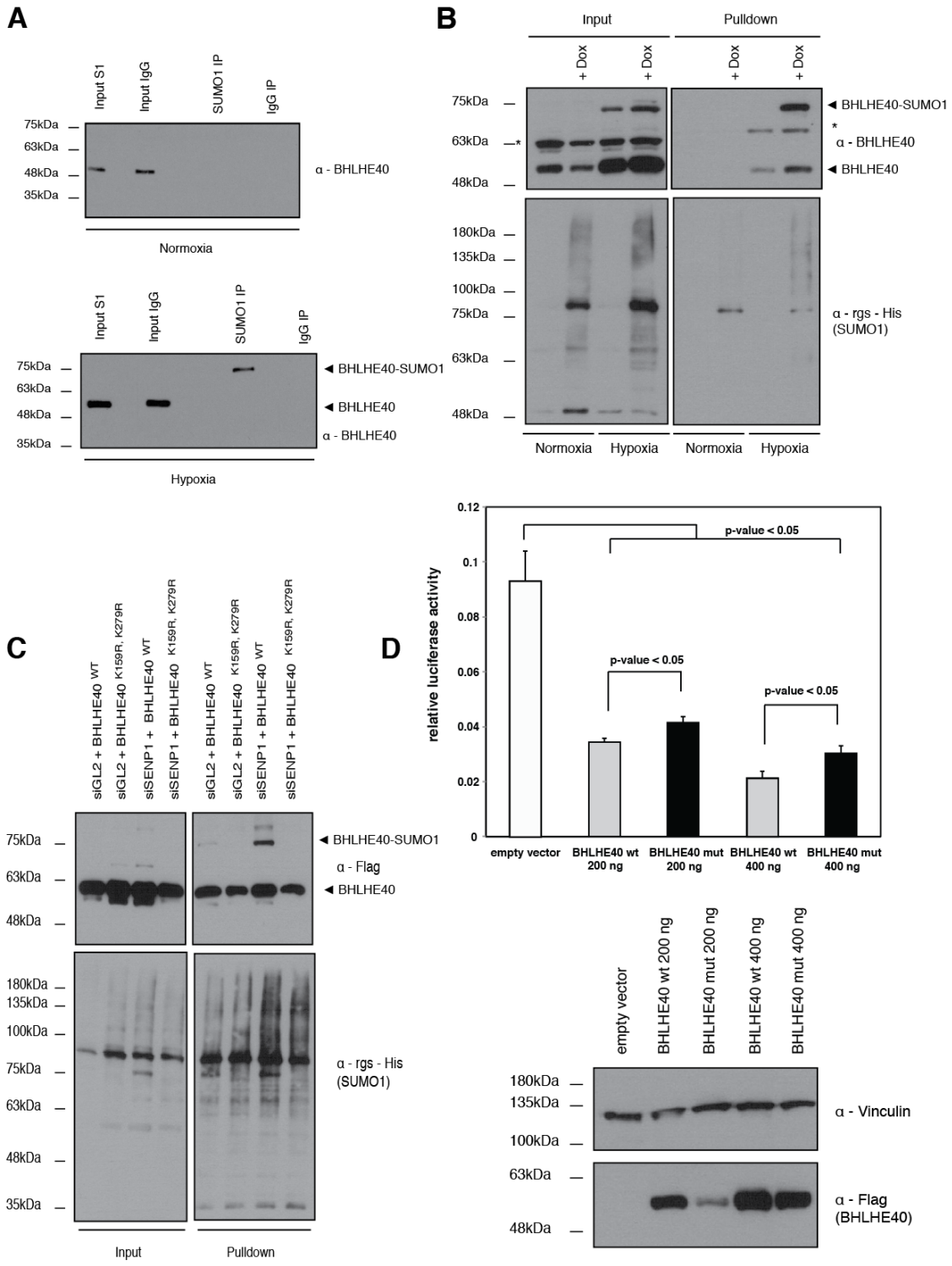

Figure 15: The transcriptional co-repressor BHLHE40 as hypoxic SUMO1 target. (A) Validation of BHLHE40 as SUMO1-modified protein under hypoxia. HeLa cells were cultured under normoxia or hypoxia for 24 h and afterwards lysed for denaturing SUMO1 IP or IgG IP as negative control. Enriched proteins as well as input material were separated by SDS-PAGE and stained against BHLHE40. **(B)** His-SUMO1 expression was induced from a Tet-inducible promoter in normoxic or hypoxic (24 h) HeLa cells on the evening before lysis. After denaturing lysis on the next day, His-SUMO1 modified proteins were enriched by Ni-NTA pulldown. Input and pulldown samples were size-separated and after transfer stained against BHLHE40 and against His-tag to control for proper expression and enrichment. Asterisk marks an unspecific band detected with the BHLHE40 antibody. **(C)** HeLa cells were depleted from SENP1 or non-targeting control by using siRNA. On the next day, wild-type BHLHE40 or SUMO-deficient mutant $BHLHE40^{K159R,K279R}$ were introduced. Denaturing lysis was followed by Ni-NTA pulldown of His-SUMO1-

modified proteins. Enriched material and input samples were blotted against His-tag of SUMO1 or Flag-tagged BHLHE40 constructs. **(D)** HeLa cells were transfected with indicated amounts of WT or SUMO mutant BHLHE40 or empty vector as negative control. Cells were lysed and dual-luciferase reporter assay was performed using a PGC-1α promoter as reporter gene. Data represent the average of at least four independent experiments (± SEM). An aliquot of input material was used for immunoblot analysis to control for proper expression of used constructs by staining against Flag-tag. Anti-vinculin antibody was used to ensure equal protein amount. From Kunz *et al.*[52].

6.2 Identification of SENP3-regulated SUMO2/3 targets

6.2.1 Validation of a U-2 OS SENP3 knockout cell line and experimental conditions for endogenous SUMO2/3 IP

After having defined a cellular subset of proteins being SUMO1-modified in response to hypoxia in a SENP1-controlled manner, we additionally set out to characterize endogenous SUMO2/3 targets under the control of SUMO-specific isopeptidases. Therefore, we applied the same methodical approach, consisting of affinity purification of endogenous SUMO2/3 targets and following LC-MS/MS analysis. For this study, we decided to investigate SUMO2/3 conjugation of proteins that are controlled by the SUMO isopeptidase SENP3. Given its preference in catalysing the deconjugation of SUMO2/3 from target proteins SENP3 seemed to be an ideal candidate for our approach. To this end, we generated a U2-OS SENP3 knockout cell line using a CRISPR-Cas9 (clustered regularly interspaced short palindromic repeats-Cas9) approach. In order to validate successful knockout of SENP3 and alteration of SUMO2/3 conjugation we performed immunoblotting on cell lysates (Figure 16 A). Therefore, U-2 OS WT and SENP3 KO cells were cultured under normal conditions or heat shocked for 30 min at 43 °C, to additionally monitor possible effects on global SUMOylation after heat stress. Cells were lysed in Laemmli buffer, separated by SDS-PAGE and stained against SENP3, SUMO2/3, PELP1 or β-tubulin as loading control. Proper knockout could be demonstrated since no residual protein migrating at 75 kDa was left in the KO samples (upper panel). Absence of SENP3 did not strongly affect the global SUMOylation under control conditions or heat stress indicating that SENP3 only targets a subset of SUMOylated proteins. To validate whether known SENP3 targets are affected in

their SUMOylation status, we tested the well-characterized target PELP1[30]. In the lower panel, samples were stained against PELP1 where the unmodified version of PELP1, migrating around 180 kDa is strongly expressed in all samples. Only in the SENP3 knockout cells, both under normal and heat shock conditions, a higher molecular weight band migrating around 200 kDa can be detected. As shown previously[30], this band corresponds to a PELP1-SUMO2 conjugate indicating that our experimental system is suitable to detect differentially regulated SUMO2/3 targets. We therefore set out to establish the protocol for the enrichment of endogenous SUMO2/3 targets according to Barysch *et al.*[53]. To control for sufficient enrichment of SUMOylated proteins after immunoprecipitation, we stained input and IP samples against SUMO2/3. Figure 16 B exemplifies the enrichment steps in one out of three replicates for each condition. A small volume of eluted proteins and TCA-precipitated samples was analysed by Western blot and showed sufficient enrichment of SUMOylated proteins after SUMO2/3 IP (upper panel). In contrast, no high-molecular weight bands of SUMO2/3 modified proteins could be enriched in samples eluted after IgG IP. With this experiment, we assured specific enrichment of SUMO2/3 targets after immunoprecipitation, functionality of IgG IP as negative control and suitability of this method for large-scale MS experiments.

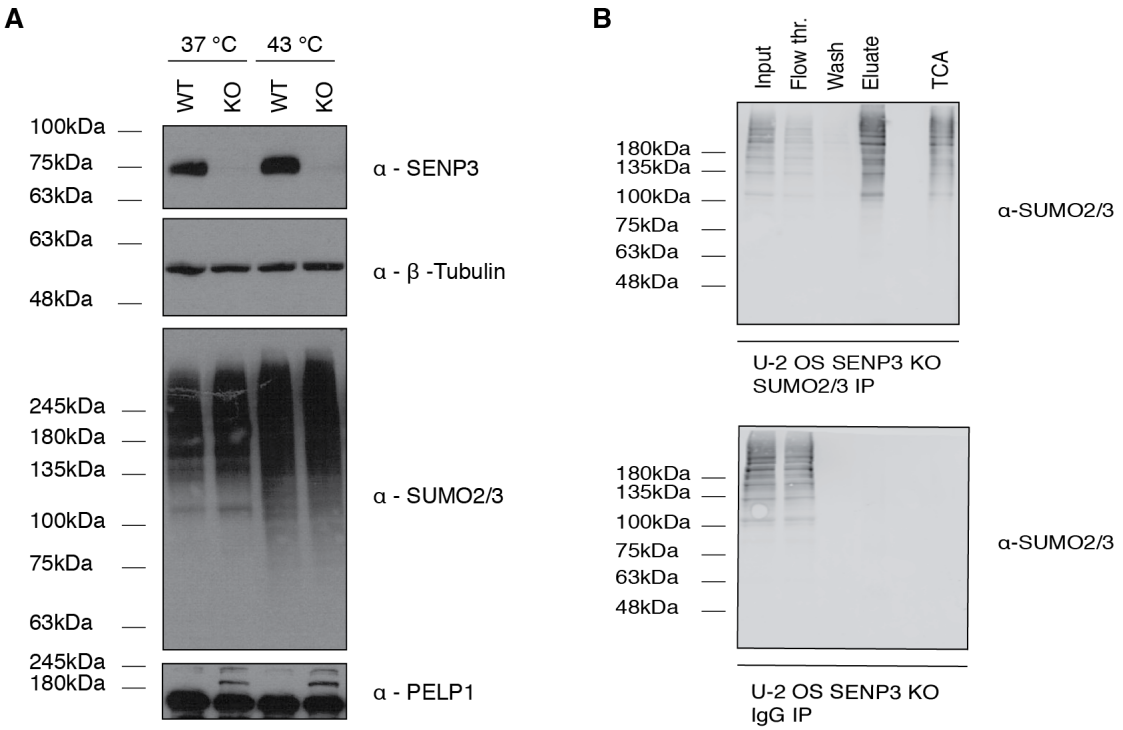

Figure 16: Validation of the U-2 OS SENP3 KO cell line and the enrichment of endogenous SUMO2/3 immunoprecipitates. (A) U-2 OS cells were depleted of SENP3 using the CRISPR-Cas9 technique and tested for SENP3-mediated effects on the SUMO2/3 pattern and target proteins under normal as well as heat stress conditions. To this end, U-2 OS WT and SENP3 KO cells were heat shocked for 30 min at 43 °C or cultured under normal conditions. Lysates were prepared in Laemmli buffer, separated by SDS-PAGE and stained for SENP3, SUMO2/3, PELP1 or β-tubulin as loading control. **(B)** Western Blot analysis of SUMO2/3 IP to test for successful enrichment of SUMO-conjugates. For MS-based targetome analysis, U-2 OS WT and SENP3 KO cells were subjected to denaturing lysis and endogenous SUMO2/3 targets were captured on SUMO2/3 beads like described in Barysch *et al.*[53]. IgG IPs were performed to exclude unspecific background binders. Experiments were performed in triplicates for each condition, exemplified here on SUMO2/3 Western blots for a SUMO2/3 IP and an IgG IP in SENP3 KO cells. Small aliquots of input material, flow through sample after overnight IP, a pre-elution wash step, the eluted material and the TCA-precipitated sample were run for SDS-PAGE and following immunostaining was done with an antibody against SUMO2/3.

6.2.2 LC-MS/MS analysis of endogenous SUMO2/3 targets in SENP3 KO and WT cells

For the large-scale experiment, U-2 OS WT and SENP3 KO cells were cultured under normal conditions and denaturing lysis was performed. A total protein amount of 8 mg was used per condition. The experiment was performed in triplicates including IgG controls to exclude unspecific binders from further analysis. Eluted and subsequently TCA-precipitated samples as well as input material for WT and KO cells (all performed in triplicates) were separated by SDS-PAGE, stained and prepared for mass spectrometry by tryptic in-gel

digestion. Raw data were processed using the MaxQuant software and label-free quantification by the MaxLFQ algorithm was applied. Filtering of data, quality control and statistical methods were done with the Perseus software. To control for the quality of the obtained data, triplicates were checked individually. For later calculations and statistics, triplicates were grouped together. Gaussian distribution of the LFQ values was verified by visual histogram analysis (Supplemental Figures 6 A and 8 C). Multiscatter plot analysis was applied and Pearson correlation coefficient was used to evaluate the reproducibility of the replicates. The IP samples showed a correlation coefficient > 0.93 among each other (Supplemental Figure 6 B, C) and also the proteomic replicates were highly similar to each other (> 0.97, Supplemental Figure 8 B). Volcano plots were used to depict significantly enriched targets (log2 ≥ 1 and -log10 p-value > 1.3) of SUMO2/3 IP over IgG IP in U-2 OS WT and SENP3 KO cells (Supplemental Figure 7 A, B). In total, we identified 78 and 97 candidate targets meeting these criteria in WT and KO cells, respectively. Among the 20 most highly enriched proteins in SUMO2/3 IP over IgG control we found the three SUMO paralogs (SUMO1/2/3), as well as known SUMO targets such as TRIM28, GTF2I, NOP58, RanGAP1 or FANCI. Additionally, 324 and 337 candidate SENP3-controlled SUMO2/3 targets were identified exclusively (at least twice) in SUMO2/3 IPs but not in IgG IPs in WT or KO samples, respectively.

To identify proteins differentially regulated in control cells versus SENP3 depleted cells we applied the following selection criteria. As *bona fide* SENP3 targets we considered proteins that exhibit an at least two-fold higher enrichment on anti-SUMO2/3 beads in SENP3 depleted cells versus control cells or those that were exclusively found in SENP3 depleted cells in at least two of the three anti-SUMO2/3 IP replicates, but not in anti-IgG IPs (Supplemental Table 1). In total 58 candidates fulfilled these criteria. Among these, 18 proteins were increased at least 2-fold in anti-SUMO2/3 IPs from SENP3 depleted cells compared to control cells and 20 proteins were found exclusively (2 out of three replicates) in anti-SUMO2/3 IPs from SENP3 KO cells, but not in control cells (Figure 17 A). The most highly SENP3-regulated

proteins are the known targets[30] Las1L (log2 ratio 4.56, -log10 p-value 5.16) and PELP1 (log2 ratio 7.32, -log10 p-value 3.89), again validating our experimental conditions. Also other proteins interacting with Las1L and PELP1 in a complex (NOL9, TEX10) were identified as stronger SUMOylated in SENP3 KO cells. For a better visualization of the results, we generated a STRING network with the 58 candidate SENP3 targets (Figure 17 B). The network reveals one central cluster, which can be subdivided into two smaller functional clusters. The largest cluster centres around the above-mentioned PELP1 complex comprising Las1L, Nol9 and TEX10. Additionally, several ribosomal proteins of the large subunit (RPL6, 26, 29, 31, 36AL) are connected to this cluster. We assigned this cluster as pre-60S cluster, given the involvement of the proteins in 28S rRNA maturation, processing and 60S biogenesis. This cluster is interconnected with another small cluster of three connected proteins (NOL10, BMS1, UTP3). This smaller cluster was defined as 90S cluster, since all three proteins included are components of the small subunit processome, fulfilling functions like rRNA maturation (NOL10) or serving as regulatory GTPase like BMS1. Besides this one big network, there are several pairs of interacting proteins from various pathways that will be discussed later.

Altogether, our data support the critical function of SENP3 in ribosome biogenesis.

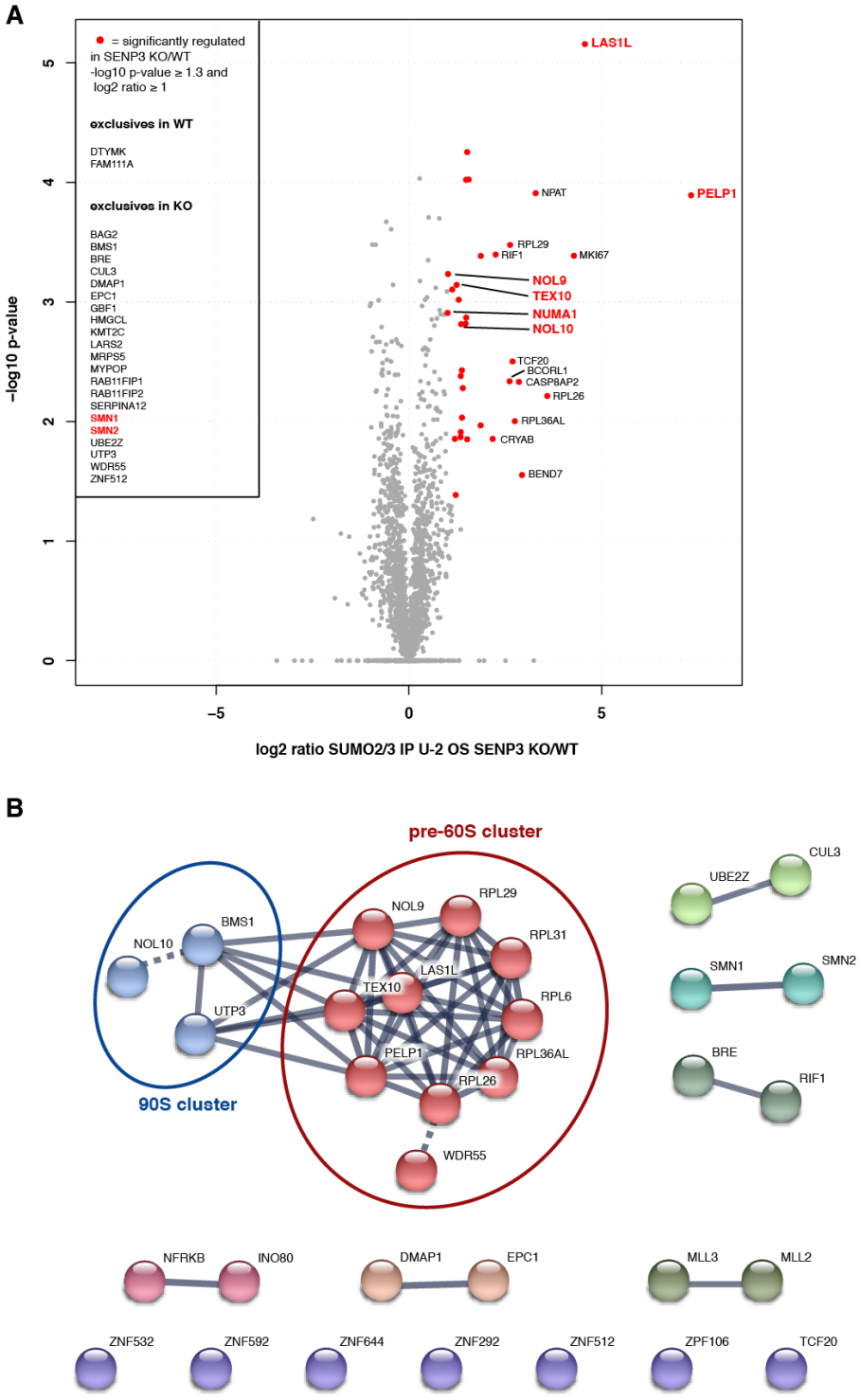

Figure 17: Identification of SENP3-dependent endogenous SUMO2/3 targets by IP-MS and the resulting STRING network analysis of high-confident target proteins. (A) Volcano plot summarizing the results of endogenous SUMO2/3 targetome analysis in U-2 OS SENP3 KO and WT cells. Only proteins that are enriched more than 2-fold in the SUMO2/3 IP from SENP3 KO cells compared to WT cells and display a p-value < 0.05 are considered as significantly regulated, high-confident targets and are depicted as red dots. Gene names marked in red are common hits in the SENP3 targetome and interactome analysis. **(B)** STRING network analysis of high-confident SENP3-regulated SUMO2/3 targets. Only hits significantly enriched in SENP3 KO versus WT cells (log2 ratio > 1 and -log10 p-value > 1.3) and proteins being identified exclusively at least twice in SUMO2/3 IPs from SENP3 KO cells were subjected to network analysis.

Next, we set out to validate MS-results also by Western blot. Therefore, we chose the two most enriched SUMO2/3 targets in the screen, PELP1 and Las1L. We took 50 μg of the corresponding input material for the MS-screen in triplicates, separated by SDS-PAGE and stained against SENP3, tubulin, Las1L and PELP1 (Figure 18). SENP3 knockout could be verified also via Western blot method by lack of the band at 75 kDa corresponding to SENP3 protein in KO (left panel) samples compared to WT samples (right panel). The use of input material instead of enriched IP samples was already sufficient to confirm elevated conjugation of SUMO2/3 to Las1L/PELP1. On the left-hand side in WT cells there is only the unmodified version of both proteins being detected. On contrary, in SENP3 KO lysates there is already a faint band visible, corresponding to the SUMO2/3-conjugated version of PELP1/Las1L, respectively (right panel).

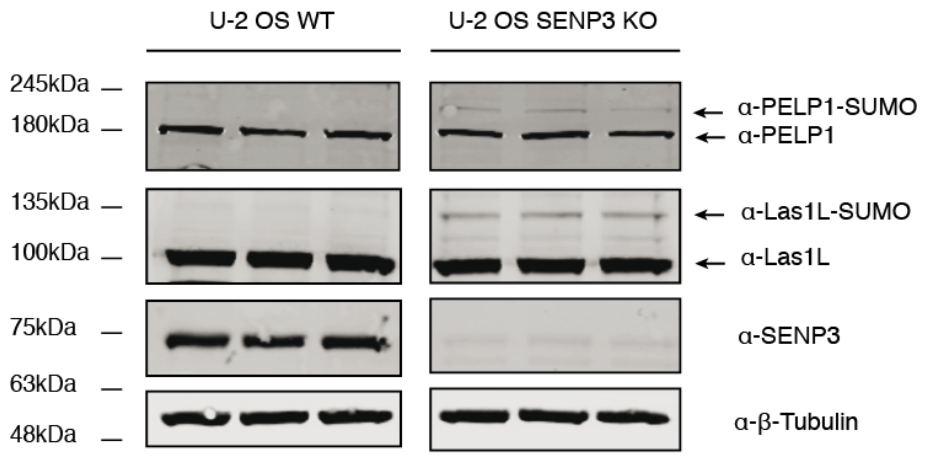

Figure 18: Validation of SENP3-mediated effects on known SENP3-regulated SUMO2/3 target proteins. Input material from U-2 OS WT and SENP3 KO cells (50 μg, in triplicates) was size-separated by SDS-PAGE and probed against PELP1, Las1L, SENP3 to confirm proper knockout and against β-tubulin to control for equal loading.

To explore whether the increase in SUMOylation of the identified SENP3-regulated target proteins results from elevated protein levels, we performed a total proteome analysis of input material from SENP3 KO and WT cells. As depicted in Supplemental Figure 8 A, there was only moderate change when comparing the proteome of WT and SENP3 KO cells. In total, we identified 7328 proteins, from which 12 were up regulated and 19 down regulated in KO

cells compared to WT cells. We defined the underlying criteria as absolute log2 ratio ≥ 1 and -log10 p-value > 1.3. None of these 31 proteins were up/down regulated more than 3.5-fold. Also no significant enriched hit included in the above-mentioned networks and volcano plots is significantly changed on proteome level. These results strengthen our observation that differentially enriched SUMO2/3 targets are indeed caused by lacking SENP3 and not by global protein level.

With this MS-based analysis of endogenous SUMO2/3 targets in SENP3 KO cells versus WT cells, we defined a subset of proteins being modified with SUMO2/3 under the control of SENP3. We termed these regulated proteins the "SENP3 targetome".

6.2.3 Comparison of SENP3 interactors and targets

The dataset of candidate SENP3-targets suggest that SENP3 controls the SUMOylation status of entire protein complexes. To see whether SENP3 is physically associated with these complexes, we integrated our dataset on SENP3 targets with an existing dataset on SENP3 associated proteins. This interactome study was performed by Tanja Piller in her master thesis, where Flag-tagged wild-type and catalytic dead versions of all SENPs were transiently expressed in HEK cells and enriched by Flag-IP. Interactors were analysed by mass spectrometric analysis. Here, we extracted the dataset of proteins associated with the catalytic dead Flag-SENP3 (C532S) for downstream analysis, which will be described in the following.

The most-enriched interactors of this study are depicted in the Volcano plot in Figure 19 A and colour-coded according their enrichment in $SENP3^{C532S}$/Mock (Supplemental Table 1). To further analyse possible connections between SENP3 interactors, we applied a STRING network analysis here, too. The results using the top hits of the MS study (> 2.5-fold enrichment over mock and p-value ≤ 0.05) are shown as network in Figure 19 B.

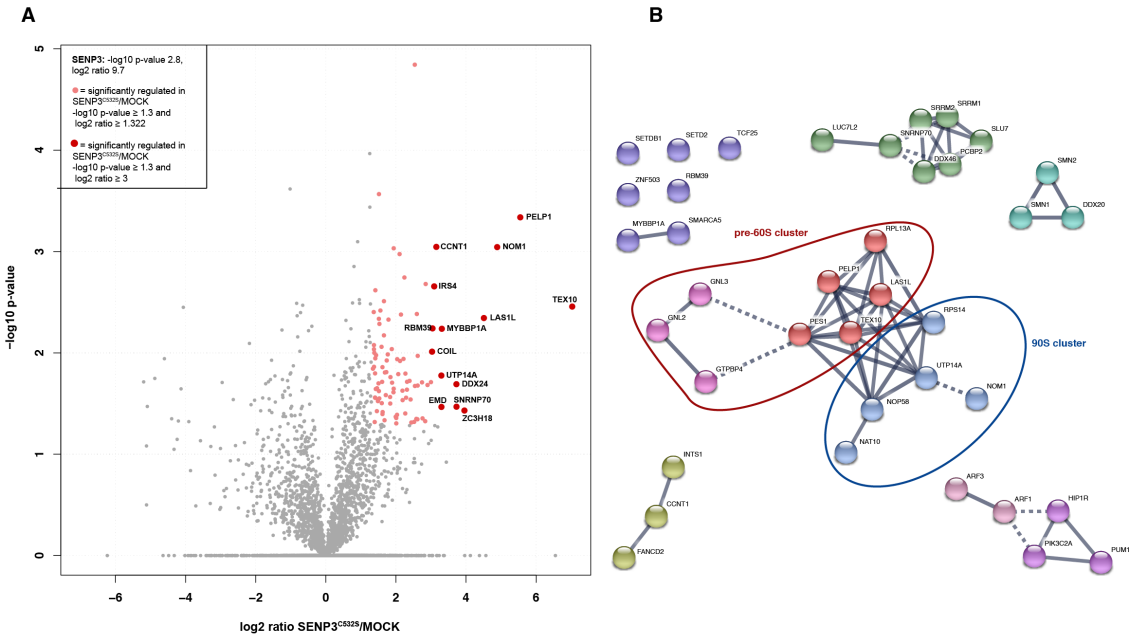

Figure 19: Interactome analysis of the catalytically inactive mutant of SENP3 and STRING network analysis of high-confident interactors. (A) HEK293T cells were transiently transfected with a Flag-tagged catalytically inactive SENP3 mutant (SENP3^{C532S}) or mock control. Interactors were enriched by Flag-IP and analysed by LC-MS/MS. The volcano plot depicts significantly enriched proteins over the mock control in colour-coded dots (at least 2.5-fold enriched and p-value < 0.05). **(B)** STRING network analysis of high-confident SENP3 interactors. Only hits matching the significance criteria defined in (A) were subjected to STRING analysis.

To investigate the overlap of SENP3-dependent SUMO2/3 targets and SENP3 interacting proteins, we compared the interactome analysis with the targetome study. Again, we only considered the best hits for further use with the above-mentioned criteria and subjected those candidates to STRING network analysis and generated a Venn diagram (Figure 20 A, B). As depicted in the Venn diagram, 93 and 52 proteins were identified as exclusive SENP3 interactors or SUMO2/3 targets, respectively. The overlap between both studies includes six proteins, being the Las1L-PELP1-TEX10 complex and SMN1, SMN2 and NUMA1. In the combined STRING network, these proteins are depicted with a red frame. A condensed network of the core clusters (90S and pre-60S) can be found in Supplemental Figure 9. In the integrated network, the biggest connected protein complex is composed of proteins involved in 60S ribosome biogenesis and 90S maturation. So we subdivided this complex into a 90S and a pre-60S cluster containing the PELP1-Las1L-TEX10 complex connected to PES1, a member of the PeBoW complex, both involved in rRNA maturation and

formation of 60S ribosomes. Additionally, these proteins show connections to three GTP-binding and Guanine-nucleotide binding proteins, functioning in the biogenesis, maturation and nuclear export of the 60S ribosomal subunit. The 90S cluster comprises for example NAT10, cleaving precursor rRNA or NOP58 which is required for 60S biogenesis. Besides this big central network, several small protein networks could be identified. One of them composed of SMN1, SMN2 and DDX20, being part of the spliceosome complex and thus involved in pre-mRNA splicing. Another network consisting of SRRM1/2, DDX46, SNRNP70, SLU7 and others, is acting in mRNA processing, pre-mRNA splicing and needed for the assembly of the spliceosome, too. Additionally, there are five proteins being interconnected, being GTP binders or vesicle components and thus all playing a role in intracellular trafficking (ARF1/3, HIP1R, PUM1, PIK3C2A).

Taken all together, we can confirm by both studies, independently from each other as well as in combination, that the major function of SENP3 interactors and targets is concentrated on the ribosome biogenesis pathway.

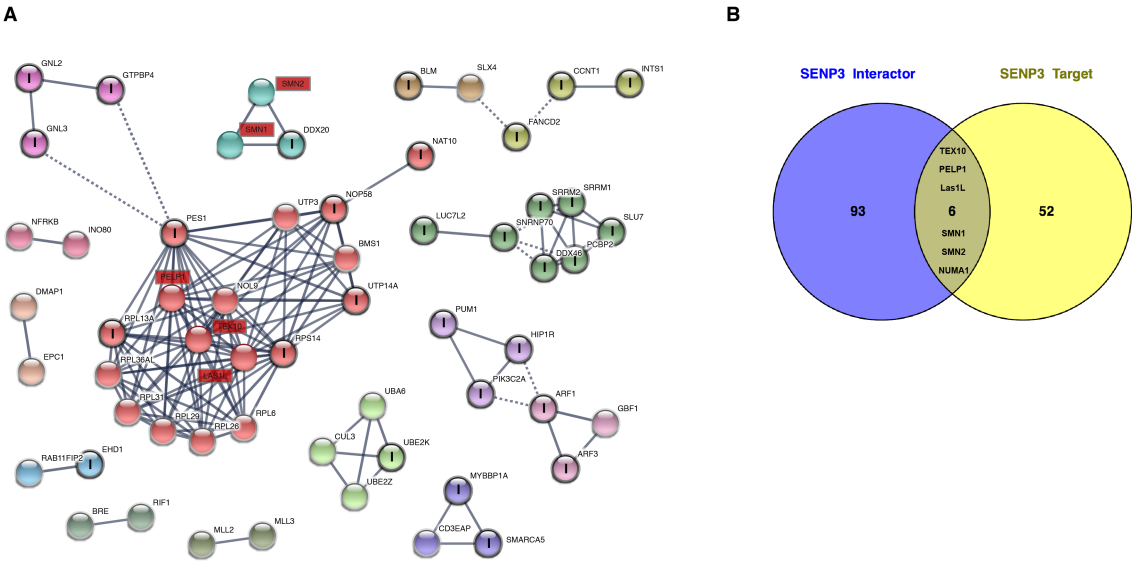

Figure 20: Comparison of SENP3 interactome and targetome analysis. (A) Integrative STRING network analysis of all identified high-confident targets and interactors of SENP3. SENP3 interactors are marked with an "I", common hits identified in both studies are depicted in red rectangles. **(B)** Venn diagram indicating the overlap (6 proteins) of SENP3 interactors and targets plus interactors (93) or targets (52) exclusively identified in the respective study. Only significantly regulated proteins matching the definition like described in Figure 17 (A) and 19 (A) are taken into consideration.

6.2.4 Investigating the role of SENP5 under loss of SENP3

The closest cellular homolog of SENP3 is SENP5. In HeLa cells, SENP5 is expressed at low levels, typically precluding its detection by MS in whole cell lysates. Interestingly however, we could detect SENP5 in the whole cell proteome analysis from SENP3 KO. We therefore asked, whether elevated SENP5 levels might partially compensate for the loss of SENP3. Consequently, we performed siRNA-mediated knockdown of SENP5 or SENP3 in U-2 OS WT cells or additionally depleted U-2 OS SENP3 KO cells from SENP5. After 48 h, samples were lysed in Laemmli buffer and separated by SDS-PAGE. Knockdown efficiency was assessed by immunostaining against SENP3, SENP5 or tubulin. Figure 21 A shows SENP3 levels in WT and KO cells. Validation of SENP5 knockdown was difficult since the endogenous SENP5 levels are relatively low (Figure 21 B). However, we confirmed the ability of the chosen SENP5 siRNA to deplete transiently overexpressed SENP5 (data not shown). Staining against PELP1 (Figure 21 C) and Las1L (Figure 21 D) revealed SUMO-modified versions of those proteins visible only under SENP3 depletion by either siRNA or by CRISPR-mediated knockout. SENP5 depletion alone did not result in enhanced SUMOylation of PELP1 or Las1. Only in combination with SENP3 knockout, SENP5 knockdown slightly enhanced SUMOylation of PELP1 or Las1L. Altogether, this demonstrates that SENP3 is the major regulator of Las1L- and PELP1-SUMOylation, but in the absence of SENP3, SENP5 may contribute to deSUMOylation.

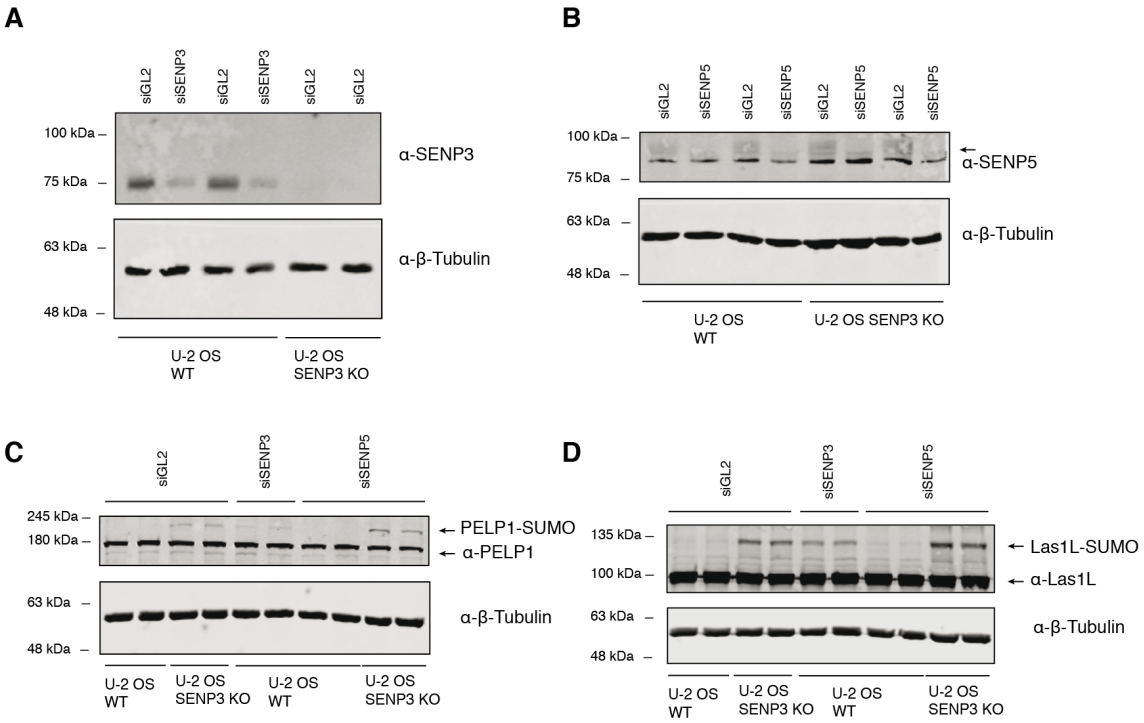

Figure 21: Effects of SENP5 depletion on SENP3-regulated SUMO2/3 target proteins. (A, B) U-2 OS WT and SENP3 KO cells were depleted from either SENP3, SENP5 or non-targeting control by siRNA (performed in duplicates). After 48 h, cells were lysed in Laemmli buffer and separated by SDS-PAGE. Efficient knockdown was confirmed by staining against SENP3 (A) and SENP5 (B). Equal loading was ensured by probing for β-tubulin. Arrow in (B) indicates faint band specific for SENP5. Lower consistently present band is unspecific. **(C, D)** The same cell extracts like in (A) and (B) were stained against PELP1 (C) and Las1L (D), β-tubulin served as loading control. In both blots, the lower arrow marks the unmodified version of the protein and the upper arrow indicates the SUMOylated form.

6.3 Identification of SENP6-regulated SUMO2/3 targets

6.3.1 Comparative analysis of SUMO2/3 targets in control HeLa cells and cells upon SENP6 knockdown

To further expand the knowledge on specific SUMO targets regulated by individual SENPs, we applied our approach of endogenous SUMO2/3 IP-MS analysis to cells following siRNA-mediated SENP6 knockdown. Our goal was to identify SENP6-controlled SUMO2/3 targets to further elucidate pathways that rely on SENP6 regulation.

Therefore, HeLa cells were transfected with siRNA against SENP6 or a non-targeting control siRNA. All experiments were performed in triplicate. 72 hours after knockdown, cells were lysed and SUMO2/3 targets were enriched as

described above. Input material and enriched samples for each replicate were tested for successful siRNA knockdown and enrichment of SUMO2/3 targets (Supplemental Figure 10, upper panel). Enrichment of SUMO2/3-modified proteins in respective replicates is visualized in anti-SUMO2/3 immunoblots by a high molecular weight smear in eluates and TCA-precipitated samples from SUMO2/3 IPs but not control IPs. SENP6 depletion upon siRNA-mediated knockdown in comparison to control cells was confirmed by immunoblotting against SENP6 (Supplemental Figure 10, lower panel). TCA-precipitated samples as well as input material for whole cell proteome were prepared for MS analysis like described for the SENP3 targetome analysis. Quality of the analysed IP and proteome data was assessed by histogram analysis to ensure normal distribution of the measured LFQ values and by Pearson correlation coefficient to evaluate the similarity of the replicates (data not shown). For whole cellular proteomes, a Pearson coefficient of > 0.96 could be reached for all replicates. Analysing all replicates of IgG and SUMO2/3 IPs from knockdown and control conditions together, we ended up with a Pearson correlation of > 0.82. Further, we filtered all identified proteins in immunopurified material for sufficient enrichment over IgG control. Only hits with a p-value < 0.05 and a log2 ratio of SUMO2/3 IP/IgG IP ≥ 1 were considered as significant candidates and included in further analysis. With these criteria, we ended up with 133 and 107 proteins significantly enriched over IgG IP for SENP6 knockdown or control conditions, respectively. Additionally, we identified 116 and 164 proteins, at least in two out of three replicates in SUMO2/3 IP and not at all found in IgG IP from cells under control conditions or SENP6 knockdown. Significantly enriched proteins in each condition are depicted as red dots in corresponding Volcano plots (Supplemental Figure 11 A, B). Known SUMO targets as well as SUMO paralogs were among the most highly enriched proteins.

Most interestingly, we revealed 78 candidate SENP6 targets (Supplemental Table 1). Among these, 40 proteins were significantly enriched in SUMO2/3 IPs from SENP6 depleted cells compared to control cell, depicted as red dots in the Volcano plot in Figure 22 A. Additionally, 38 proteins were exclusively identified in at least two out of three SUMO2/3 IPs from SENP6 depleted cells and not in

control cells. To further identify connections and pathways involving high confident targets, we subjected these proteins to STRING network analysis (Figure 22 B). Among the top hits of these candidates, we identified a central cluster of centromere proteins (CENPB, CENPC), involved in assembly of the kinetochore and needed for proper mitotic progression and chromosome segregation. Also the endonuclease SLX4, required for genome integrity, and several components of the mammalian cohesin complex (PDS5A, SMC1, SMC3, STAG1, STAG2, RAD21) were identified. Through the SUMO E3 ligase RanBP2, also known as Nup358, and through Nup133, this core cluster is interconnected with several other nuclear pore complex proteins and PML as prototypical SUMO2/3-modified protein under the control of SENP6.

To exclude that the increase in SUMOylation is not simply caused by changes in protein abundance upon SENP6 depletion, we performed whole cell proteome analysis of control cells or cells under SENP6 knockdown. In summary, we revealed 120 proteins up-regulated and 199 proteins down-regulated under SENP6 knockdown (absolute log2 ratio ≥1 and p-value < 0.05) within a total of 6771 proteins identified in both conditions (Supplemental Figure 12 A). Among the down-regulated hits under SENP6 depletion, we found FANCD2, a member of the Fanconi anemia complex, which is crucial for DNA damage repair. This loss of FANCD2 could also be confirmed by Western blotting cell lysates of control cells or cells under depletion of SENP6 (Supplemental Figure 12 B).

We also tested the input material for the IPs for RNF4 protein levels (Supplemental Figure 12 C) to investigate a previously described negative effect of SENP6 depletion on RNF4 stability[57]. Indeed, we could observe a significant decrease in RNF4 levels under simultaneous SENP6 knockdown.

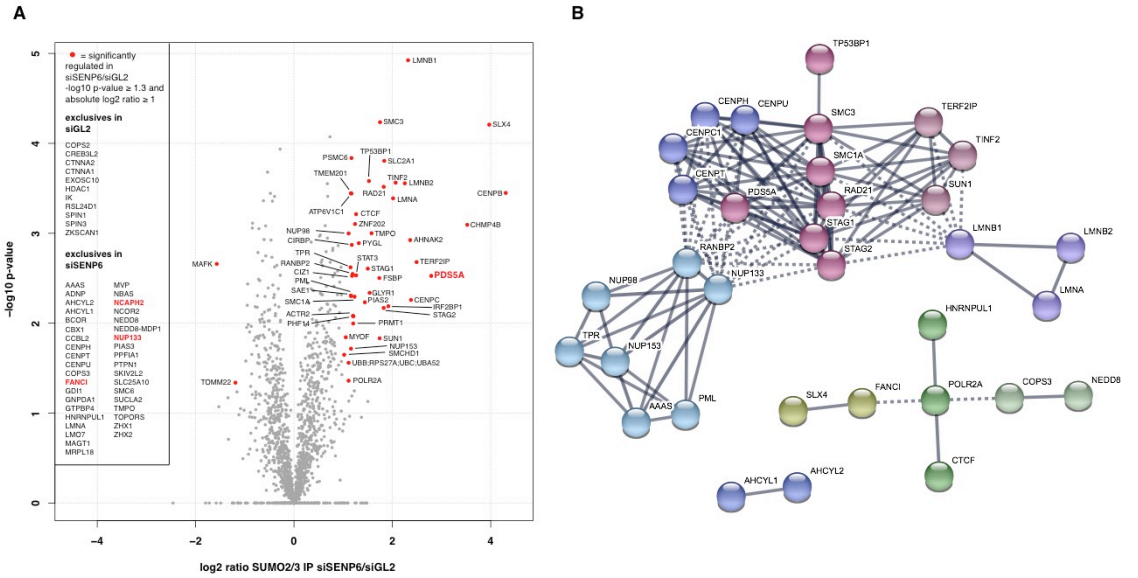

Figure 22: LC-MS/MS-based analysis of SENP6 target proteins. (A) HeLa cells were depleted from SENP6 or non-targeting control using siRNA, following denaturing SUMO2/3 IP. IgG IP was performed as negative control. Volcano plot depicts SUMO2/3-modified proteins significantly enriched in siSENP6 treated cells versus control cells as red dots (absolute log2 ratio ≥ 1 and –log10 p-value > 1.3). Gene names in red are common hits found as SENP6 targets and interactors. Experiments were made in triplicates for each condition. **(B)** High-confident SENP6-regulated SUMO2/3 targets were subjected to STRING network analysis. Only proteins significantly regulated in cells lacking SENP6 compared to control cells and targets at least found twice exclusively under siSENP6 were taken into consideration.

To categorize the SENP6-regulated SUMO targets according to their cellular function, we performed GO BP (gene ontology biological process) enrichment analysis. Processes depicted in Figure 23 represent a selection of the 20 most-enriched GO BP terms of the complete analysis. As shown, SENP6-regulated SUMO targets are involved in negative regulation of DNA endoreduplication. This includes per definition any process that stops, prevents or reduces the frequency, rate or extent of DNA endoreduplication.

Taken all together, network and GO term enrichment analysis indicate that SENP6-regulated targets are preferentially involved the regulation of mitotic spindle assembly, sister chromatid cohesion, nuclear pore organization and the SUMO machinery itself.

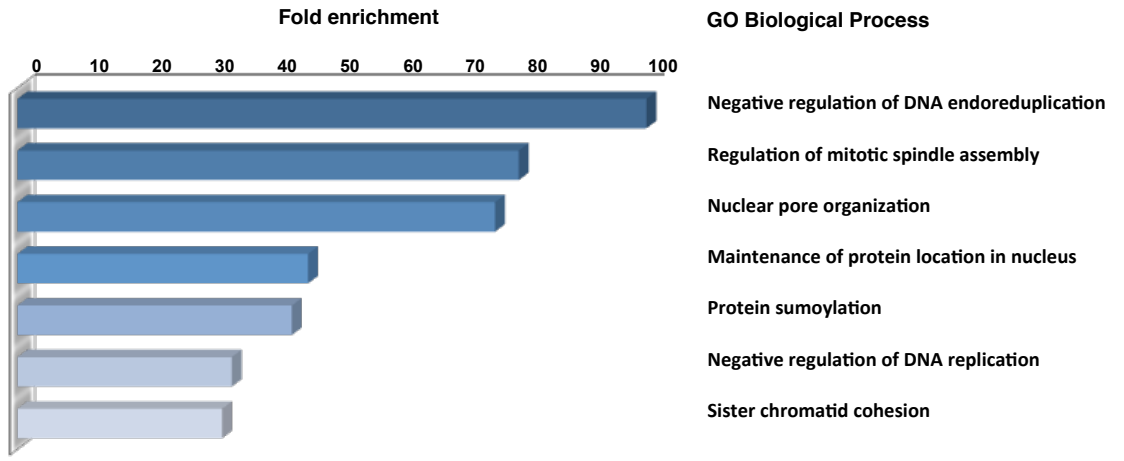

Figure 23: GO BP enrichment analysis of SENP6 target proteins. SENP6-regulated SUMO2/3 targets matching the criteria defined for STRING network analysis were considered for GO term analysis. Annotation was performed using complete GO biological process and a binominal test type including the Bonferroni correction for multiple testing. Depicted is a selection of the 20 most enriched GO BP terms.

6.3.2 Comparison of SENP6-regulated SUMO2/3 targets and SENP6 interactome analysis

To get a deeper understanding whether SENP6 is also physically associated with the candidate SENP6-regulated SUMO2/3 targets, we once again made use of the SENP interactome analysis previously conducted by Tanja Piller in our lab. We therefore extracted the dataset for the catalytically inactive mutant of SENP6 (SENP6^{C1030A}). This mutant was used to trap SENP6-bound interactors like shown in Hattersley *et al.*[27]. Proper expression and localization of the catalytic inactive SENP6 mutant was monitored by Western blot analysis and immune fluorescence microscopy (Figure 24 A, B). Expression levels of SENP6 WT and SENP6^{C1030A} construct are comparable and the mutant SENP6 is localizing to the nucleoplasm like already described by Mukhopadhyay *et al.*[58]. Significantly enriched (log2 ratio ≥ 1.322 and -log10 p-value ≥ 1.3) interactors of SENP6^{C1030A} in respect to mock control are depicted as colour-coded dots in Volcano plot (Figure 24 C, Supplemental Table 1). In total, we enriched 94 interactors, among those also FANCI and FANCD2 as FA core complex components and well-established SENP6 targets have been identified[34]. STRING network analysis was performed with those high-confident interactors, depicted in Figure 24 D.

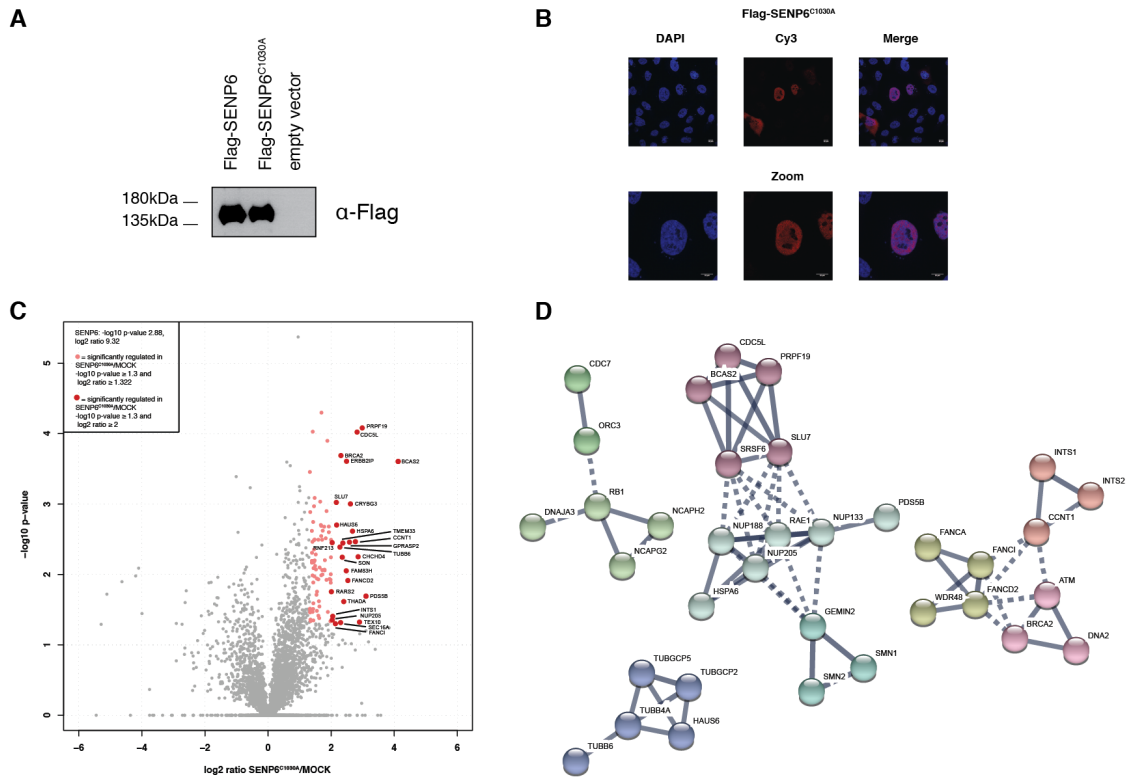

Figure 24: Identification of SENP6 interactors. (A) HEK293T cells were transiently transfected with Flag-SENP6 or Flag-SENP6^{C1030A} or empty vector. After lysis, proteins were separated by SDS-PAGE and stained against Flag-tag to control for proper expression of the constructs. **(B)** Immunofluorescence of HeLa cells expressing Flag-SENP6^{C1030A} to ensure correct localization. Cells were stained with primary antibody against Flag-tag, Cy3 was used as secondary antibody. Nuclei were stained with DAPI (4',6-diamidino-2-phenylindole). Fluorescence microscopy was carried out on a Leica SP8 confocal microscope and images were visualized with ImageJ. Scale bar = 10 μm. **(C)** Flag-SENP6^{C1030A} or a mock control was expressed in HEK293T cells and SENP6 interactors were enriched by Flag-IP. Significant results of the subsequent analysis by LC-MS/MS are depicted as red dots in the volcano plot. Proteins enriched more than 2.5-fold over the mock control and with a p-value < 0.05 were considered as high-confident targets. **(D)** STRING network analysis depicting only high-confident SENP6 interactors. A confidence-based analysis was performed by application of the highest confidence filter (0.9) and only connected proteins are visualized.

To compare SENP6-regulated SUMO2/3 target proteins and SENP6 interactors, we generated a combined STRING network of all high-confident SENP6 targets and interacting proteins (Figure 25 A). Shared proteins enriched in both studies are marked in red. We categorized proteins in different clusters according to their cellular functions. One cluster is associated with DNA repair processes, comprised of the human PSO4 complex (PRP19, CDC5L, BCAS2) and members of the FA repair pathway (FANCI, FANCA, FANCD2, WDR48, SLX4). The PSO4-associated cluster is connected with several proteins of the nuclear pore complex (Nup133, Nup188, Nup205, RanBP2). Furthermore, these nuclear

pore proteins are connected to the cohesin complex members and centromere proteins identified as SENP6-dependent SUMO2/3 targets. Comparing both MS-based studies, we identified in total 80 significantly regulated SUMO2/3 targets and 94 interactors, with four proteins significantly enriched in both studies, as depicted in the Venn diagram in Figure 25 B. These shared proteins are PDS5A/B belonging to the mammalian cohesin complex, NCAPH2 as condensin-2 complex subunit, FANCI involved in the FA repair pathway and Nup133, a nuclear pore protein, localizing to the kinetochores during mitosis[59].

Applying this visual combination of both MS studies by STRING network analysis, we found that SENP6-regulated targets and direct SENP6 interactors mostly act in the cell nucleus. We identified proteins of the cohesin and condensin complex, needed for proper chromosome assembly and segregation during mitosis. Obviously, SENP6 is additionally acting on several nuclear pore complex proteins. And finally we could also reproduce the already well-established functions of SENP6 in the FA/DDR (DNA damage response) pathway.

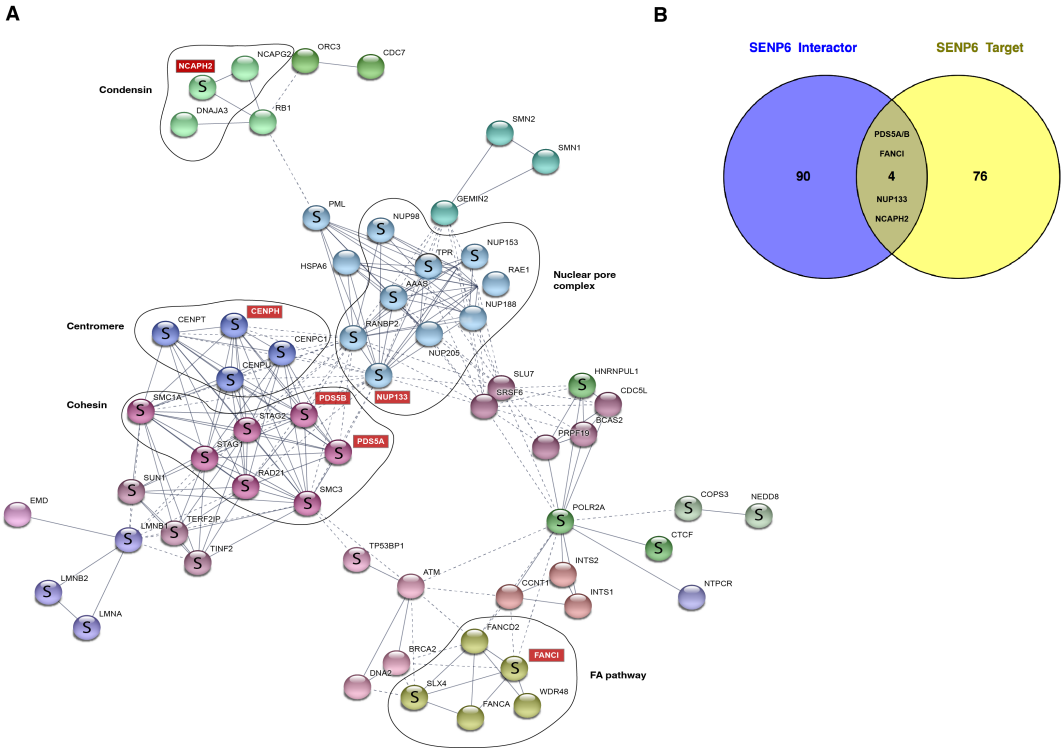

Figure 25: Comparison of significantly regulated SENP6 targets and interactors identified by LC-MS/MS analysis. (A) Integrated network analysis of high-confident SUMO2/3 targets under the control of

SENP6 and SENP6 interactors. Significantly regulated proteins identified in both studies are marked with a red rectangle. SENP6-dependent SUMO targets are labelled with an "S". **(B)** Venn diagram depicting the overlapping four proteins found in the targetome as well as the interactome analysis. Additionally, the exclusive hits found in every dataset are shown.

6.3.3 SENP6 regulates functions in mammalian cohesin complex and DNA damage repair

We next aimed to validate the proteomic data and dissect the physiological relevance of our findings. To this end, we concentrated on components of the cohesin and hPSO4/PRP19 complex, which were the most strongly enriched proteins in the SENP6 targets and interactome screens.

To confirm the interaction of SENP6 with the cohesin subunit PDS5B, HEK293T cells were transfected with Flag-SENP6 or Flag-SENP6^{C1030} and cellular fractionation of cells was performed to obtain a soluble and a chromatin-bound fraction. After the separation, an anti-Flag-IP was conducted for both fractions separately. Eluted material was probed against Flag-tag to detect SENP6 or against endogenous PDS5B (Figure 26 A). Proper separation of both fractions was monitored by immunostaining against histone H3 for the chromatin-bound fraction and β-tubulin for the soluble fraction (Supplemental Figure 14). Histone H3 was only detected in the chromatin fraction, while tubulin was only present in the soluble fraction. In the input material, SENP6 is found in both, the soluble and chromatin fraction, whereas PDS5B is mostly enriched in the chromatin-bound fraction. In the IP samples, however, interaction of endogenous PDS5B with SENP6 WT as well as the catalytic inactive version can be recognized in both fractions to a similar extent visualized by a band between 160 and 180 kDa.

We additionally wanted to demonstrate not only interaction of cohesin components with SENP6 but also check for SENP6-dependent SUMOylation of the targets. We therefore depleted HeLa cells from SENP6 using siRNA and transiently transfected cells with a plasmid containing His-SUMO2. After 48 hours of transfection, we performed enrichment of SUMOylated proteins by

denaturing Ni-NTA-pulldown. Bead-bound samples were recovered in Laemmli buffer, separated by SDS-PAGE and stained against the cohesin component Stag2 (Figure 26 B). A strong increase of SUMOylated Stag2 is apparent in the pulldown sample under SENP6 depletion in comparison to cells treated with control siRNA. The same experimental design was applied to demonstrate SENP6-dependent SUMOylation of Lamin B1, another candidate SENP6 target identified in our screen (Supplemental Figure 13).

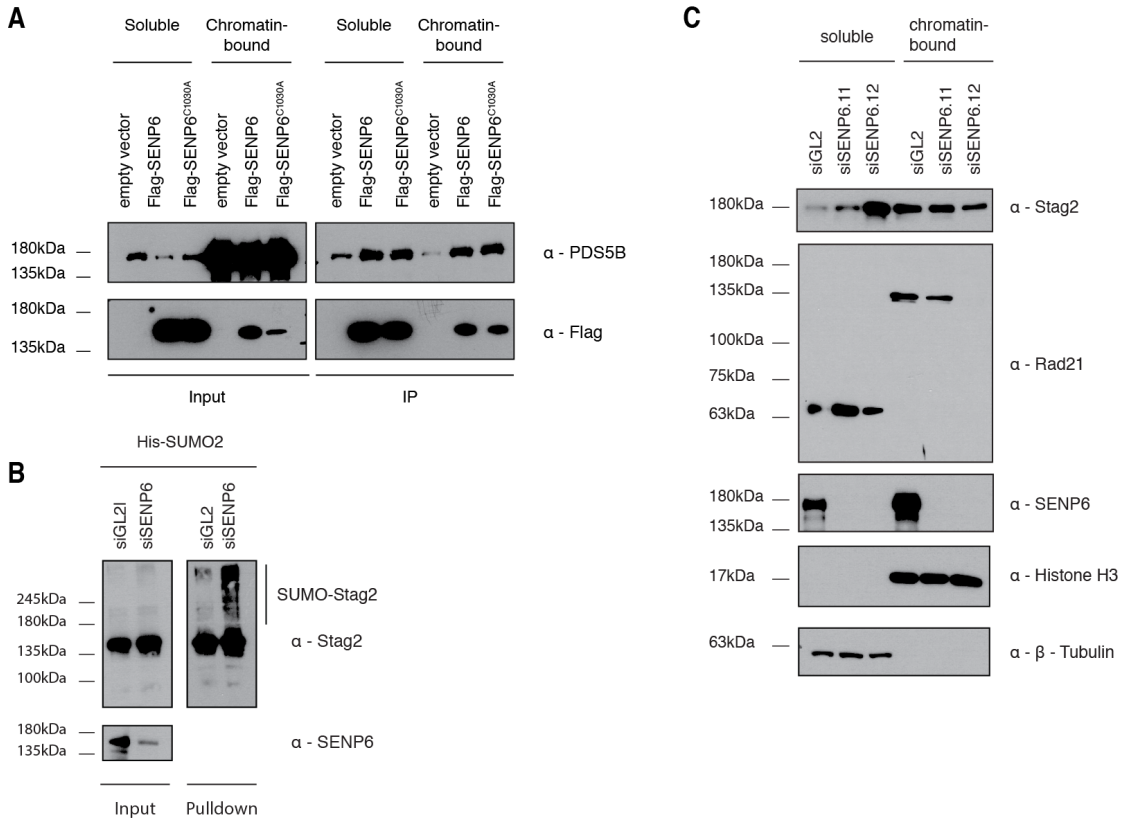

Figure 26: SENP6-dependent functions on cohesin complex components. (A) Interaction of PDS5B with SENP6 was shown in HEK293T cells expressing Flag-SENP6 or Flag-SENP6^{C1030A}. Cells were lysed and separated in a soluble and a chromatin-bound fraction. Following Flag-IP was performed and bead-bound material was released in Laemmli buffer. Protein separation was achieved by SDS-PAGE and staining of input and IP samples was performed with antibodies directed against PDS5B and the Flag-tag of SENP6 constructs. **(B)** HeLa cells were depleted of SENP6 or control by siRNA-mediated knockdown. On the next day, His-SUMO2 was introduced. Denaturing lysis and following Ni-NTA pulldown were performed and bead-bound material was released in Laemmli buffer. SDS-PAGE and transfer onto membranes was performed. Staining against SENP6 was used to confirm valid knockdown. Input and pulldown samples were additionally probed against Stag2. **(C)** HeLa cells were depleted of SENP6 using two different siRNAs. Cells were lysed and fractionated in soluble and chromatin-bound material. Subsequent SDS-PAGE and immunoblot analysis was performed with antibodies against Stag2 and Rad21. Staining against SENP6 was used to validate knockdown efficiency and histone H3 and tubulin served as controls for proper fractionation.

To further elucidate SENP6-dependent functions on the cohesin complex, we investigated the chromatin-association of cohesin core subunits in cells depleted of SENP6. For this purpose, HeLa cells were depleted of SENP6 using two different siRNAs or a non-targeting control siRNA. After cell lysis, the recovered material was separated into soluble and chromatin-bound fractions. Staining against Stag2 and Rad21 revealed a complete loss or a strong decrease of those proteins in chromatin-bound material from cells lacking SENP6 (Figure 26 C).
Taken together, we confirmed the interaction of SENP6 with PDS5B and provide evidence, that SENP6 regulates the SUMOylation status and chromatin-residency of cohesin complex subunits.

Next, we concentrated on the validation of the interaction between SENP6 and the hPSO4/PRP19 complex, comprised of PRP19, CDC5L, BCAS2 and PLRG1. To prove the association of hPSO4/PRP19 subunits with SENP6, we transfected HEK293T cells with Flag-SENP6 or Flag-SENP6^{C1030A} and performed a Flag-IP with following elution in Laemmli buffer. Eluted proteins were immunoblotted against BCAS2, CDC5L and PRP19 (Figure 27 A). Consistent with the MS data, we could confirm interaction of all three tested proteins with SENP6. In the immunoprecipitated samples of SENP6 WT and the catalytically inactive version, bands migrating around 30 kDa, 63 kDa and 100 kDa can be seen, corresponding to BCAS2, PRP19 and CDC5L, respectively.
Additionally, we performed a reverse experiment to test for interaction of PRP19 with endogenous SENP6. To this end, we immunoprecipitated endogenous PRP19 from HEK cell lysate, eluted bead-bound proteins and subjected them to Western blot analysis (Figure 27 B). Successful enrichment of PRP19 in anti-PRP19 immunoprecipitates can be recognized by a prominent band around 63 kDa corresponding to PRP19 (lower panel). Staining for SENP6 and CDC5L showed interaction of both proteins with endogenous PRP19 as indicated by bands in the PRP19 IP sample migrating around 140 kDa for SENP6 and 100 kDa for CDC5L.

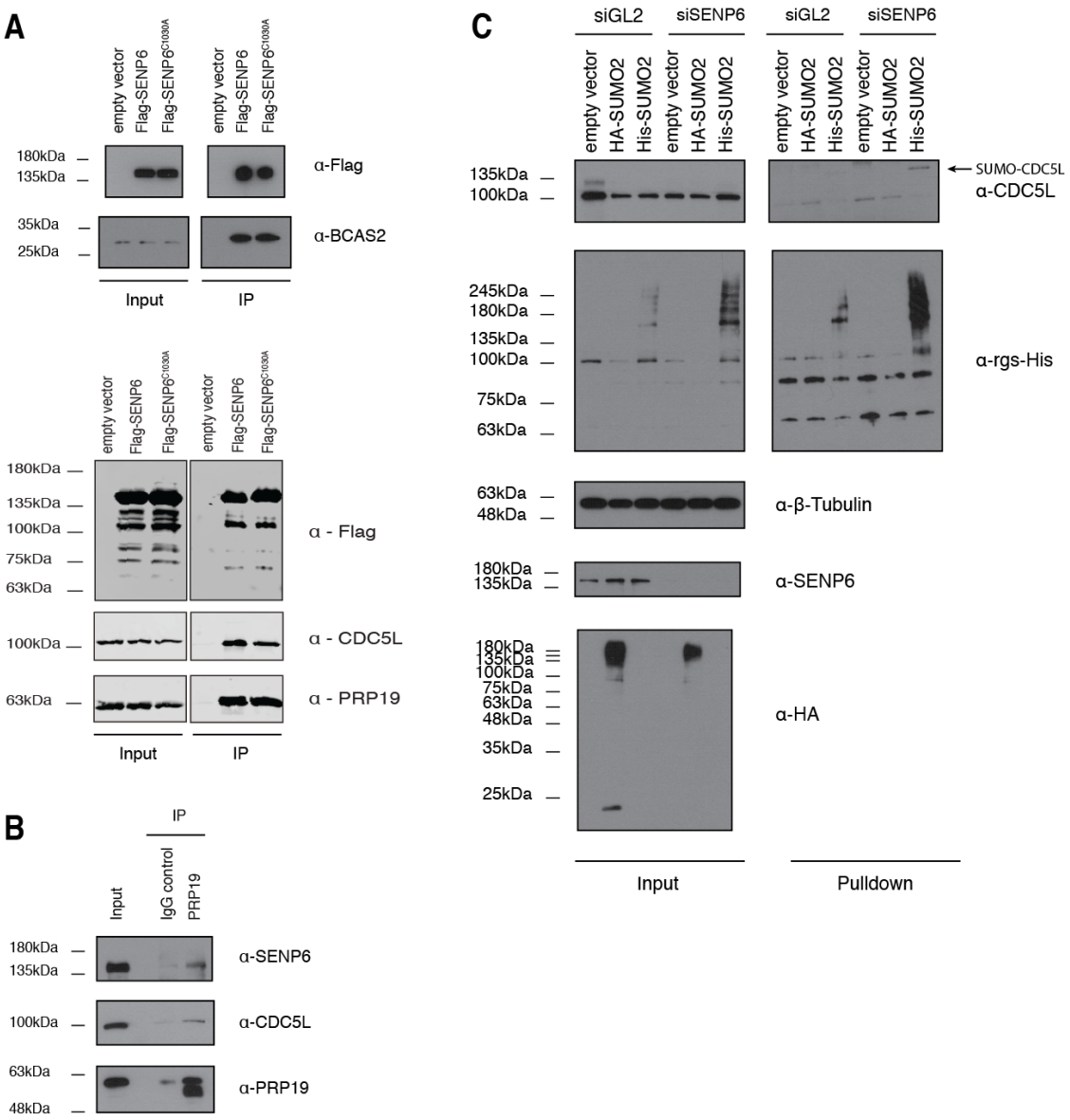

Figure 27: SENP6 interacts with the PRP19 complex. (A) Flag-SENP6 or Flag-SENP6^{C1030A} were expressed in HEK293T cells. After lysis, Flag-IP was performed and retained material was dissolved in Laemmli buffer. After separation by SDS-PAGE, input and IP samples were stained against Flag-tag, BCAS2 (upper panel) or CDC5L and PRP19 (lower panel). **(B)** Endogenous PRP19 IP was performed in HEK293T cells including IgG IP as negative control. Immunoprecipitates were dissolved in Laemmli buffer, separated and transferred onto membranes. Staining was performed with antibodies against SENP6, CDC5L and PRP19. **(C)** HeLa cells were depleted from SENP6 or non-targeting control by siRNA. 24 h later, His-SUMO2 or HA-SUMO and an empty vector, both serving as negative control, were expressed. Denaturing lysis was performed and His-SUMO2 conjugates were enriched by Ni-NTA pulldown. Input and pulldown samples were separated and stained against CDC5L and His-tag of SUMO2 to control for effective pulldown. Additionally, the input samples were probed for SENP6 to ensure efficient knockdown and for β-tubulin as loading control. Blotting against HA-tag controls expression of the HA-SUMO2 construct. Arrow indicates CDC5L-SUMO conjugate.

To test for SENP6-dependent SUMOylation of PRP19 complex members, we performed denaturing Ni-NTA pulldown of His-SUMO2 modified proteins in cells

depleted of SENP6 like described before. HA-SUMO2 was included as negative control. Recovered material was separated by SDS-PAGE and stained against CDC5L (Figure 27 C). We additionally probed the input material against β-tubulin as loading control, against SENP6 to control for sufficient knockdown and against HA-tag to ensure proper expression of the HA-SUMO2 construct. Successful expression and enrichment of the His-SUMO2 plasmid was verified by staining against the His-tag in input and IP samples. Importantly, we were able to detect the SENP6-dependent SUMOylation of CDC5L as indicated by a faint band around 135 kDa in the His-SUMO2 sample after pulldown (last lane). This band is exclusive for the His-SUMO2 samples and not present in the HA-SUMO2 transfected sample, showing the specific modification of CDC5L by His-SUMO2.

Given the involvement of the hPSO4/PRP19 complex in the DDR pathway, we followed the idea that SENP6 is part of the DDR network. The hPSO4/PRP19 complex is particularly critical for the cellular response to replication stress and the activation of the ATR-CHK1 pathway. We therefore introduced replication stress by treating cells with aphidicolin, which specifically inhibits eukaryotic DNA polymerases. Cells depleted from SENP6 or control siRNA were treated for 2 or 4 hours with aphidicolin at different concentrations. Afterwards they were lysed and proteins were separated by SDS-PAGE (Figure 28 A, B). Successful knockdown was verified by staining against SENP6, vinculin or tubulin served as loading control. Probing for the DNA damage marker γH2AX showed in both experiments already increased levels of γH2AX in untreated samples in absence of SENP6. When the cells were additionally treated with aphidicolin, this effect was even stronger. Blotting against the phosphorylated version of threonine 68 in CHK2 revealed that the lack of SENP6 activates CHK2. Importantly, in contrast to CHK2, CHK1 activation is impaired under SENP6 depletion. The activation of CHK1 was followed by checking phospho-CHK1 (Ser296) levels. While no activation was detectable in DMSO (dimethyl sulfoxide) treated cells, aphidicolin strongly enhances phospho-CHK1 (Ser296) levels. Under low doses of aphidicolin (0.5 μg/ml) for 2 or 4 hours, we observed

a consistent impairment of CHK1 activation in cells lacking SENP6. This effect is strongest for mild replicative stress. To exclude that these results are based on off-target effects of a single SENP6 siRNA, we performed the analogous experiment (0 - 4 μg/ml aphidicolin for 4 h) using two different siRNAs (Supplemental Figure 15). Importantly, also this experiment confirmed the reduced CHK1 activation under loss of SENP6.

To reveal the potential molecular mechanism of the impaired CHK1 activation in SENP6-depleted cells, we monitored the SENP6-dependent chromatin-association of the ATR cofactor ATRIP, since ATRIP recruitment depends on the hPSO4/PRP19 complex. Therefore, HeLa cells were transfected with control siRNA or siRNA against SENP6 and 72 hours later, cells were treated with DMSO or 0.5 μg/ml aphidicolin for 1 h, then fractionated in soluble and chromatin-bound material and separated by SDS-PAGE. Staining against histone H3 or tubulin ensured proper separation of the fractions (Figure 28 C). Effective depletion of SENP6 was checked by immunostaining. Blotting against PRP19 and CDC5L revealed no significant changes in the distribution between soluble or chromatin-bound fraction upon treatment with aphidicolin. In contrast, the ATR cofactor ATRIP showed increased protein levels in the soluble fraction upon lack of SENP6.

The results obtained from these additional experiments further support our findings revealed by both MS-screens and prove functions of SENP6 in controlling SUMOylation events involved in sister chromatid rearrangements and the DNA damage response.

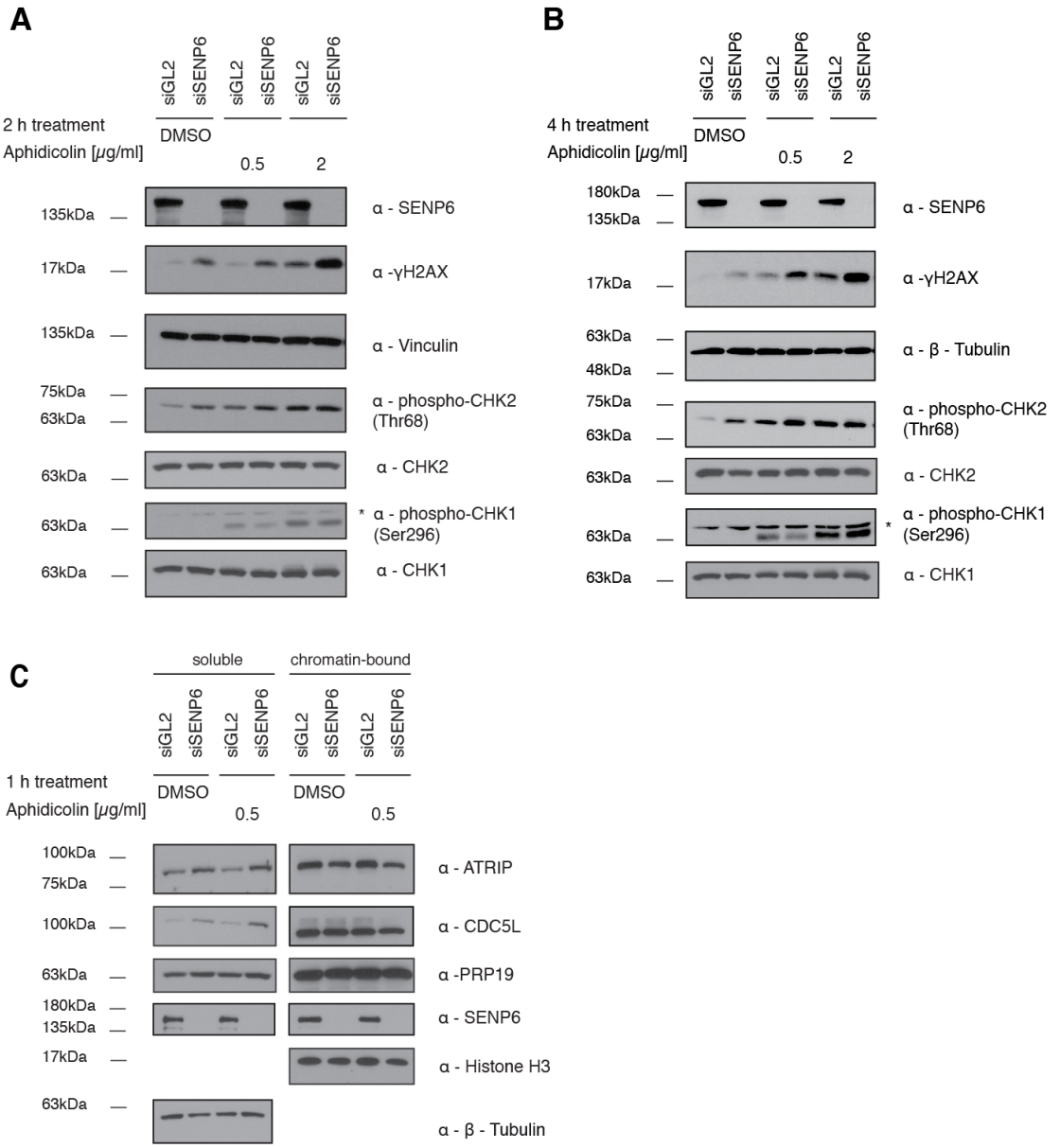

Figure 28: The ATR-CHK1 checkpoint under control of SENP6. (A, B) SiRNA-mediated knockdown of SENP6 or a non-targeting control was carried out in HeLa cells. 72 hours after transfection, cells were lysed in Laemmli buffer. Prior to lysis, cells were treated with indicated concentrations of aphidicolin for 2 h (A) or 4 h (B). Cell extracts were subjected to SDS-PAGE and following transfer. Staining was done with antibodies against SENP6, γH2AX, vinculin, phospho-CHK2, CHK2, phospho-CHK1 and CHK1. **(C)** After 72 hours of SENP6 or control knockdown, HeLa cells were treated with aphidicolin or DMSO (0.5 μg/ml) for 1 h prior to lysis. After lysis, cells were fractionated into soluble and chromatin-bound material. Extracts were separated by SDS-PAGE and stained against ATRIP, CDC5L, PRP19 and SENP6. Proper fractionation was controlled by probing against histone H3 and β-tubulin.

7 Discussion

SUMO conjugation or deconjugation of target proteins represents a quick and dynamic way to control activity, interaction or localization of substrates. As outlined earlier, SUMOylation therefore acts as versatile regulator of many different cellular pathways and mechanisms. The transient nature of the SUMOylation process enables the cell to promptly react to internal or external stimuli that require regulatory changes. A fine-tuned balance of modification and demodification of substrate proteins is a prerequisite for proper functioning of SUMO-regulated cellular processes. In mammalian cells, the SENP family of SUMO-specific isopeptidases acts as most prominent deconjugases of SUMO. The six members differ in their specificity of cleaving SUMO1, SUMO2/3 or SUMO chains and hence fulfil different functions in cleaving mono- or poly-SUMO modified target proteins.

To date, not much is known about distinct stimuli controlling SENP activity. Only for several SENP family members a regulation in response to gene expression or protein turnover is known[37–40]. Also information on specific SUMO targets under the control of individual SENPs is lacking. In this work, we investigated the influence of hypoxia on SUMO signalling and in particular on the activity of SENP1 and SENP3. Furthermore we expanded our knowledge on SENP3 and SENP6 interactors and target proteins using a combined IP-MS approach. Finally, we explored the role of SENP6 in DNA damage response, contributing to ATR/CHK1 activation under replicative stress.

7.1 Regulation of SENP activity by hypoxia

Generally, elevated SUMOylation upon different stress situations is thought to have cytoprotective functions. Global increases in SUMO2/3 levels are seen after heat shock or for instance in models of brain ischemia[38,47], but the physiological consequences of these alterations are not well-established. With our experiments we could confirm a pronounced increase in SUMO1-modified

targets under hypoxia. Using proteomic tools we identified a subset of proteins whose SUMO1-modification is highly increased under low oxygen levels. Our data are in line with the idea that the adaption of the cellular metabolism to the hypoxic situation is facilitated by hyperSUMOylation of distinct proteins. As part of this adaption mitochondrial aerobic metabolism is attenuated and anaerobic glycolysis is activated. We identified the transcriptional co-repressor BHLHE40 as one hyperSUMOylated SUMO1 target under hypoxia, possibly contributing to the metabolic switch by repressing genes that participate in oxidative metabolism[54]. In particular, we showed the repressive function of SUMOylated BHLHE40 on PGC-1α in a luciferase assay. PGC-1α is a transcriptional coactivator and master regulator of oxidative metabolism[56,60]. Therefore, we propose that the inactivation of SENP1 under hypoxia, leading to hyperSUMOylated BHLHE40 and following repression of PGC-1α, contributes to cellular adaption upon a decrease in oxygen levels. Additionally, PGC-1α was shown to be modified with SUMO1 itself. Cai and co-workers showed that SENP1 is the SUMO isopeptidase responsible for deconjugating PGC-1α. DeSUMOylated PGC-1α shows elevated transcriptional activity, promoting expression of mitochondrial genes and thereby fostering mitochondrial biogenesis and oxidative metabolism[61].

Also our proteomic data from normoxic versus hypoxic whole cell extracts point to a shift from aerobic metabolism to glycolysis. We see the glucose transporter GLUT1 that is responsible for basal glucose uptake stronger SUMOylated and additionally upregulated in the proteome of hypoxic cells. This may contribute to anaerobic glycolysis by promoting glucose uptake. In fact, an increase of the glycolytic flux has been shown for mammalian cells overexpressing SUMO1[41]. In general, we find some more enzymes of the glycolytic pathway to be increased on proteome level under hypoxia. These are for example fructose-bisphosphate aldolase C (ALDOC) or gamma-enolase (ENO2), both known to be induced upon hypoxia[62]. This further proves the reliability of our experimental conditions.

All these results strengthen our hypothesis of the hypoxic inactivation of SENP1 facilitating the switch from aerobic metabolism to glycolysis under hypoxia.

Comparing our dataset with previous studies on SUMOylation under hypoxic conditions, we find several common hits. Yang *et al*. subjected neuronal cells to oxygen/glucose-deprivation and investigated changes in SUMO3 conjugation by SILAC-based proteomics[50]. Among their 22 identified hits, PML, PIAS2 and IRF2BP1 were common to our dataset. Also the transcriptional repressors NAB1/2 are common in both studies. Additionally, a downregulation of the two proteins RSF1 and BRD8 under hypoxia was observed in both datasets. Besides those examples, the overlap is rather limited what may be explained by different experimental setup and conditions. On the one hand, Yang and co-workers exposed their cells to 6 h of oxygen and glucose deprivation simultaneously, followed by a reoxygenation period of 30 min. In our study, we applied hypoxia for prolonged period of 24 h without any reoxygenation or lack of glucose. These different environmental circumstances may have diverse effects on the cellular system. On the other hand, we investigated SUMO1-conjugation in HeLa cells triggered by hypoxia whereas Yang *et al.* used a neuroblastoma cell line under stable expression of HA-SUMO3, likely explaining the different findings in both studies.

The effect of hypoxia on enhanced SUMOylation is best exemplified on BHLHE40. Previous studies already identified the SUMOylation sites in BHLHE40 and furthermore showed an enhanced repressive activity of its SUMOylated form. SUMOylation of the respective lysine residues prevents ubiquitination and thereby increases the stability of BHLHE40[55]. This is in line with our observations where we see consistently lower levels of the SUMO-mutant version BHLHE40^{K159R,K279R} compared to BHLHE40 wild-type.

In the context of hypoxia-induced SENP1 inhibition and its contribution to changes in the cellular metabolism, one must also consider the hypoxic master regulator HIF1α. HIF1α is the key transcription factor regulating the transcriptional response to hypoxia. Its target genes include erythropoietin, glucose transporters, many enzymes of the glycolytic system and others that mediate the adaption of the cellular system to changes in oxygen supply. Intriguingly, HIF1α itself has been identified as SENP1-regulated hypoxic SUMO target[63]. Cheng *et al*. showed that SENP1 is the responsible SUMO-

specific isopeptidase deconjugating SUMOylated HIF1α. Under normoxic conditions, HIF1α is hydroxylated at two distinct proline residues thus binding to VHL, a member of an E3 ubiquitin ligase complex, leading to its subsequent proteasomal degradation. Cheng *et al.* proposed that SENP1-mediated deconjugation of HIF1α contributes to its stability in hypoxia since SUMOylation of HIF1α promotes its interaction with VHL. We did not detect HIF1α as a SUMO target in our screen therefore we can not make any statement on HIF1α SUMOylation under prolonged hypoxia. We can only speculate that the inactivation of SENP1 under prolonged hypoxic conditions may act as a negative feed back to restrict HIF1α levels.

Notably also, SENP3 has already been shown to function as redox sensor under oxidative stress to regulate HIF1α transcriptional activity[39]. SENP3 activity is needed for ROS-induced HIF1α transactivation where the direct substrate for SENP3-mediated deSUMOylation is not HIF1α itself but its co-activator p300. Removing SUMO2/3 from p300 fosters its binding to HIF1α. Also in this process, inactivation of SENP3 under prolonged hypoxia may be used to limit HIF1α activity.

An important question concerns the mechanism of SENP inactivation under hypoxia. The exact mechanism of SENP1 and SENP3 inactivation under low oxygen is not clear. One may assume, that distinct SENPs are able to react to changes in the cellular oxygen level and thereby act as a switch to control the consequences. Like it was already shown for several deubiquitinases, also SENPs could be reversibly inactivated through ROS by targeting their catalytic cysteine[64,65]. SENP1 and SENP3 are primarily nuclear proteins. Under normal conditions, ROS are produced as by-product of the respiratory chain in the mitochondria. Under hypoxic conditions however, it has been demonstrated, that mitochondria cluster into the perinuclear region, thereby increasing nuclear ROS[66]. This may explain the reversible hypoxic inactivation of SENP1 and SENP3 despite their nuclear localization. The catalytic cysteine residue of both proteins is known to be influenced by changes in redox state. The active Cys (cysteine) 603 of SENP1 is forming a disulphide bond with Cys 613 under H_2O_2,

most likely to prevent irreversible inactivation[49]. For SENP3, sulfenylation of the catalytic cysteine 532 has been identified in a cellular model upon H_2O_2 treatment (500 μM, 5 min). These examples illustrate the susceptibility of cysteine residues in the SUMO system to reversible modifications under redox stress.

Taken together, in the first part of this work, we gained insight into the hypoxic regulation of SUMO1 targets by inactivation of SENP1. Furthermore, we identified the transcriptional repressor BHLHE40 as hyperSUMOylated under hypoxia, thereby possibly restricting PGC-1α activity on oxidative metabolism. Thus, low oxygen-induced SENP1 inactivation could be linked to a switch of the cellular metabolism into anaerobic glycolysis (Figure 29). Additionally, we also find SENP3 inactivated but the consequences for distinct target proteins and physiological functions still have to be determined.

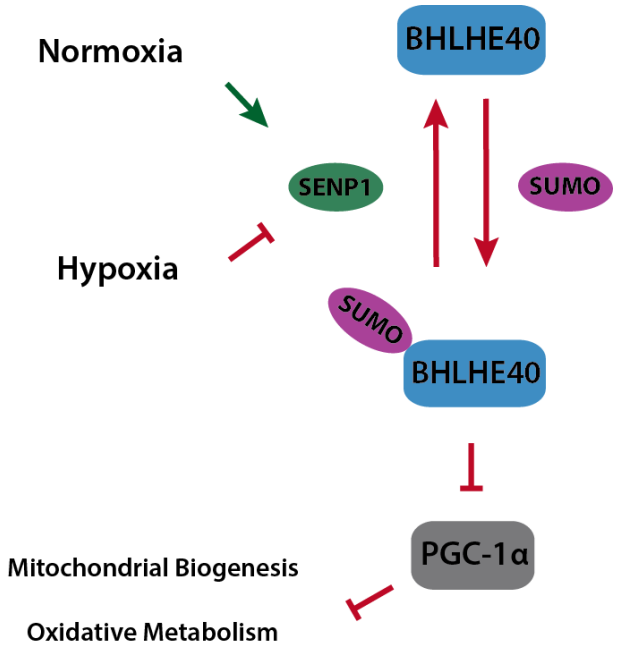

Figure 29: Model illustrating how SENP1 inactivation under hypoxia contributes to adaption of the cellular metabolism under low oxygen. Under hypoxic conditions, SENP1 is inactivated, leading to increased SUMOylation of BHLHE40. This supports its repressive function on PCG-1α and thereby contributes to the switch from oxidative metabolism to glycolysis under lack of oxygen. From Kunz *et al.*[52].

7.2 SENP3 function is tightly linked to mammalian ribosome biogenesis

The SUMO isopeptidase SENP3 predominantly localized to the nucleolus and nuclear targeting is determined by its interaction with the nuclear scaffold protein NPM1[29]. SENP3 exhibits a preference for cleaving SUMO2/3 conjugates and plays a crucial role in ribosome biogenesis[30,67].

The eukaryotic ribosome biogenesis is a highly complex and tightly controlled process. The translation of genetic information into functional proteins demands high energy costs from the cell and involves many proteins of different enzyme classes. In mammalian cells, the process starts with the transcription of the 47S pre-rRNA in the nucleolus, which undergoes subsequent processing steps, finally giving rise to the 18S, 5.8S and 28S rRNA. In this pathway, the 47S pre-rRNA initially associates with a number of proteins to form the 90S preribosome, which later splits into the pre-60S subunit and the pre-40S subunit. Pre-60S and pre-40S particles pass through the nucleolus and the nucleoplasm, where remodelling processes of the particles and processing of rRNAs take place to assure the export of mature 40S and 60S ribosomes. These maturation steps, which are considered as proofreading and quality control processes involve many assembly and transport factors collectively termed trans-acting factors. Our understanding of mammalian trans-acting factors and their role in these quality control pathways is still fragmentary. Data from our group elucidated an important role for SENP3 in the pathway of 60S maturation. As already outlined in the introduction, a SENP3-associated complex consisting of the core components PELP1, TEX10 and WDR18 was initially identified by mass spectrometry. Functional studies demonstrated that the mammalian PELP1-TEX10-WDR18 complex represents the functional counterpart of the Rix1-Ipi1-Ipi3 complex in *Saccharomyces cerevisiae*, a well-characterized subcomplex functioning in pre-60S ribosomal maturation. The PELP1-TEX10-WDR18 complex was shown to be involved in the 28S rRNA maturation and PELP1 was identified as SENP3-sensitive SUMO target. Subsequent work demonstrated that SUMO modification of PELP1 facilitates

the SIM-dependent transient recruitment of the AAA ATPase MDN1 to pre-60S particles. Like its yeast counterpart Rea1, MDN1 is a critical remodelling factor at pre-60S particles. Importantly, at a later stage of the maturation process MDN1 and PELP1 are released from pre-60S particles in a SENP3-dependent process.

While these data tightly link SENP3 function to ribosome maturation, we wanted to get unbiased, system-wide insight into SENP3-controlled cellular pathways by our MS-based proteomic screening approach. To this end, we compared the SUMO2/3 targets in control cells and cells depleted from SENP3 by CRISPR-Cas9. Altogether, we identified around 550 *bona fide* SUMO2/3 targets in control cells or SENP3 KO cells, respectively. In this dataset we find a good overlap with known SUMO targets. Importantly, when comparing SENP3 KO cells versus control cells, around 60 proteins exhibit an elevated SUMOylation status. Among these, PELP1 and Las1L are the most prominent hits showing a strong induction of SUMO2/3 conjugation under lack of SENP3. As shown in our dataset, SENP3 is counteracting SUMOylation of the PELP1 complex and associated proteins (Las1L, NOL9, TEX10), which is in line with the concept of protein group demodification by SENPs. The idea of SENP3 functioning as group demodifier is further strengthened by the finding that a number of large ribosomal subunit proteins (RPL26, RPL36, RPL29, RPL31) exhibits enhanced SUMOylation in the absence of SENP3. Elevated SUMOylation of these ribosomal proteins may be seen for different reasons. First, it is known, that impairments at any stages of ribosomal biogenesis leads to nucleolar stress. This results in a release or accumulation of free ribosomal proteins in the respective compartment. Interfering with ribosomal biogenesis by depletion of SENP3 may lead to an increase in unassembled ribosomal proteins which are SUMOylated and potentially degraded by the proteasome like it was shown in yeast[68]. Also recent MS-based screens in human cells demonstrate the proteasomal degradation of excess ribosomal proteins[69]. Alternatively, depletion of SENP3 may cause a general accumulation of SUMO2/3-modified proteins at pre-60S ribosomes. Because SENP3 is associated with pre-60S ribosomes, its

lack may lead to unrestricted SUMOylation of large subunit proteins. This latter possibility is in line with the model of SUMO group modification/demodification.

In addition to pre-60S associated SENP3-controlled proteins, we defined a cluster of 90S associated proteins in our combined STRING network of SENP3 interactors and targets. This cluster includes BMS1, NOP58 or UTP3, which are all involved in maturation, cleavage and processing steps of the small subunit processome. Since we find these proteins either highly SUMOylated under lack of SENP3 or being SENP3 interactors, we propose additional SENP3-regulated functions in the 90S biogenesis. However, the specific consequences on 90S formation under SENP3 depletion remain to be determined.
Although the main function of SENP3 seems to be concentrated on ribosome biogenesis, we find several SENP3-regulated targets involved in different pathways. The ubiquitin E2 enzyme UBE2Z, for instance, is connected to the Ubiquitin E3 ligase Cullin-3, SMN1 and SMN2, are part of the spliceosome or BRE and RIF1 play a role in DNA double strand repair. Additionally, we found several transcriptional regulators (e.g. NFRKB-INO80, DMAP1-EPC1, MLL2-MLL3). Finally, we included also a few non-connected proteins, most of them belonging to the zinc finger family. Not much is known so far about their function besides that they all might be involved in transcriptional regulation. The role of SENP3 in transcriptional regulation is well established and can be exemplified on the MLL/SET methyltransferase complex, where it facilitates the complex assembly by deconjugation of SUMO2/3 from the subunit RbBP5. Thereby, SENP3 promotes transcriptional activity of a subset of HOX genes.

7.3 Identification of SENP6-controlled SUMO2/3 targets

Protecting the genomic DNA is one of the cell's most important and challenging task. Numerous sources of endogenous and environmental DNA damaging agents cause distinct types of DNA lesions, including single- and double-strand breaks or other chemical modifications that endanger the genome integrity. To combat these consequences of DNA damage, the cell maintains several

different and complex organised DNA repair pathways, many of them regulated at the level of PTMs. Imperfect repair leads to genomic instability that fosters cellular aging, transfer of incorrect genetic information or diseases including neurodegenerative disorders and cancer.

SUMO conjugation/deconjugation events are critically involved in the regulation of various DNA repair pathways. Accordingly, disturbances of general SUMOylation result in phenotypes characterized by inadequate genome maintenance[70,71]. This includes hypersensitivity to DNA-damaging agents[72] due to defective HR (homologous recombination) resulting in chromosomal rearrangements[73]. To date, several key factors of DNA repair are known to be SUMO-modified but it is not clear how the SUMOylation status of these factors is regulated. In particular the involvement of SUMO-specific isopeptidases in these processes has remained largely unclear.

With our work, we define a cellular network of SENP6-regulated SUMO2/3 targets and provide evidence that SENP6 is regulating the chromatin-association of several protein complexes, involved in cell cycle control, DNA damage response and maintenance of genome stability. We applied an endogenous IP-MS approach to enrich for SUMO2/3 substrates in cells lacking SENP6 to pinpoint SENP6-driven regulation of target proteins. The resulting dataset confirms already known findings and expands our knowledge on SENP6 functions. Previous work identified SENP6 as an antagonist of the StUbL RNF4 in the Fanconi anemia repair pathway[74]. Two subunits of the FA core complex, FANCI and FANCD2 are SUMOylated in response to stalling of replication forks. Subsequent polyubiquitination of FANCI/FANCD2 by RNF4 results in elimination of the FA complex from sites of DNA lesions by the segregase p97 in conjunction with the adaptor DVC1. In this pathway, SENP6 restrains SUMO chain formation on the subunit FANCI and thereby antagonizes RNF4 action. In our experiments, we confirm the interaction of SENP6 with components of the FA repair pathway because interactomics revealed interaction of SENP6 with FANCA, FANCI and FANCD2. In addition, we observed an increased SUMO2/3 modification of FANCI in our screen for

SENP6-regulated SUMO targets. This is in line with the model proposed by Gibbs-Seymour *et al.*. Remarkably though, we see a strong decrease of FANCD2 in the cellular proteome of cells lacking SENP6. This observation was also verified by Western Blot analysis suggesting that FANCD2 is not simply extracted from DNA damage sites but furthermore addressed to proteasomal degradation by the StUbL pathway. In line with this idea, RNF4-mediated degradation of the subunit FANCA by the proteasome has already been demonstrated[75].

As another target, which is functionally linked to the FA pathway, we identified SLX4, also known as FANCP. SLX4 was one candidate with the most highly induced SUMOylation in SENP6 depleted cells. SLX4 is a scaffold protein with important implications in DNA repair. It harbours two ubiquitin-binding zinc finger domains that are necessary for its action in the repair of ICLs (interstrand crosslinks) through the FA pathway[76]. Additionally, it contains multiple SIMs, enabling it to bind poly-SUMO chains. Previous studies identified the SLX4 complex acting as SUMO E3 ligase, able to SUMOylate itself[77,78]. It was shown that SLX4 possesses SUMO-dependent functions that are essential in response to local replication stress.

Summarizing our results of SENP6 interactome and target MS screen, we identified multiple FA members being controlled by SENP6 and thereby confirming an important role of SENP6 in this pathway.

Another protein cluster identified in our network analysis of SENP6-dependent SUMO targets are the centromere proteins CENPC, CENPH, CENPT and CENPU. Physical interaction of SENP6 with CENPH was confirmed in the interactomics dataset whereas elevated SUMOylation was seen for the others CENPs in SUMO2/3 IPs from SENP6 depleted cells. These centromere proteins partially belong to the CENPA-NAC complex, playing an indispensable role in the assembly of kinetochore proteins, chromosome segregation and mitotic progression. Previous data already established SENP6 as crucial for the assembly of the inner kinetochore. Cells lacking SENP6 show phenotypes of defective spindle assembly caused by RNF4-mediated proteasomal

degradation of CENPI. The CENP H/I/K complex is not properly formed at centromeres/kinetochores under depletion of SENP6 resulting in failure of mitotic progression by disturbed spindle assembly[79]. Since we see enhanced SUMOylation of the CENPA-NAC complex (CENPC, CENPH, CENPT, CENPU), this may result in the recruitment of RNF4 and subsequent degradation or extraction of the complex from chromatin. Recent mass spectrometric screens in *S. pombe (Schizosaccharomyces pombe)* identified the inner kinetochore subunit mis17 (corresponding to mammalian CENPU) as target of the SLX8/CDC48 pathway[80] (corresponding to the RNF4/p97 pathway in mammals). These data further support our findings of mammalian centromere proteins being SUMOylated upon loss of SENP6 and potentially targeted by RNF4 for degradation/extraction.

The dataset in *S. pombe* further identified the SMC5/6 and condensin complexes being highly SUMOylated in SLX8 mutants. The mammalian SMC complexes (structural maintenance of chromosomes) belong to a multisubunit family of ATPases that function in chromosome dynamics and organization. Human SMC proteins are part of distinct but related complexes: SMC1/3 belong to the cohesin complex, which controls cohesion of sister chromatids. SMC2/4, also known as condensin complex, facilitate the condensation of chromosomes and the SMC5/6 complex is specialized in the maintenance of genomic stability. SMC protein complexes share a conserved structural composition, exemplified by the cohesin complex. A heterodimer of SMC proteins (SMC1/3) is stabilized by a single α-kleisin subunit (Rad21) connecting them via its N- and C-terminus to form a trimeric ring-shaped structure. Associated via the kleisin subunit are HeatA/B repeats (PDS5A/B, Stag1/2) or tandem-WHD domains that orchestrate the activity of the core complex. PDS5A/B are responsible for the dynamic interaction of cohesin and chromatin, whereas Plk1-mediated phosphorylation of Stag2 leads to removal of the cohesin complex from chromatin. Recent studies also implicated functions of Stag2 at DNA intermediates in pathways of genome maintenance[81].

Importantly, we find the cohesin member PDS5B interacting with SENP6. Furthermore, we demonstrate enhanced SUMOylation of the cohesin subunit

Stag2 in cells lacking SENP6 and showed reduced chromatin-association of Stag2 and Rad21 under SENP6 depletion. In the yeast *S. cerevisiae*, PDS5 has been shown to maintain sister chromatid cohesion in pre-anaphase cells by preventing poly-SUMO-mediated proteasomal degradation of the cohesin complex. Scc1 (corresponding to mammalian Rad21) has been identified as important target in this process since lack of PDS5 promotes SUMOylation of Scc1 followed by its ubiquitin/proteasome-mediated degradation via the StUbL SLX5/8 pathway. Accordingly, blocking the StUbL pathway limits Scc1 turnover and restores sister chromatid cohesion[82,83]. SUMOylation of cohesin subunits has also been reported in *S. pombe*, where the SMC1/3 homologues psm1 and psm3 were found to be StUbL substrates[80]. With our data, we propose a model where the chromatin-residency of the cohesin complex is likely mediated via a SENP6-RNF4-regulated mechanism. Altogether, this strengthens the idea of an evolutionary conserved function of SUMO-mediated regulation of the cohesin complex. Thus, StUbL-mediated degradation of cohesin may for instance enable sister chromatid separation to facilitate DNA damage repair.

In response to DNA damage or replication stress, the cellular DDR pathways are activated. The checkpoint response can be subdivided in the ATR-CHK1 and the ATM-CHK2 branches. ATR is activated in response to DNA lesions that generate single-stranded DNA. One critical component of ATR-CHK1 activation is the human PSO4/PRP19 complex. PSO4, also termed PRP19, has been first identified in *S. cerevisiae* as a component of the interstrand crosslink repair pathway. Yeast PSO4/PRP19 shows a strong structural and functional conservation with its mammalian counterpart. Mammalian PRP19/hPSO4 is part of a protein complex, comprised of the core components PRP19, BCAS2, CDC5L and PLRG1. This complex plays a crucial role in sensing DNA lesions by interacting with the ATR signalling network. In recent studies is has been shown that hPSO4/PRP19 directly binds to RPA, colocalizes with PCNA and is needed for stabilization and restart of stalled replication forks in response to replicative stress[84,85]. Interestingly, we found three members of the human PRP19 core complex, namely of PRP19, CDC5L and BCAS2 as SENP6

interacting proteins identified by IP-MS and validated by Western blot analysis. To further investigate a possible role of SENP6 in the DNA damage response, in particular in response to replication stress, we explored cellular DDR following SENP6 depletion under replicative stress induced by aphidicolin. We therefore monitored the activation of ATR-CHK1 in control cells or SENP6 deficient cells. Upon DNA damage, ATR binds as stable heterodimer to its co-activator ATRIP, forming a mutually depending partnership in DDR. The ATR-ATRIP dimer is then localizing to sites of DNA lesions by ATRIP interacting with RPA-modified single-stranded DNA stretches building up at stalled replication forks[86]. The hPSO4 complex fosters ATR autophosphorylation and ATRIP recruitment upon DNA damage, resulting in subsequent phosphorylation of downstream targets like CHK1. In our experiments, we demonstrated that in response to aphidicolin-induced replication stress, cells depleted of SENP6 show impaired chromatin-recruitment of ATRIP and reduced CHK1 activation, leaving cells prone to DNA damage caused by replication stress. Since this process is paralleled by enhanced SUMOylation of CDC5L and a slight reduction of CDC5L residency at chromatin we hypothesize that loss of SENP6 affects ATRIP recruitment via uncontrolled CDC5L SUMOylation. This additionally promotes the hypothesis that SENP6 plays a critical role in maintaining SUMOylation status of hPSO4 complex components and possibly other chromatin-associated proteins and that loss of SENP6 negatively influences chromatin recruitment of these complexes. In recent studies is was shown that replicative stress triggers SUMOylation of ATR-activating proteins such as TOPBP1 and ATRIP[87]. Additionally, a non-SUMOylatable mutant of ATRIP exhibited diminished interaction with multiple proteins including ATR, TOPBP1 and others and failed to support ATR activation[88]. Although this might seem contradictory at first, the differential roles of mono- and polySUMOylation, in particular in the regulation of protein assembly on chromatin have to be considered here. While monoSUMOylation facilitates protein assembly by SUMO-SIM-mediated interactions, polySUMOylation rather functions as a signal for disassembly via the RNF4/p97 pathway, also conserved in lower eukaryotes as Slx5/Slx8-CDC48 pathway. Together with our data on impaired CHK1

activation under lack of SENP6 this supports a model where SENP6 is an essential key player in balancing SUMOylation of chromatin-associated proteins involved in DDR like the hPSO4 complex and thereby regulating their chromatin-residency (Figure 30).

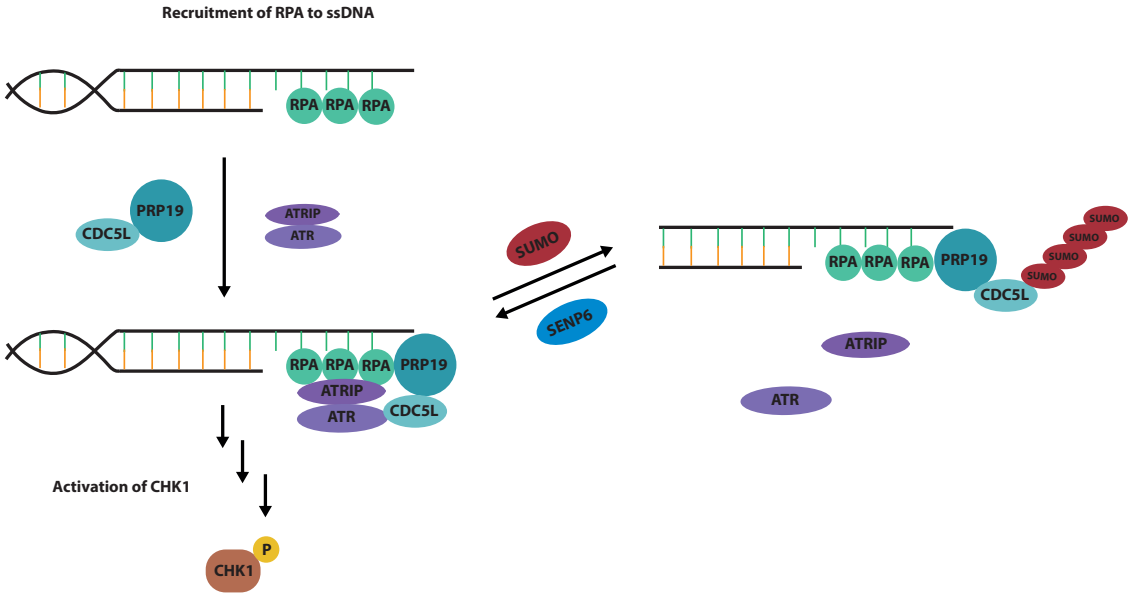

Figure 30: Model of SENP6 functioning in the DDR pathway. Upon DNA damage resulting in single-stranded DNA, RPA is recruited to sites of DNA lesion. In presence of SENP6, the hPSO4/PRP19 complex triggers subsequent recruitment of the ATR-ATRIP heterodimer to chromatin, finally leading to CHK1 activation by phosphorylation. In cells lacking SENP6, chromatin recruitment of ATRIP is impaired resulting in diminished activation of CHK1. Furthermore, CDC5L is SUMOylated in a SENP6-dependent manner.

7.4 Conclusion

With our current work we contribute to a better understanding of regulation and activity of distinct SUMO isopeptidases on specific targets and protein networks. By an unbiased, system-wide proteomic approach, we defined a cluster of differentially SUMO1-modified proteins under hypoxia, which is most likely the consequence of hypoxic inactivation of SENP1. Furthermore, we were able demonstrate that hyperSUMOylation of the transcriptional co-repressor BHLHE40 contributes to metabolic changes under low oxygen supply. Applying endogenous SUMO2/3 IP-MS, we confirmed and extended the critical involvement of SENP3 in ribosomal maturation as shown by identified protein clusters involved in pre-60S and 90S processing. With respect to SENP6, we

uncovered interactors and SENP6-dependent SUMO targets functioning at kinetochores, centromeres, chromatin cohesion and DNA damage response. Finally, we provide strong evidence that SENP6 function is needed to maintain genome stability by enabling efficient CHK1 activation during replicative stress. Generally we strengthen the idea that SENP6 acts as antagonist of the StUbL pathway by limiting polySUMOylation of chromatin-associated protein complexes. We propose that SENP6 controls the chromatin-residency of various chromatin-associated protein complexes by targeting multiple subunits of these complexes.

8 Materials and Methods

8.1 Reagents and Chemicals

Methods described in this chapter were done with chemicals purchased from AppliChem (Darmstadt), Fluka (Seelze), Fisher scientific (Schwerte), Merck (Darmstadt), Roth (Karlsruhe) or Sigma-Aldrich (Taufkirchen), if not stated otherwise. Peptides for elution of enriched SUMO substrates were synthesized by PanaTecs® (Heilbronn). Sequencing of plasmids was done by Seqlab (Göttingen) and Eurofins Genomics (Ebersberg). DNA oligonucleotides and siRNA's were ordered from Eurofins Genomics.

Other materials and kits used in this work:

Reagent	Supplier
GeneJET Plasmid Mini-/Midiprep Kit	Thermo Scientific
FastGene Gel/PCR Extraction Kit	Nippon Genetics
Universal RNA Purification Kit	Roboklon
Transcriptor First Strand cDNA Synthesis Kit	Roche
2x LightCycler 480 SYBR Green I Master	Roche
DC™ Protein Assay	Bio-Rad
T4 DNA ligase and restriction enzymes	New England Biolabs
Pfu Polymerase	Bio & Sell
FastRuler	Thermo Scientific
Protein Marker prestained (11 – 245 kDa)	Neofroxx
InstantBlue™	Expedeon
Dual-Luciferase® Reporter Assay	Promega

8.2 Microbiological methods

8.2.1 *E. coli (Escherichia coli)* strain used

Experiments involving *E. coli* were performed using XL10 Gold® from Stratagene with the following genotype: Tet^{r}Δ(*mcrA)*183 Δ(*mcrCB-hsdSMR-*

mrr)173 endA1 supE44 thi-1 recA1 gyrA96 relA1 lac Hte [F´ *proAB lacI*^{q}*ZΔM15* Tn*10* (Tet^{r}) Amy Cam^{r}]

8.2.2 Generation of competent *E. coli*

For the preparation of competent *E. coli*, 50 ml LB (lysogeny broth) medium (0.5% (w/v) NaCl, 0.5% (w/v) yeast extract, 1% (w/v) tryptone, sterilized by autoclaving) were inoculated with respective bacteria from a glycerol stock and incubated overnight at 37 °C. On the next day, 500 ml fresh LB medium were inoculated with an OD_{600} of 0.1 using the overnight culture. The culture was grown at 37 °C until an OD_{600} value between 0.4 – 0.6 was reached, then cooled down on ice for up to one hour. Bacterial cells were pelleted by centrifugation at 3000 g for 15 min at 4 °C. Afterwards, the pellet was resuspended in 100 ml FB (freezing buffer) (100 mM KCl, 50 mM $CaCl_2x2H_2O$, 10% (w/v) glycerol, 10 mM potassium acetate, pH 6.4, sterile filtered) and kept on ice for another hour. Bacteria were pelleted by centrifugation (3000 g, 15 min, 4 °C), resuspended in 40 ml FB medium and frozen in 500 µl aliquots at -80 °C.

8.2.3 Storage and cultivation of *E. coli*

Frozen stocks of *E. coli* were kept at -80 °C. For cultivation, bacteria were grown in LB medium at 37 °C while shaking at 200 rpm. To obtain single colonies, bacteria were streaked on LB-agar plates (LB medium, 1.5% (w/v) agar) and incubated at 37 °C.

8.2.4 Transformation of plasmid DNA in *E. coli*

For the transformation of *E. coli* with DNA, bacteria were thawed on ice. 10 µl of a ligation reaction or 1 µl of plasmid DNA (= 100 – 500 ng DNA) were added to 100 µl of resuspended bacteria and incubated on ice for 20 min. The uptake of the plasmid DNA was stimulated by incubation *of E. coli* at 42 °C for 1 min. Afterwards, bacteria were incubated in 1 ml of LB medium at 37 °C for 30 min.

For a liquid overnight culture, transformed bacteria were added to 100 ml of LB medium supplemented with appropriate antibiotics and incubated shaking at 37 °C. To culture bacteria on a plate, cells were pelleted by centrifugation for 2 min at 2000 g, supernatant was reduced to 100 µl. Bacteria were resuspended in the remaining supernatant and streaked on an LB-agar plate containing respective antibiotic. To select for transformed bacteria, ampicillin (50 µg/ml) was added to the LB medium or LB-agar plates.

8.3 Cell-biological methods

8.3.1 Cell lines used

Cell line/supplier	Cell type/origin
HeLa/ATCC (CCL-2)	Human cervix adenocarcinoma
HeLa His-SUMO1	Ullmann *et al.*[89], 2012
HeLa His-SUMO2	Ullmann *et al.*[89], 2012
U-2 OS/ATCC (HTB-96)	Human osteosarcoma
HEK293T/ATCC (CRL-3216)	Human embryonic kidney cells stably expressing T-antigen

8.3.2 Mammalian expression vectors used

Name	Source
pCI	Promega
pcDNA™5/TO	Invitrogen

8.3.3 Cultivation and treatment of mammalian cell lines

HeLa and U-2 OS cells were cultured under standard conditions at 37 °C and 5% CO_2 in DMEM (Dulbecco's Modified Eagle Medium). The medium was supplemented with 10% FCS (fetal calf serum) and 1% PS (Penicillin/Streptomycin, 100 U/ml) to provide optimal growth conditions. Cells were subcultured every three days in a new 10 cm dish. Therefore,

monolayered cells were washed once with 10 ml PBS (phosphate-buffered saline) (137 mM NaCl, 2.68 mM KCl, 10.14 mM Na_2HPO_4, 8.82 mM KH_2PO_4, sterilized by autoclaving) and incubated in 1 ml Trypsin/EDTA (ethylenediaminetetraacetate) for 5 min at 37 °C. After detachment, 10% of the cells were supplied with 10 ml fresh medium in a new dish for further cultivation. Prior seeding of cells for an experiment, they were counted with the TC20™ cell counter from Bio-Rad.

For experiments involving the His-SUMO1/2 expressing HeLa cell lines, induction of His-tagged SUMO was achieved by treatment of cells with doxycycline (1 μg/ml) overnight.

Experiments under hypoxic conditions were performed in a hypoxia chamber, were cells were incubated for 2, 4 or 24 hours in normal DMEM at 37 °C and 1% O_2. Hypoxic samples were harvested in the hypoxia chamber; all buffers used (PBS, lysis buffer) were degassed for several hours to ensure the given oxygen content of 1%. In case of reoxygenation experiments, hypoxic samples were incubated for 30 minutes in a normal incubator at 37 °C and 5% CO_2.

Heat shock was performed for 30 min in an incubator set at 43 °C and 5% CO_2.

Treatment of cells with aphidicolin was done for 1, 2 or 4 hours at a final concentration of 0.5, 2 or 4 μg/ml. After incubation time, cells were subsequently washed in PBS and scraped in lysis buffer containing 4% SDS. DNA was sheared by sonication and samples were heated to 99°C for 10 min, then centrifuged at 14000 rpm for 10 min. Before the cell lysate was used for Western blot analysis, protein content was determined using Lowry assay.

8.3.4 Storage of cell lines

For long-term storage, cells were frozen in aliquots at -150 °C. Therefore, a confluent 10 cm dish was washed in PBS and detached using trypsin like described above. Then cells were pelleted by centrifugation at 800 g for 3 min at room temperature and the remaining medium was aspirated. Cells were resuspended in 10 ml FCS supplied with 10% DMSO and aliquots of 1 ml were prepared in special cryo vials. These tubes were placed in a polystyrene box overnight at -80 °C and the next day transferred to cardboard boxes at -150°C.

When thawing cell for a new culture, the tube was put into a waterbath to defrost as fast as possible. After centrifugation for 3 min at 800 g and RT (room temperature), DMSO-containing freezing medium was aspirated and cells were resuspended in 10 ml DMEM in a 10 cm plate.

8.3.5 Transfection of cells with siRNA

Transfection of mammalian cells with siRNA was done using Lipofectamine™ RNAiMAX according to manufacturer's instructions. If not stated otherwise, siRNA transfections in this work were done in reverse for 72 hours. For reverse transfection in a 12 well plate, 50 pmol siRNA were mixed with 200 µl Opti-MEM™ and 3 µl Lipofectamine RNAiMAX. After incubation for 20 minutes at RT, the siRNA mix was pipetted at the bottom of the 12 well plate and 1 ml of cell suspension with a cell number of $1x10^5$ cells/ml (HeLa, 72 h) was added on top. Cells and siRNA mix were distributed evenly in the plate and incubated for 72 h in the incubator. For siRNA transfections in larger plates, the volumes of cells and transfection mix were adjusted. For siRNA transfections carried out in the SENP3 part of this work, involving siSENP3 and siSENP5 in HeLa and U-2 OS cells, following cell numbers were used for 48 h and 72 h:

Cell line/time point	Cell number per 12 well
HeLa 48 h	$1.5x10^5$/ml
HeLa 72 h	$1x10^5$/ml
U-2 OS 48 h	$2.5x10^5$/ml
U-2 OS 72 h	$1.5x10^5$/ml

In the first part of this work, involving SENP1 and SENP3 activity under hypoxia in Figure 13 A, HeLa cells were transfected twice within five days. On day 1, cells were reverse transfected with a total of 250 pmol siRNA per 60 mm dish. On day 3, the procedure was repeated and cells were harvested on day 5.

Different siRNAs targeting SENP6 were used in experiments, where not indicated, like in the following:

- siSENP6.4: Figures 22, 26 B, 27 C, Supplemental Figures 10, 12 B + C
- siSENP6.12: Figure 28 and Supplemental Figure 13.

Following siRNAs were used in this work:

siRNA	Sequence 5'→ 3'
siGL2 (= non-targeting control)	(CGU ACG CGG AAU ACU UCG A)TT
siSENP1	(AUU CAG UAC AUG AUU CAG U)TT
siSENP3	(ACG UGG ACA UCU UCA AUA A)TT
siSENP5	(AGA AAG CUC UUC AAA UCC A)TT
siSENP6.4	(UGA GUC UAC UGG ACC AUU A)TT
siSENP6.11	(GGA CAA AUC UGC UCA GUG U)TT
siSENP6.12	(GAA CGU CAA UUC AUC AGA A)TT

8.3.6 Transfection of cells with plasmid DNA

Transfection of U-2 OS and HeLa cells with plasmid DNA was done using FuGENE® HD transfection reagent (Promega) according to manufacturer's instructions. For transfection of a 10 cm dish, $2x10^6$ cells (HeLa) in total were seeded on day one. The day after, plasmid DNA transfection was carried out. Therefore 7.5 µg DNA were mixed with 500 µl Opti-MEM and 25 µl FuGENE. After 25 minutes incubation at RT, the mixture was added drop-wise to the cells. Transfected cells were incubated for another 48 h and then used for the experiment. For transfections performed in different-sized dishes, cell number and transfection mix were calculated according to surface area of the plates.

HEK293T cells were transfected using the calcium phosphate transfection method. Therefore, cells were seeded in 10 cm dishes with a total concentration of $3x10^6$ cells/dish. For calcium phosphate transfection on the following day, 18 µg DNA were mixed with 36.9 µl $CaCl_2$ in a total volume of 300 µl (fill up with ddH_2O). In a second tube, 300 µl HBS (HEPES-buffered saline) (50 mM HEPES

(4-(2-hydroxyethyl)-1-piperazineethanesulfonic acid), 280 mM NaCl, 1.5 mM Na_2HPO_4, pH 7.05, sterilized by filtration) was pre-dispensed. Under constant mixing, the $CaCl_2$-DNA solution was pipetted into the HBS-containing vial and after incubated for 10 min at RT pipetted drop wise onto the cells. For Figure 27 A, B, transfection were calculated to a total volume of 500 µl HBS. This required 25 µg DNA and 61.5 µl $CaCl_2$ per 10 cm dish.

8.3.7 Generation of knockout cell line with CRISPR-Cas9

Following guide RNAs were pooled and used to target SENP3:

Guide RNA	Sequence 5' → 3'
Guide 1 forward	gggctccttactctgtacgc
Guide 1 reverse	gcgtacagagtaaggagccc
Guide 2 forward	cctccacctgacttgagtcg
Guide 2 reverse	cgactcaagtcaggtggagg
Guide 3 forward	cagcaatgtgtgcagcatcg
Guide 3 reverse	cgatgctgcacacattgctg

Digestion sites for the restriction enzyme BSMBI were added to the guide RNA oligos. Guides were shortly heated up to 95 °C and then directly used for ligation with the pre-digested pLentiCRISPR V2 plasmid. Transfection of this final plasmid together with the envelope plasmid pMD2.G and the packaging plasmid psPAX2 was carried out in HEK293T cells under S2 cell culture conditions. On day 1, $1.3x10^6$ cells were seeded in a 6 well plate in a total volume of 2 ml DMEM. The day after, plasmids were transfected using Lipofectamine 2000 reagent. For a 6 well, 21 µl Lipofectamine 2000 were mixed with 150 µl Opti-MEM and incubated for 5 min at RT. In a second tube, 2.7 µg psPAX2, 1 µg pMD2.G and 3.3 µg guide RNA mix were added to 150 µl Opti-MEM. The plasmid mix was added to the first tube, incubated another 15 min at RT and finally added drop-wise to the HEK293T cells. The next morning, supernatant was removed and cells were supplied with 2 ml fresh DMEM. On day 4, the lentiviral-containing supernatant was harvested and stored at 4 °C.

Cells were supplemented with 2 ml fresh DMEM. The day after, supernatant was harvested again and pooled with the supernatant from the first harvest. Cells were inactivated by autoclaving. Pooled supernatants were filtered through a 0.45 µm filter, and frozen in aliquots at -80 °C. To generate a SENP3 knockout, U-2 OS cells were seeded in a 6 well plate on day 1 and incubated with 1 ml of the viral supernatant. After 48 hours, viral supernatant was removed and cells were selected with DMEM containing puromycin (10 µg/ml). As negative control one well of U-2 OS cells was included, which had not been transduced with virus. All cells were kept in selection medium until control cells died. After 14 days of subculture in S2, cells could be transferred in S1 cell culture and successful knockout of SENP3 was verified by immunoblotting.

8.4 Molecular biological methods

8.4.1 PCR (polymerase chain reaction)

For amplification of DNA, following reagents were mixed and subjected to the temperature program given in the table below:

Reagent	Volume [µl]
Template DNA [100 ng/µl]	1
5'-Primer	1.5
3'-Primer	1.5
dNTPs [10 mM]	1
Pfu reaction buffer [10x]	5
Pfu DNA polymerase [5U/µl]	1
DNase-free water	Ad 50

Step	Temperature [°C]	Time [min]
1. Initial Denaturation	94	2
2. Denaturation	94	1
3. Annealing	T_m-5	1
4. Elongation	72	1/0.5 kb

For sufficient amplification of DNA, steps 2-4 were repeated 35 times. Afterwards, a final extension step for 10 min at 72 °C was included followed by a cool down step to 4 °C. Finally, the PCR reaction was stored at 4°C until use. T_m stands for the melting temperature of the used primers.

8.4.2 Agarose gel electrophoresis

To visualize PCR products and to control for correct size of the amplified DNA, agarose gel electrophoresis was used to separate DNA by size. Agarose gels were composed of 0.5 – 2% agarose in TAE (tris-acetate-EDTA) buffer (40 mM tris base, 2 mM EDTA, 0.1% (v/v) acetic acid). The mixture was heated in the microwave until it was fluid. After a short cool down, agarose was mixed with 0.5% (v/v) Roti®-GelStain and the gel was casted into a horizontal gel tray including a sample comb. Once the gel was solidified again, the gel comb was carefully removed. DNA samples were mixed with 10x loading dye (2 mg/ml Orange G and 30% (v/v) glycerol in water, sterile filtered) (e.g. 1/10 of the PCR reaction + 5 μl loading buffer) and loaded onto the agarose gel. Additionally a size marker for determination of the DNA length was included. Gel electrophoresis was carried out at 100 V for 20 - 30 min and the stained DNA was visualized using an UV illuminator at 515 nm.

8.4.3 Purification of DNA from agarose gels

To purify DNA samples from agarose gels, target bands were visualized under UV light and corresponding bands were cut out with a scalpel. For extraction, the FastGene Gel/PCR Extraction Kit was used according to manufacturer's instructions. In brief, DNA in agarose was mixed with supplied buffer and liquefied by heating. Then the mixture was transferred onto a DNA-binding membrane in a spin-column. After several wash steps, DNA was eluted from the membrane with a water-based buffer.

8.4.4 Restriction and ligation

Restriction reactions were performed with chosen enzymes after determination of optimal reaction conditions using the online tool “Double Digest Calculator” from Thermo Scientific. PCR samples were incubated with respective restriction enzymes in appropriate buffer and suggested temperature and time. After restriction was completed, digested samples were loaded onto an agarose gel and corresponding bands were cut out and purified like described above. For digest reactions with only one restriction endonuclease, 1 µg of DNA was incubated with 10 U restrictions enzyme in the suitable buffer at optimal temperature for 1 h.

8.4.5 Ligation of DNA

To insert digested PCR products in the final vector, T4 DNA ligase was used. In a total volume of 10 µl, fragment and vector were added 10:1 and mixed with 1 µl T4 DNA ligase buffer and 1 µl T4 DNA ligase. DNase-free water was added up to 10 µl. The mixture was incubated for 2 h at RT and then used for transformation of *E. coli*.

8.4.6 Mutagenesis

For site-directed mutagenesis, suitable primers were designed and used in a PCR reaction to achieve desired mutation of DNA by exchange of one or multiple base pairs. The used reagents and temperature program are described in chapter 8.4.1 PCR. In contrast to a normal PCR reaction, for site-directed mutagenesis PCR reactions, steps 2 – 4 of the program were repeated only 18 times. After cool down, the samples were supplied with 1 µl of the restriction enzyme DpnI and incubated at 37 °C for 2 h.

8.4.7 Used plasmids

The following plasmids were used in this work:

Name	Source
pCI-Flag-BHLHE40 ^{WT}	Kunz *et al.*[52], 2016
pCI-Flag-BHLHE40 ^{K159R,K279R}	Kunz *et al.*[52], 2016
pCI-Flag-SENP6 ^{WT}	Markus Haindl
pCI-Flag-SENP6 ^{C1030A}	Markus Haindl
pCI-Flag-SENP3 ^{C532S}	Haindl *et al.*[29], 2008
pSG5-His-SUMO2-GG	Stefan Müller
pcDNA-HA-SUMO2-GG	Ullmann *et al.*[89], 2012
pRL-SV40 Renilla Luciferase Control Reporter Vector	Promega
PGC-1 α promoter 2kb luciferase	Addgene #8887
psPAX2	Addgene #12260
pMD2.G	Addgene #12259
pLentiCRISPR V2	Addgene #52961
GFP-LMNB1	Addgene #57141

8.4.8 Isolation of plasmid DNA from *E. coli*

Bacteria transformed with plasmid DNA were grown overnight at 37 °C in 3 ml LB for mini preps or 100 ml LB medium for midi preps. Isolation of DNA was done using mini or midi prep kits from Thermo Scientific according to provided instructions. Cells were pelleted by centrifugation at 2000 g for 15 min, supernatant was removed and cells were resuspended in provided resuspension buffer. By addition of an SDS/alkaline buffer, cells were lysed to release plasmid DNA. After neutralization, cell debris and SDS precipitates were pelleted by centrifugation. The mixture was applied to a silica column binding the DNA. Bound DNA was cleared by several wash steps and was eluted in a small volume of ddH_2O. Purity and concentration of extracted DNA was measured by Nanodrop (Peqlab) spectrophotometer. After blank measurement, 1 µl of DNA was applied and concentration in ng/µl was determined using the absorption coefficient at 260 nm. Additionally the ratio 260/280 nm was used to control the purity of isolated DNA. Ratios around 1.8 were considered as pure extracted DNA.

8.4.9 Isolation of RNA from cells

To isolate RNA from human cells, the Universal RNA Purification Kit from Roboklon was used as specified by the manufacturer. After elution in RNAse-free water, concentration and purity of isolated RNA was determined with Nanodrop like described for DNA. RNA was considered as pure with a 260/280 nm ratio around 2.0.

8.4.10 Reverse transcription of RNA in cDNA

For the generation of cDNA from RNA the Transcriptor First Strand cDNA Synthesis Kit from Roche was used like described in the supplied manual. 1 μg of RNA was reverse transcribed with anchored-oligo $(dT)_{18}$ primers and 1 μl of resulting cDNA was used for quantitative real-time PCR experiments.

8.4.11 Quantitative real-time PCR

Quantitative PCR reactions in real time were performed with a LightCycler 480 system (Roche) using the 2x LightCycler 480 SYBR Green I Master (Roche) as reagent together with previously isolated cDNA (complementary DNA). The ready-to-use hot-start PCR reaction mix from Roche already contained a FastStart Taq DNA polymerase in appropriate reaction buffer with $MgCl_2$, a dNTP mix with dUTP (deoxyuridine triphosphate) instead of dTTP (deoxythymidine triphosphate) and the SYBR green I dye. This dye enables real-time quantification of newly synthesized DNA by detection of fluorescence (530 nm) emitted by DNA-bound SYBR green dye. The increase of the fluorescence signal upon DNA binding is directly proportional to the newly generated double-stranded DNA.

Real-time PCR reactions were set up in 384 well plates as follows:

Reagent	Volume [µl]
cDNA	1
5'-Primer [10 mM]	0.5
3'-Primer [10 mM]	0.5
2x SYBR Green I Master	5
DNase-free H_2O	3

Following program was used for q-RT-PCR (quantitative real-time PCR):

Step	Temperature [°C]	Time [min:sec]	Cycle
Initial denaturation	95	15:00	1
Denaturation	95	00:10	
Annealing	55	00:20	45
Elongation	72	00:30	

After amplification of DNA, melting curves were generated and a standard curve was determined using different dilutions of the primers to ensure their specificity and efficiency. Subsequently samples were cooled down and amplification of DNA was calculated in direct comparison to the control sample.

Following primer sequences were used for q-RT-PCR:

Primer	Sequence 5' → 3'
SUMO1 forward	TTCAACTGAGGACTTGGGGG
SUMO1 reverse	TGGAACACCCTGTCTTTGAC
SUMO2 forward	GCCGACGAAAAGCCCAAGG
SUMO2 reverse	TGACAATCCCTGTCGTTCACAA
SUMO3 forward	CCCAAGGAGGGTGTGAAGAC
SUMO3 reverse	ATTGACAAGCCCTGCCTCTC
TBP forward	GGGCCGCCGGCTGTTTAACT
TBP reverse	AGCCCTGAGCGTAAGGTGGCA

8.5 Protein biochemistry methods

8.5.1 SDS-Polyacrylamide gel electrophoresis

Protein mixtures from cell lysates were separated according to their molecular weight by SDS-PAGE. To prepare cell lysates for SDS-PAGE, cells were washed with PBS, lysed in 1x Laemmli buffer and heated for 5 min at 95 °C. For separation, lysates were loaded onto self-made acrylamide gels of appropriate percentage. Gel casting systems of Bio-Rad were used to first prepare the separating gel with a top layer of ddH_2O to ensure a smooth surface. After polymerization, the water layer was removed and a stacking gel was casted on top, completed with a sample comb to generate sample wells. Finally the Laemmli lysates were pipetted into these wells and the gel was run at 100 V first for 10 min until the whole sample was crossing over to the separating gel. Then SDS-PAGE was continued at 140 V until sufficient separation was reached. Mapping of the correct size of the separated proteins was achieved using a molecular weight marker running together with the samples on the gel.

Composition for stacking and separation gel is given in following table:

Reagent	Volume [per 10 ml] for separating gel (7.5%, 10%, 12.5%)	Volume [per 5 ml] for stacking gel (4%)
4x Buffer for stacking gel		1.25 ml
4x Buffer for separating gel	2.5 ml	
Acrylamide/Bisacrylamide solution, 40% (29:1)	Needed % acrylamide solution for respective percentage	0.5 ml
APS (ammonium persulphate) (20% in H_2O)	60 µl	35 µl
TEMED (tetraethylmethylenediamine)	6 µl	3.5 µl
ddH_2O	Ad 10 ml	Ad 5 ml

Following buffer systems were used for SDS-PAGE:

Buffer	Ingredients
4x Buffer for stacking gel	0.5 M Tris-HCl, pH 6.8, 4 g/l SDS
4x Buffer for separating gel	3 M Tris-HCl, pH 8.85, 4 g/l SDS
6x SDS sample buffer (Laemmli)	0.2 M Tris-HCl pH 6.8, 8% SDS, 20% glycerol, 10% DTT, 0.1 mg/ml bromphenol blue
SDS running buffer	25 mM Tris base, 192 mM glycine, 0.1% (w/v) SDS

8.5.2 Western blot

For the detection of separated proteins by SDS-PAGE, proteins were transferred onto nitrocellulose membranes by semi-dry blot or wet-blot method using blotting systems from Biometra or Bio-Rad and blotting buffer consisting of SDS running buffer with 20% methanol. The nitrocellulose membrane was pre-incubated in blotting buffer for several minutes first. Then the gel was washed once in deionized water and placed onto the membrane. Both were then packed as sandwich between Whatman papers sucked into blotting buffer. This stack was placed then into the blotting chamber and was run at constant 55 V for 90 min (wet blot) or 180 mA for 70 min (semi-dry blot).

After successful transfer, the membrane was washed once in deionized H_2O and subsequently blocked in 5% milk in PBST (PBS + 0.1% Tween® 20). Afterwards, the membrane was incubated with primary antibody dilution in 5% milk-PBST overnight at 4 °C. On the next day, the antibody was removed and the membrane was washed 3x 10 min in PBST to remove residual primary antibody solution. Thereafter, incubation with HRP-coupled secondary antibody was carried out for 1 h at RT. Another three washing steps in PBST were included before incubation with ECL (enhanced chemiluminescence) substrate for 1 min enabled detection of emitted chemiluminescence on medical X-ray films (Fujifilm) in the darkroom. In several experiments, the IR®-Dye 800 CW goat anti-mouse/rabbit secondary antibodies from Licor were used to detect near-infrared signals with the Odyssey CLx machine from Licor.

Following primary antibodies were used in this work:

Antibody	Company	Product number	Host	Dilution
Anti-ATRIP	Merck Millipore	07-625	Rabbit	1:2000
Anti-BCAS2	Santa Cruz	sc-376554	Mouse	1:1000
Anti-BHLHE40	Bethyl	A300-649-M	Rabbit	1:1000
Anti-CDC5L	Atlas	HPA011361	Rabbit	1:1000
Anti-CHK1	Cell Signaling	2360	Mouse	1:1000
Anti-CHK2	Cell Signaling	6334	Rabbit	1:1000
Anti-FANCD2	Santa Cruz	sc-20022	Mouse	1:1000
Anti-Flag M2	Sigma-Aldrich	F1804	Mouse	1:1000
Anti-GFP	Clontech	632592	Rabbit	1:10000
Anti-HA	Covance	Clone 16B12	Mouse	1:2000
Anti-HIF1α	Novus	NB100-449	Rabbit	1:500
Anti-Histone H3	Abcam	Ab1791-100	Rabbit	1:15000
Anti-IgG1 mouse control	BD Pharmingen	557372	Mouse	1 μg
Anti-Las1L	Sigma-Aldrich	AV34629	Rabbit	1:1000
Anti-PDS5B	Novus	NB100-755	Rabbit	1:1000
Anti-PELP1	Bethyl	A300-876A	Rabbit	1:5000
Anti-phospho-CHK1	Cell Signaling	2349	Rabbit	1:2000
Anti-phospho-CHK2	Cell Signaling	2197	Rabbit	1:3000
Anti-PRP19	Santa Cruz	sc-514338	Mouse	1:500
Anti-rgs-His	Qiagen	34610	Mouse	1:2500
Anti-RNF4	Gift from Vertegaal group	FI-5	Rabbit	1:2000
Anti-SENP1	Cell Signaling	D16D7	Rabbit	1:1000
Anti-SENP2	Eurogentech SA, Belgium	Custom-made anti-peptide antibody	Rabbit	1:1000

Anti-SENP3	Cell Signaling	D20A10	Rabbit	1:4000
Anti-SENP5 *	Abin	abin459856	Rabbit	1:500
Anti-SENP5 **	Proteintech Europe	19529-1-AP	Rabbit	1:5000
Anti-SENP6	Sigma-Aldrich	HPA024376	Rabbit	1:1000
Anti-SENP7	Eurogentech SA, Belgium	Custom made anti-peptide antibody	Rabbit	1:1000
Anti-Stag2	Santa Cruz	sc-81852	Mouse	1:1000
Anti-SUMO1	Hybridoma supernatant	Clone 21C7	Mouse	1:50
Anti-SUMO2/3	MBL	M114-3	Mouse	1:2000
Anti-Vinculin	Sigma-Aldrich	V9131	Mouse	1:20000
Anti-β-Tubulin	Developmental Studies Hybridoma Bank	Clone E7	Mouse	1:3000
Anti-γH2AX	Cell Signaling	9718	Rabbit	1:1000

* This SENP5 antibody was used in the SUMO-1 IP, normoxia and hypoxia part of this work.

** This SENP5 antibody was used for experiments in the SUMO2/3 IP part and work in U-2 OS SENP3 KO cells.

Used secondary antibodies:

Antibody	**Company**	**Host**	**Dilution**
Peroxidase-conjugated AffiniPure = HRP-anti-mouse	Dianova	Goat anti-mouse	1:15000
Peroxidase-conjugated AffiniPure = HRP-anti-rabbit	Dianova	Goat anti-rabbit	1:15000
IR®-Dye 800 CW mouse	Licor	Goat anti-mouse	1:15000
IR®-Dye 800 CW rabbit	Licor	Goat anti-rabbit	1:15000

8.5.3 Immunofluorescence

HeLa cells were grown on cover slips and one day later transfected with Flag-SENP6^{C1030A}. After 48h of transfection, cells were washed with ice cold PBS and then fixed with 4% PFA (paraformaldehyde) in PBS for 15 min. Permeabilization was done using 0.5% Triton X-100 for 10 min. Afterwards, cells were pretreated with 2% BSA (bovine serum albumin) for 20 min, then incubated with anti-Flag antibody for 30 min. Following secondary antibody incubation with anti-mouse Cy3 fluorophor was carried out for 30 min in the dark. Nuclei were stained using DAPI. All incubation steps were carried out by room temperature and followed by wash steps in PBS to remove excessive liquid. Cover slips were sealed and preserved with ProLong Gold antifade mountant. Confocal images were acquired on a Leica TCS SP8 microscope and visualized using ImageJ software.

Antibodies used for immunofluorescence:

Antibody	Company	Product number	Host	Dilution
Anti-Flag M2	Sigma-Aldrich	F1804	Mouse	1:500
Anti-mouse Cy3	Dianova	115-165-146	Goat	1:300

8.5.4 SUMO-AMC measurements

To determine SUMO protease activity in human cell lysates, SUMO1/2-AMC cleavage assays were performed. Therefore, HeLa cells were cultured under hypoxia or control conditions for indicated time points. To ensure rapid lysis and conservation of given conditions, SEM (sucrose-EDTA-MOPS) buffer was prepared in advance and supplemented with protease inhibitors (Aprotinin 1:5000, Leupeptin 1:5000, Pepstatin A 1:1000, PMSF (phenylmethylsulfonyl fluoride) 1:200, DTT 1:1000); all steps were carried out on ice. Only to the lysis buffer for negative control 10 mM NEM was added. Hypoxic samples were lysed in the hypoxic chamber. Cells were washed 3x in PBS, lysed in 1 ml SEM buffer per 10 cm dish and sonicated briefly. Protein concentration was

determined (DC protein assay, Bio-Rad) and samples were adjusted with SEM buffer to equal protein content (e.g. 1 mg/ml). Aliquots of the samples were snap-frozen in liquid nitrogen and stored at -80 °C.

For AMC-measurements, 7.5 µg or 14 µg of HeLa cell extract were incubated with 500 ng of SUMO1-AMC or SUMO2-AMC substrate, respectively. Therefore, cell lysates were dispensed in a 384 well plate (flat bottom, black) on ice. For blank measurement, one well was included where cell lysate was replaced by corresponding volume of SEM buffer. A master mix was prepared using 500 ng SUMO-AMC substrate in activity assay buffer. Total volume was adjusted to 50 µl minus volume of the lysate. Finally the appropriate amount of this master mix was added to cell lysates in the plate. After quick spin down, the measurement was started immediately. Therefore, a Synergy H1 plate reader was set to following wavelength to record emitted AMC fluorescence: λ_{Ex} = 380 nm, λ_{Em} = 460 nm. Data analysis was done by Gen5 software in combination with Microsoft Excel.

Following reagents and buffers were used for SUMO-AMC assays:

Buffer	Ingredients/Concentration
SEM buffer	0.25 M Sucrose, 20 mM MOPS-KOH (pH 7.4), 1 mM EDTA-NaOH (pH 8)
Aprotinin	10 mg/ml in H_2O
Pepstatin A	1 mg/ml in DMSO
Leupeptin	10 mg/ml in H_2O
DTT	1 M in H_2O
NEM	1 M in DMSO
PMSF	0.2 M in Isopropanol
Activity assay buffer	50 mM Tris-HCl (pH 7.5), 0.1 mg/ml BSA, 10 mM DTT
SUMO1/2-AMC	Enzo Life Sciences/Boston Biochem

8.5.5 SUMO-VS assays

To determine SUMO protease activity by SUMO1/2-VS adduct formation, cell lysates in SEM buffer ± NEM were prepared like described for SUMO-AMC assay. For a single reaction, 100 µg cell lysate was incubated with 50 ng HA-SUMO1-VS or HA-SUMO2-VS (Boston Biochem) for 15 min at 25 °C. The reaction was stopped by the addition of 6x Laemmli buffer and heating to 95 °C for 5 min. Aliquots of the sample were separated by SDS-PAGE and stained against HA-antibody or individual SUMO isopeptidases. NEM was used as negative control to block the reaction.

8.5.6 Dual-Luciferase Reporter Assays

To measure activating or repressive functions of BHLHE40^{WT} or BHLHE40$^{K159R, K279R}$ on a PGC-1 α promoter, dual-luciferase reporter assay (Promega) was performed. Therefore, HeLa cells were seeded on day one in a 12 well plate with a total cell number of 1x10^5 cells/well. On the second day, the promoter construct, BHLHE40^{WT} or BHLHE40$^{K159R, K279R}$, pCI empty vector and a Renilla control plasmid were introduced using FuGENE as transfection reagent like previously described. The exact amounts and conditions are given in the table below. After 48 h of transfection, cells were washed once in PBS and lysed by the addition of 250 µl passive-lysis buffer provided with the kit (Promega). Lysis was carried out for 15 min at RT while shaking. Afterwards, lysed cells were resuspended and transferred into an Eppendorf tube. For the measurement, the lysate was diluted 1:5 with ddH_2O. 100 µl of LAR II buffer were pre-dispensed into a clear luminometer tube, then 20 µl of the diluted lysate was added, briefly mixed by vortexing and firefly luciferase activity was measured for 10 s. Subsequently, the signal was quenched by 100 µl of Stop & Glo reagent added manually to the tube and Renilla luciferase activity was recorded for another 10 s. Measurements were performed always in duplicates and recorded with an Berthold Lumat LB 9507 by manual insertion of the tubes and reagents. The difference of Firefly and Renilla luciferase activity was calculated by division of

the RLU Firefly luciferase/RLU Renilla luciferase. Data analysis and calculations were performed with Microsoft Excel.

HeLa cells were transfected in following conditions for luciferase reporter assays (* Mut = BHLHE40$^{K159R, K279R}$):

PGC-1 α promoter 2 kb luciferase	pCI empty vector	BHLHE40 WT or Mut *	pRL-SV40 Renilla luciferase
200 ng	400 ng		10 ng
200 ng	200 ng	WT 200 ng	10 ng
200 ng	200 ng	Mut 200 ng	10 ng
200 ng		WT 400 ng	10 ng
200 ng		Mut 400 ng	10 ng

8.5.7 Ni-NTA pulldown

To pull-down SUMOylated versions of a target protein, optionally after knockdown of individual SENPs, His-tagged SUMO isoforms were transiently expressed in HeLa cells. When indicated, experiments were performed in HeLa cells stably expressing His-SUMO1/2 from a tetracycline-inducible promoter. For experiments in His-SUMO expressing cells under siRNA knockdown of an individual SENP, one 10 cm dish per conditions was seeded with a total cell number of 2x10^6. Reverse transfection of desired siRNA was done according to manufacturer's instructions. On day 3, the expression of His-SUMO1/2 was induced by addition of doxycycline in a final concentration of 1 µg/ml overnight. The following day, cells were washed twice in PBS and scraped in 1 ml of lysis buffer (6 M guanidine-HCl, 0.1 M $NaH_2PO_4x2H_2O$, 0.1 M tris, 0.05% Tween, pH 8) per 10 cm dish. Lysates were heated to 99 °C for 15 min, then centrifuged for 20 min at 18000 g at RT. The supernatant was transferred in a new tube, 100 µl were taken for TCA precipitation. Therefore, 20 µl TCA (50%) was added to the lysate mixed by vortexing and incubated on ice for 15 min. After centrifugation at 18000 g for 15 min at 4 °C, supernatant was discarded and the pellet was resolved in 200 µl of ice-cold ethanol (100%). One more centrifugation step

(20 min/18000 g/4 °C) was needed to pellet the precipitate again. The supernatant was carefully discarded and the remaining pellet was dried at 42 °C in the Speed-Vac for 10 min. Then the pellet was resolved in 200 µl Laemmli buffer and heated to 95 °C for 10 min. Input material was now ready for Western blot analysis and was stored at –20 °C.

For pulldown of proteins modified by His-SUMO the remaining lysate was incubated with 30 µl magnetic Ni-NTA-beads (Qiagen) per 10 cm dish on a rotating wheel overnight. On the next day, the supernatant was removed and beads were washed 3x with 1 ml buffer A (8 M urea, 0.1 M $NaH_2PO_4x2H_2O$, 0.01 M tris, 0.05% Tween, pH 8), 2x with buffer B (8 M urea, 0.1 M $NaH_2PO_4x2H_2O$, 0.01 M tris, 0.05% Tween**,** pH 6.4) and a final wash step in PBS. To release His-SUMO-modified proteins, beads were incubated in 30 µl Laemmli buffer for 10 min at 95 °C. Input and a small volume of the pulldown samples were analysed by immunoblotting against His-tag to control for efficient enrichment of SUMOylated proteins. The remaining pulldown samples were stained against protein of interest and its potentially SUMO-modified version. Additional blots were included to check for successful knockdown of chosen SUMO protease.

In case of His-pulldown experiments without involvement of siRNA-mediated knockdown, the reverse transfection was omitted and the protocol was carried out exactly like described above.

8.5.8 Flag-IP

Immunoprecipitation of Flag-tagged proteins was done in 10 cm dishes of HEK293T cells, transfected with the respective plasmids by calcium phosphate method. When HeLa cells were used, transfection was performed using FUGENE as transfection reagent. 48 hours after transfection, cells were washed in PBS and lysed in (radioimmunoprecipitation assay) buffer (50 mM tris pH 7.5, 150 mM NaCl, 1% NP40, 1 mM EDTA, 0.1% sodium deoxycholate) supplemented with protease inhibitors (Aprotinin 2 mg/ml, Pepstatin A 1 mg/ml, Leupeptin 2 mg/ml, PMSF 1 mM). After the lysate was cleared by centrifugation

the remaining supernatant was incubated with 20 µl Flag-M2-beads (washed in RIPA buffer) (Sigma-Aldrich) for 3 h at 4 °C. In the following, beads were washed in lysis buffer and proteins bound to Flag-beads were eluted with Flag-peptide (60 µl, 1:25 in PBS, 30 min at 4 °C) or by direct incubation in Laemmli buffer at 95 °C for 5 min. Eluted samples were used for Western blotting.
For Flag-IP in Figure 26 A, HEK293T cells were lysed in lysis buffer containing 50 mM pH 7.5, 150 mM NaCl, 1.4 mM $MgCl_2$, 1 mM EDTA, 10% (v/v) glycerol, 1% (v/v) Triton-X-100. Flag-IP was carried out like described above wit 20 µl beads per sample at 4 °C overnight. Elution was done by incubation with Flag-peptide (1:25 in PBS) and samples were used for Western blotting.

8.5.9 Endogenous PRP19 IP

To immunoprecipitate endogenous PRP19, HEK293T cells were lysed in RIPA buffer supplemented with inhibitors like described for Flag-IP. After clearance by centrifugation, the supernatant was precleared for 1 h with 15 µl protein A/G agarose (Santa Cruz). The lysate was then incubated for 2 h with 5 µl anti-PRP19 antibody or 2 µl (= 1 µg) IgG mouse antibody as negative control. After these 2 h, 20 µl protein A/G agarose were added to each sample and rotated at 4 °C for another 2 h. Thereafter, beads were washed in lysis buffer and enriched proteins bound to beads were eluted by direct boiling in Laemmli buffer. Eluates were then used for immunoblotting.

8.5.10 Fractionation of cells

To separate HeLa cells in a soluble and a chromatin-bound fraction, one 10 cm dish per condition was washed twice in PBS and scraped in 1 ml of PBS on ice. Centrifugation for 3 min at 800 g and 4 °C was sufficient to pellet the cells. Afterwards they were resuspended in 0.5 ml buffer A (10 mM tris pH 8, 10 mM KCl, 1.5 mM $MgCl_2$, 0.34 M sucrose, 10% glycerol, 0.1% Triton-X-100, 2 µg/ml Aprotinin, 1 µg/ml Pepstatin A, 2 µg/ml Leupeptin, 1 mM PMSF, 10 mM NEM) and incubated on ice for 5 min. Another centrifugation step (2000 g, 5 min, 4 °C) separated the supernatant as soluble fraction. The remaining pellet was washed

in 1 ml of buffer A and centrifuged again. Afterwards, the pellet was resolved in 0.5 ml of buffer B (50 mM tris pH 7.5, 150 mM NaCl, 1% NP40, 0.1% SDS, 1 mM $MgCl_2$, benzonase 1:100, 2 µg/ml Aprotinin, 1 µg/ml Pepstatin A, 2 µg/ml Leupeptin, 1 mM PMSF, 10 mM NEM) and incubated for 15 min at 37 °C while shaking. Centrifugation at 16000 g for 10 min at 4 °C separated the supernatant as chromatin-bound fraction.
In experiments where Flag-tagged proteins were immunoprecipitated from fractionated cells, Flag-beads were washed prior use in buffer A/B without sucrose/SDS and then used for Flag-IP like described above. This method was applied for experiment in Figure 26 A.

Separation of HeLa cells into a cytoplasmic fraction, a soluble and an insoluble nuclear fraction was done for experiment in Figure 28 C to control for the distribution of distinct proteins on chromatin. Therefore, cells were washed in PBS and then scraped off using 1 ml of cold PBS. After centrifugation at 700 g for 4 min at 4°C, the pellet was resuspended in 0.5 ml buffer A (10 mM HEPES pH 7.9, 10 mM KCl, 1.5 mM $MgCl_2$, 0.34 M sucrose, 10% glycerol, 1 mM DTT, 0.1% Triton-X-100, 2 µg/ml Aprotinin, 1 µg/ml Pepstatin A, 2 µg/ml Leupeptin, 1 mM PMSF) and incubated on ice for 5 min. Afterwards, centrifugation was carried out at 1300 g for 4 min at 4°C. The supernatant was taken as cytosolic fraction. After repeated centrifugation (15 min/20000 g/4°C), the pellet was washed once in 1 ml buffer A and centrifuged again (4 min/13000 g/4°C). The supernatant was discarded and the pellet was dissolved in 0.5 ml buffer B (3 mM EDTA, 0.2 mM EGTA (ethylene glycol-bis(2-aminoethylether)-*N,N,N′,N′*-tetraacetic acid), 1 mM DTT, 2 µg/ml Aprotinin, 1 µg/ml Pepstatin A, 2 µg/ml Leupeptin, 1 mM PMSF). After centrifugation at 1700 g for 4 min at 4°C, the supernatant was taken as soluble nuclear fraction and the pellet was washed once in 1 ml buffer B. An additional centrifugation step at 1700 g and 4°C for 4 min was needed to separate the supernatant from the pellet. The supernatant was discarded and the remaining pellet was solved in 500 µl 4% SDS/0.1 M tris pH 7.6. Sonication was carried out for 15 s, then the solution was heated to

95°C for 5 min. Those remaining proteins were taken as insoluble nuclear fraction.

8.5.11 Endogenous SUMO1 and SUMO2/3 IPs

Endogenous SUMO1 and SUMO2/3 IPs were performed like described in Barysch *et al*., 2014[53]. Therefore, affinity matrix was prepared using 8 mg of SUMO1 (clone 21C7) or SUMO2/3 (clone 8A2) antibody cross-linked to protein-G-agarose. As negative control, the same amount of mouse IgG antibody was used. Preparation of the cell lysate for IP and following mass spectrometric analysis was done exactly like described in the above-mentioned publication. To control for successful enrichment, a small aliquot of the IP sample was stained against SUMO1 or SUMO2/3 by immunoblotting. Mouse IgG coupled to protein-G-agarose was used as negative control for immunoprecipitation. Experiments were performed in triplicates for each condition to enable proper statistics in following mass spectrometric analysis.

For SUMO1 IPs 13 mg of HeLa cell lysate were used for each condition. For SUMO2/3-enrichment from U-2 OS cells, 8 mg per IP were used and for SUMO2/3 IP from SENP6-depleted HeLa cells, 17 mg were used. Additionally, 20-30 μg input samples were taken and subjected to in-gel digestion for proteome measurements by LC-MS/MS.

8.6 Liquid chromatography and mass spectrometry

8.6.1 Sample preparation for LC-MS/MS analysis

8.6.1.1 In-gel digestion

TCA-precipitated IP samples and proteome samples from endogenous SUMO IPs were separated by SDS-PAGE using 4-20% gels (Mini-PROTEAN® TGX™ Gels, Bio-Rad). The gel was shortly rinsed with MilliQ water and then stained for 20 min with InstantBlue. After staining, the gel was rinsed again 3x with MilliQ-water, then individual bands were sliced into equal small pieces (≈ 1 mm per side) and placed into a 96 deep well plate. Unless otherwise stated, all following

steps were performed at RT in a 96 well format. Gel pieces were washed 3x for 15 min with 150 µl 50 mM ABC (ammonium bicarbonate)/50% ethanol, then dehydrated by incubation 2x in 150 µl ethanol (100%). Afterwards, gel pieces were dried in the Speed-Vac for 5 min. Proteins were reduced by incubation in 150 µl 10 mM DTT (in 50 mM ABC) for 45 min at 56 °C. Solution was discarded afterwards and alkylation was carried out subsequently by addition of 150 µl 55 mM CAA (chloroacetamide) (in 50 mM ABC) for 30 min in the dark. Afterwards, several wash and dehydration steps were included. Gel pieces were incubated for 15 min first in 150 µl 50 mM ABC, then in 150 µl ethanol (100%), followed by 150 µl 50 mM ABC again. Finally, samples were dehydrated twice in 150 µl ethanol (100%) and dried for 5 min in the Speed-Vac. Proteins were digested by the addition of 40 µl trypsin (Sequencing-grade, Promega, 12 ng/µl in 50 mM ABC). After swelling of gel pieces at 4 °C for 15 min, another 80 µl 50 mM ABC were added and incubation was performed at 37 °C overnight. On the following day, peptide-containing supernatant was separated from gel pieces and stored in a new plate. Residual peptides were extracted from the gel pieces by incubation with buffers containing increasing concentrations of acetonitrile and corresponding supernatants were collected. First, gel pieces were incubated in 100 µl 30% ACN (acetonitrile)/3% TFA for 20 min. The supernatant was combined with the digested peptide solution in the 96 well plate. For further extraction, gel pieces were incubated twice in 70% ACN for 20 min, then in 100 µl ACN (100%) for another 20 min. Finally, the volume of all collected supernatants was reduced to 80 µl in a Speed-Vac at 30 °C. Dried down samples were acidified by addition of buffer C (5% ACN, 1% TFA (trifluoroacetic acid) in MilliQ water) in a 1:1 ratio.

8.6.1.2 Stage-tipping

For concentration and desalting of the samples, the Stage tipping technique was applied. Therefore, two layers of C18 (octadecylsilane) material were assembled in a 200 µl pipette tip and washed for activation and equilibration with different buffers. All centrifugation steps were carried out in 96 well pipet tip boxes for 2 min at 750 g and RT. First, C18 material was activated by 50 µl

methanol (100%), then equilibrated with 50 µl buffer B (80% ACN and 0.1% FA (formic acid) in MilliQ water), following two wash steps in 50 µl buffer A (0.1% FA in MilliQ water). Samples mixed with buffer C were loaded onto the Stage tips and centrifuged until no liquid was left on top of the C18 material. A final wash step with 50 µl buffer A was included before Stage tips were dried using a syringe and stored at 4 °C until use.

For elution of peptides from Stage tips, C18 material was incubated with 30 µl buffer B for 15 min at RT (covered). Samples were eluted directly into a 96 well plate (e.g. from Greiner, suitable to be inserted into the HPLC) and concentrated to 2-3 µl using a Speed-Vac. The remaining volume was filled up to 10 µl with buffer A, the plate was covered with a lid, gently mixed, centrifuged and then subjected to LC-MS/MS analysis.

8.6.1.3 In-solution digestion

For proteome measurements independent of IP samples (Supplemental Figure 1 A), cells were rinsed in PBS, lysed in 4% SDS buffer (4% SDS in 0.1 M tris-HCl pH 7.6) and heated to 95 °C for 5 min. Then the lysate was sonicated to shear DNA and cleared by centrifugation (16000 g, 5 min). After determination of protein content, 20 µg of each sample was precipitated for 1 h at -20 °C by adding 4 volumes of cold (-20 °C) acetone (100%). The precipitated proteins were pelleted by centrifugation at 15000 g for 10 min at 4 °C and the pellet was washed with 100 µl cold (-20 °C) acetone (90%). After another centrifugation step, the supernatant was removed completely, the pellet was dried at RT for 10 min and then resolved in 20 µl 6 M urea/2 M thiourea (in 10 mM HEPES pH 8). Disulphide bonds were reduced by incubation with 1 µl DTT (1 M) for 30 min. The following alkylation was performed by adding 1 µl CAA (550 mM) and incubation in the dark for 20 min. Thereafter, proteins were digested with LysC (Wako) at an enzyme:substrate ratio 1:100 for 1 h at RT, then the sample was diluted with 50 mM ABC to generate a 2 M urea buffer system, where the protease trypsin is able to cleave. Trypsin was added to the sample (protein:trypsin ratio 100:1) and incubated overnight at 37 °C. On the following day, digest was stopped by the addition of 80 µl buffer C to acidify the sample.

Samples were now ready for desalting and concentration on Stage tips like described above. For further LC-MS/MS analysis involving label-free quantification, samples were always prepared in triplicates for proper statistical analysis.

8.6.2 Instrument settings

LC-MS/MS analysis for SUMO1-enriched targets was carried out by Soraya Hölper at the MPI in Bad Nauheim using instruments and settings described in the following. For mass spectrometric analysis, a quadrupole-based Q Exactive HF mass spectrometer coupled via a nano-electrospray ionization source to a NanoLC 1000 was used. Enriched peptides were separated by their hydrophobicity on an in-house packed, 20 cm long column, filled with 1.9 μm C18 beads (Dr. Maisch GmbH). The binary buffer system for UHPLC (ultra high performance liquid chromatography) system consisted of buffer A and B (described in chapter 8.6.1.2). For SUMO1 IP and proteome samples, a 35 min gradient/75 min gradient was used, respectively. The gradient increased from 7-38% buffer B in 20 min/55 min in a linear fashion, followed by an increase to 95% B within 5 min/10 min. Finally, a re-equilibration step to 5% B was included.

The instrument settings are listed in the following table:

Description	Settings for IPs	Settings for proteomes
AGC target for acquired MS spectra	$3x10^6$	$3x10^6$
Maximal injection time	20 ms	20 ms
Resolution at 200 m/z (mass/charge)	60000	15000
MS/MS spectra of top 15 intense peaks were generated using HCD (higher-energy collisional dissociation) fragmentation		
Resolution for MS/MS spectra at 200 m/z	30000	15000

AGC target for MS/MS spectra	$1x10^5$	$1x10^5$
Maximal injection time	64 ms	25 ms
Isolation window	1.8 Th	2.2 Th

The instrumentation for LC-MS/MS analysis of endogenous SUMO2/3 IPs and proteome samples in Frankfurt was composed of an Easy-nLC 1200 coupled via nano-electrospray ionization source to a Q Exactive HF mass spectrometer. In-house packed, 17 cm long, 75 μm ID columns filled with 1.9 μm C18 beads were used to separate the peptides according to their hydrophobicity. Like described above, the buffer system for UHPLC and mass spectrometry consisted of buffer A and B. Proteome samples were measured with a linear gradient of 75 min (7-38% B in 53 min). Following an increase up to 60% B in 5 min and a final concentration of 100% B reached within 5 min. In the last 5 min of the gradient, a re-equilibration to 5% B was included. For SUMO2/3-enriched samples, a shorter gradient of 35 min was applied. Here, a concentration of 38% B was reached in 23 min, followed by an increase up to 60% in 2 min. Finally, the proportion of buffer B was increased to 100% in 2 min for a duration of 5 min with a subsequent decrease to 5% B in 2 min.

Instrument settings for LC-MS/MS analysis of SUMO2/3 IPs and proteomes:

Description	**Settings for IPs**	**Settings for proteomes**
AGC target for acquired MS spectra	$3x10^6$	$3x10^6$
Maximal injection time	20 ms	20 ms
Scan range	300-1650 m/z	300-1750 m/z
Resolution	60000	60000
MS/MS spectra of top 15 intense peaks were generated using HCD fragmentation		
Resolution for MS/MS spectra	30000	15000
AGC target for MS/MS spectra	$1x10^5$	$1x10^5$
Maximal injection time	64 ms	25 ms
Isolation window	1.6 m/z	1.6 m/z

8.6.3 Downstream data analysis

Raw files from SUMO1 IP LC-MS/MS analysis were processed using MaxQuant (version 1.5.3.12) and its implemented Andromeda search engine. Fragmentation spectra generated by ESI-MS/MS were correlated with the Uniprot human database (version 2015), including a list of common contaminants, to assign proteins. Tryptic digest and default settings for mass tolerances of MS and MS/MS spectra were applied to perform the searches. Carbamidomethyl was defined as fixed modification at cysteines, whereas acetylation at N-termini and oxidation of methionine were set as variable modifications. The minimal peptide length was set to seven amino acids and the FDR (false discovery rate) for proteins and peptide-spectrum matches was designated to 1%. Using the MaxLFQ algorithm integrated into MaxQuant, relative label-free quantification of proteins was carried out with a minimum LFQ ratio count of 2 and enabled FastLFQ option. The match-between-run feature was used with a time window set to 1 min.

Further data analysis and statistics were done with the Perseus software (version 1.5.0.31). First, contaminants and reverse entries, as well as proteins only identified by a modified peptide were removed. The log2 value of all LFQ intensities was calculated and samples were grouped into triplicates. In the SUMO1 IP dataset, missing values were replaced by the imputation function of the Perseus software. Therefore, proteins that were quantified less than 3 times in one of the experimental groups were excluded from further analysis. Afterwards, the missing values were imputed column-wise applying a downshifted (median-1.8) Gaussian distribution, simulating the detection limit of the machine. Using the histogram analysis function of the software, normal distribution of the LFQ values was visually checked. Good correlation of the experimental replicates was assured by multiscatter plot analysis. The dataset was exported and used for further analysis in Microsoft Excel. Volcano plots were generated using the RStudio software.

Downstream analysis of raw files from SUMO2/3 IPs were analysed like described above using the MaxQuant software (version 1.5.8.0). In contrast to

the settings used for SUMO1 IP described above, here the Uniprot human database from 2017 was used and the minimal unique peptides for identification were set to 1. The match time window was defined as 0.7 min and only unique peptides were allowed for protein quantification.
Filtering and analysis of the dataset with the Perseus software (version 1.5.8.5) was done like described for the SUMO1 IP dataset except for the imputation of missing values. This option was not used for the SUMO2/3 IP datasets. Visual representation of the data was achieved using the RStudio program (version 0.99.893).

8.7 Functional protein network and enrichment analysis

The Panther gene list analysis tool (http://www.pantherdb.org) was used to reveal the most enriched GO BP terms of the SUMO2/3 IP dataset under SENP6 knockdown. As annotation dataset, the GO BP complete list was used and a binominal test-type was applied. Additionally, the option for Bonferroni correction for multiple testing was enabled. As reference list, all SUMO targets with a log2 value > 1 plus the ones at least twice exclusive in siSENP6 were used.

STRING networks of interacting proteins from SUMO2/3 IPs were generated using the freely available STRING database (https://string-db.org, version 10.5). For all analyses, the parameters were set to highest confidence level and the MCL (Markov clustering) function with an inflation of 3 was used. The use of experimental data and databases was enabled and non-connected proteins were excluded from the visualized networks. For networks of interactome data, only proteins with a log2 ratio > 1.35 were used, for targetome data this value was set > 1. Here, targets at least twice exclusive in siSENP6 or SENP3 KO conditions were included.

9 Supplement

9.1 Supplemental Figures

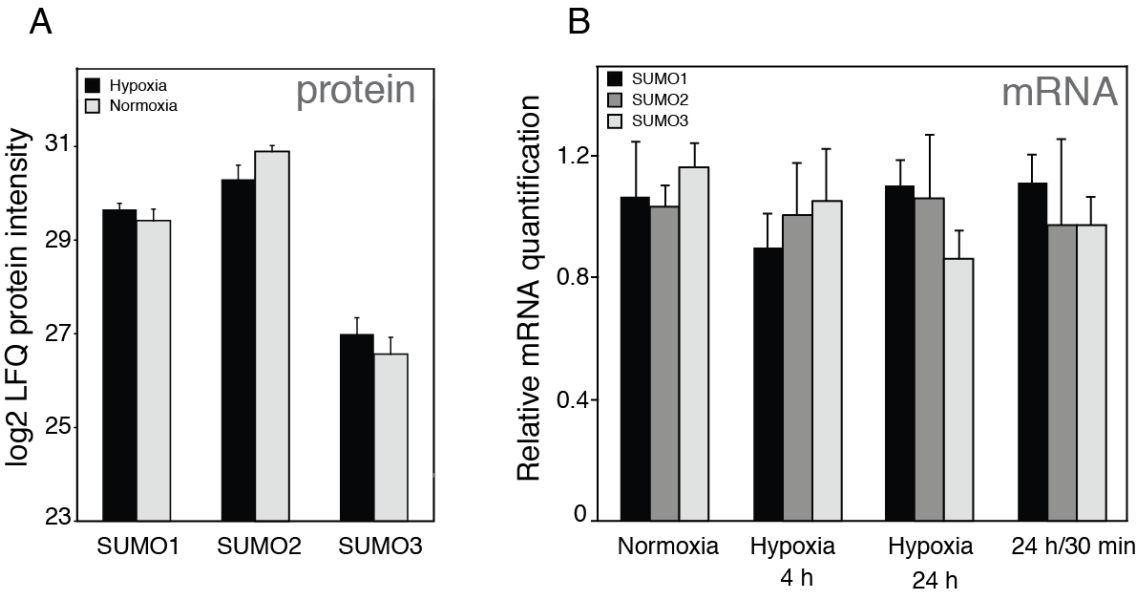

Supplemental Figure 1: Protein and mRNA levels of SUMO1, SUMO2 and SUMO3 in normoxic and hypoxic cells. (A) Quantitative LC-MS/MS analysis of whole cell proteomes of normoxic and hypoxic (24 h) HeLa cells. Label-free quantification enabled the comparison of log2 LFQ protein intensities for SUMO1, SUMO2 and SUMO3. **(B)** HeLa cells were cultured for indicated time points under normoxia or hypoxia. One sample was reoxygenated after 24 h for 30 min. Then, mRNA expression for all three SUMO isoforms were quantified using RT-q-PCR. Given values were normalized for TBP levels and represent the average (± SD (standard deviation)) of triplicates from two independently performed experiments. From Kunz *et al.*[52].

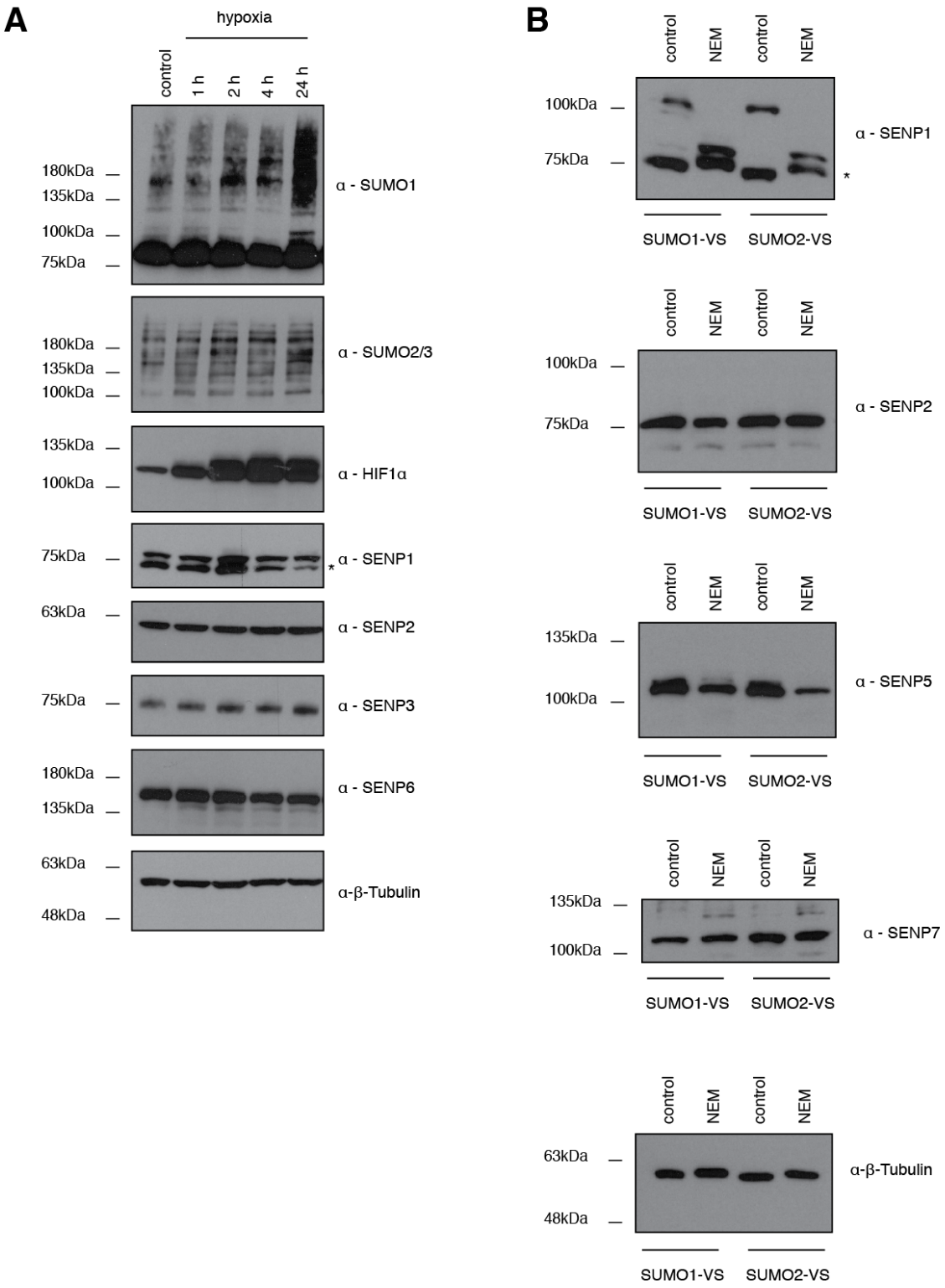

Supplemental Figure 2: Protein levels and activity of SENPs under normoxic and hypoxic conditions. (A) Cell extracts from HeLa cells under normoxia or hypoxia for indicated time points were separated by SDS-PAGE and blotted against SUMO1, SUMO2/3, HIF1α, SENP1, SENP2, SENP3, SENP6 and β-tubulin. Asterisk indicates an unspecific band of the SENP1 antibody. **(B)** HeLa cell extracts were prepared in SEM buffer ± NEM. Incubation with SUMO1-VS or SUMO2-VS was carried out at 25 °C for 15 min. Proteins were separated by SDS-PAGE and stained against SENP1, SENP2, SENP5, SENP7 and β-tubulin. Asterisk marks an unspecific band detected with the SENP1 antibody. From Kunz *et al.*[52].

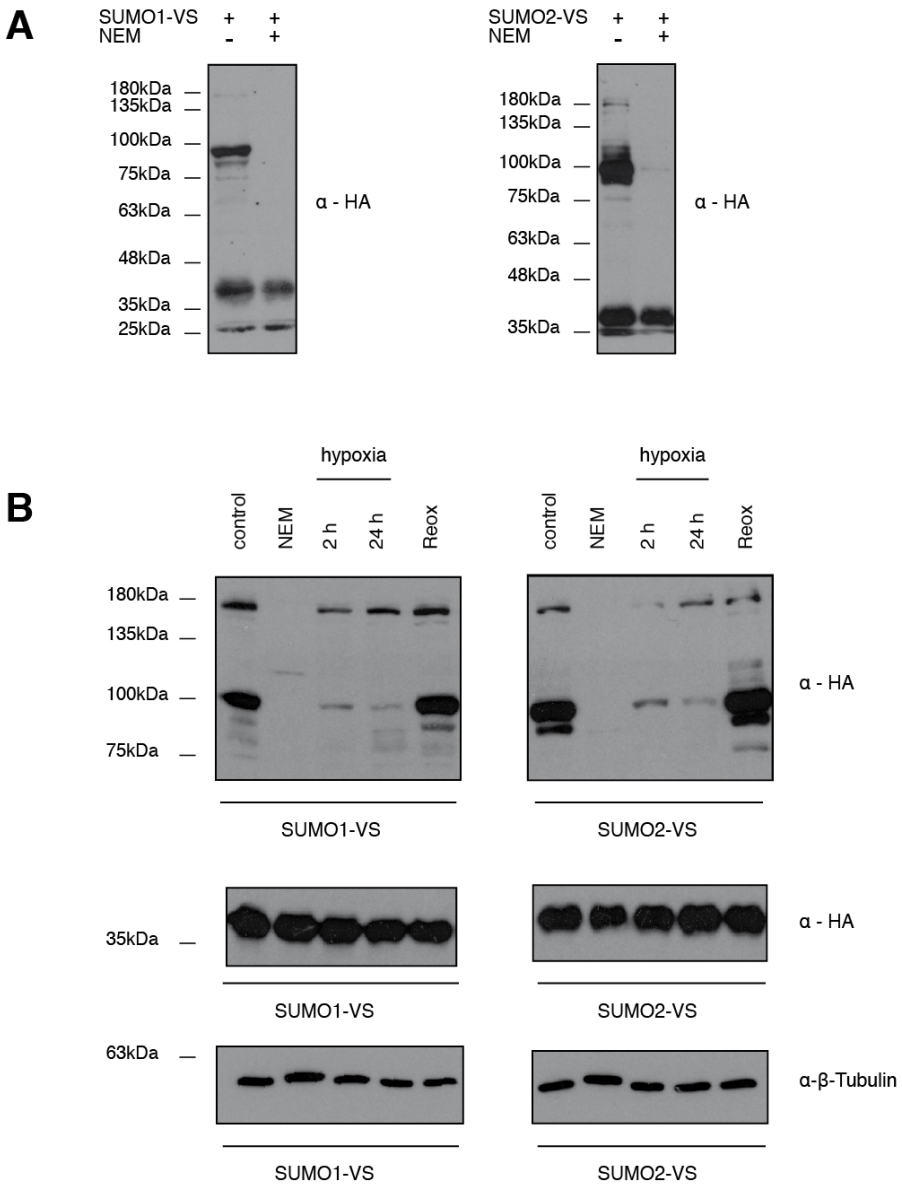

Supplemental Figure 3: Staining against HA-tag of SUMO-VS substrates in normoxic and hypoxic cell extracts. (A) HeLa cell extracts from Supplemental Figure 2 B were stained against the HA-tag of the SUMO1-VS (left panel) or SUMO2-VS (right panel) substrate. In the second lane of each blot, NEM was added as negative control. **(B)** HeLa cells were cultured under normoxic or hypoxic conditions for indicated time points. One sample was reoxygenated for 30 min after 24 h of hypoxia. Cells were lysed in SEM buffer, to the sample in lane 2, NEM was added to abolish SENP activity. Then, extracts were incubated with either SUMO1-VS or SUMO2-VS for 15 min at 25 °C, then the reaction was stopped by the addition of Laemmli buffer and proteins were separated by SDS-PAGE. Staining against the HA-tag of the SUMO-VS substrate revealed conjugated substrate in the upper panel whereas the middle panel shows free HA-SUMO-VS substrate. Probing against β-tubulin served as loading control. From Kunz *et al.*[52].

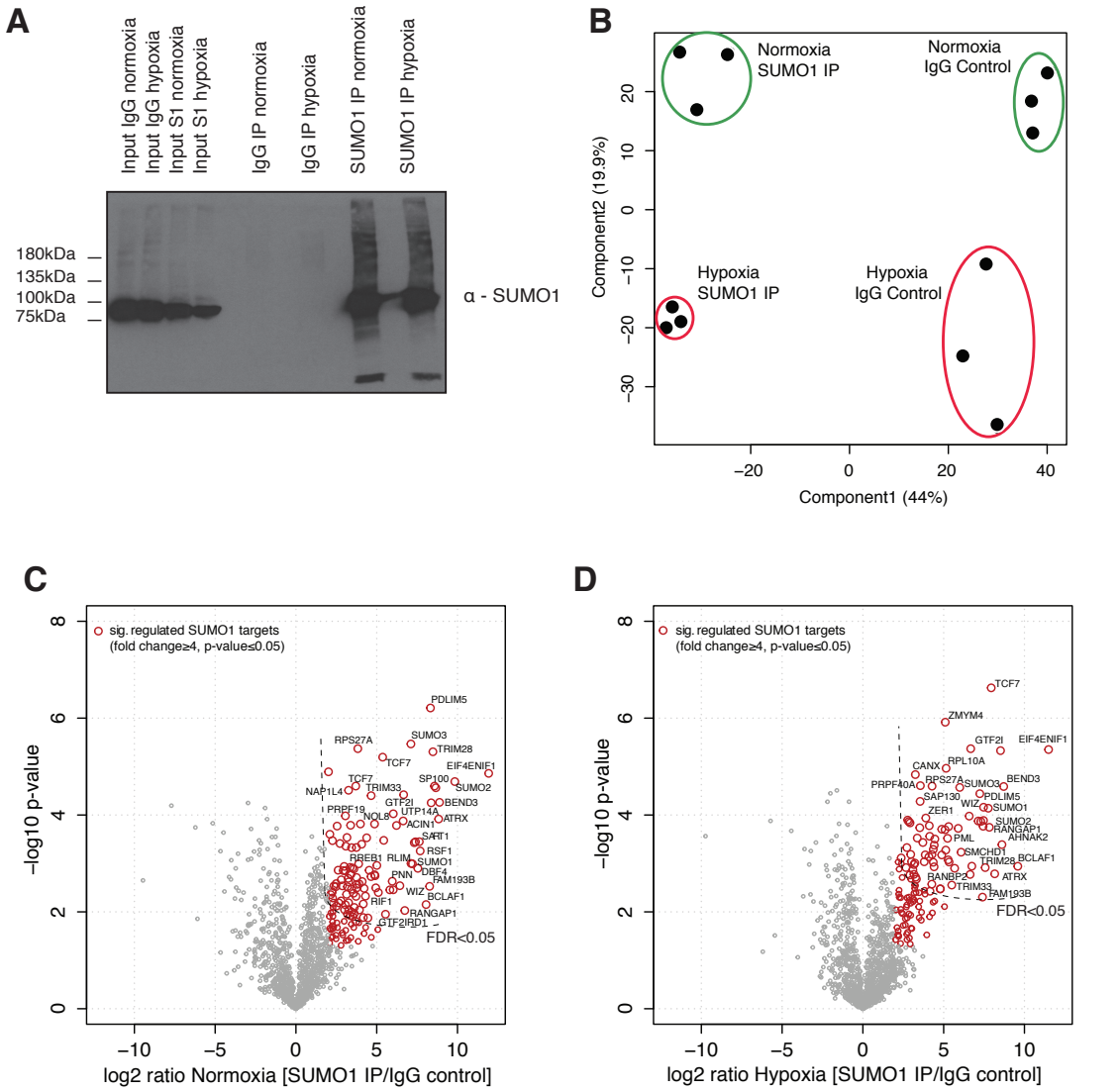

Supplemental Figure 4: Quantitative SUMO1 IPs from normoxic and hypoxic cells. (A) Western blot analysis of input and IP samples of SUMO1 or IgG IP in normoxic and hypoxic HeLa cells. Represented is one out of three replicates for each condition to ensure efficient enrichment of SUMO1-conjugates for subsequent MS-based analysis. Therefore, a small aliquot of input material of SUMO1 IP or IgG IP from normoxic and hypoxic HeLa cells as well as IP samples were probed against SUMO1. **(B)** Principle component analysis of SUMO1 or IgG IP from normoxic or hypoxic cells shows high similarity of the respective triplicates. **(C, D)** Significantly enriched SUMO1 targets after IP from normoxic (C) or hypoxic (D) cells. Only proteins with a p-value < 0.05 and a 4-fold enrichment over the IgG control are considered as significantly regulated and are depicted as red circles. From Kunz *et al.*[52].

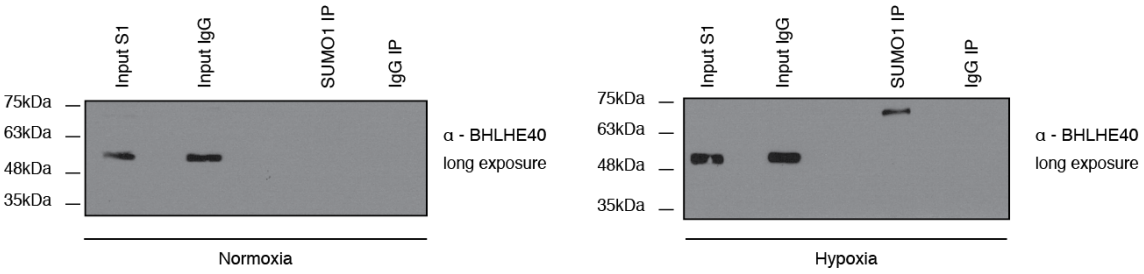

Supplemental Figure 5: Hypoxic SUMOylation of the transcriptional co-repressor BHLHE40. Long exposure of Figure 15 A. From Kunz *et al.*[52].

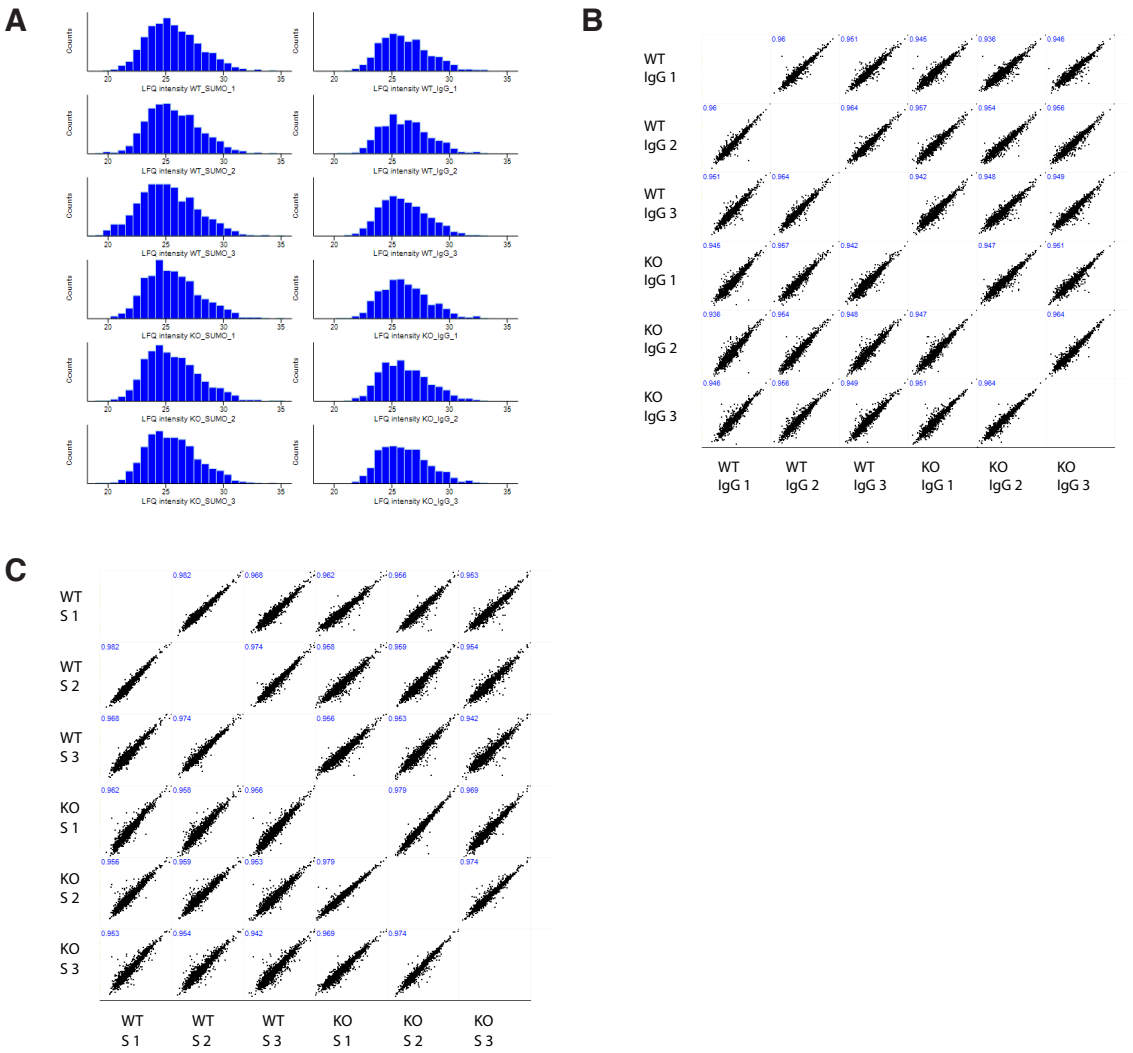

Supplemental Figure 6: Quality control of endogenous SUMO2/3 IP-MS results from U-2 OS WT and SENP3 KO cells. (A) Distribution of the LFQ intensities visualized by histogram analysis to ensure Gaussian distribution of the values. **(B, C)** Multiscatter plot analysis was performed separately for all proteins measured in IgG control IPs (B) or SUMO2/3 IPs (C) from WT and KO cells. Pearson correlation coefficient was included to monitor similarity among the triplicates.

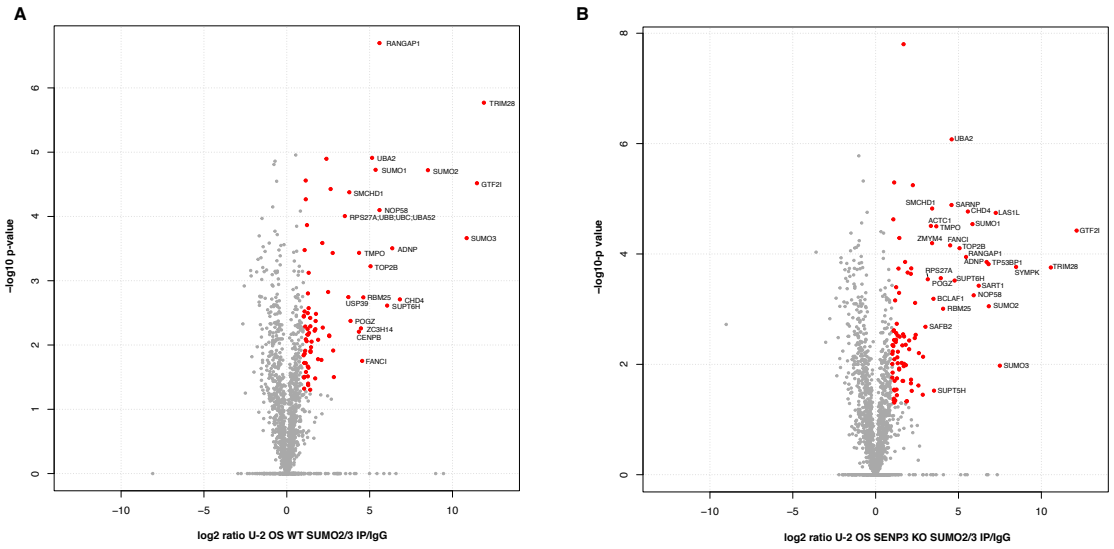

Supplemental Figure 7: Enrichment of SUMO2/3 conjugates from U-2 OS WT and SENP3 KO cells over the IgG control. (A, B) Volcano plot depicting significantly enriched proteins in SUMO2/3 IP over IgG IP in U-2 OS WT cells (A) or SENP3 KO cells (B). Proteins marked with red dots are high-confident hits with a p-value < 0.05 and an enrichment over IgG control of more than 2-fold.

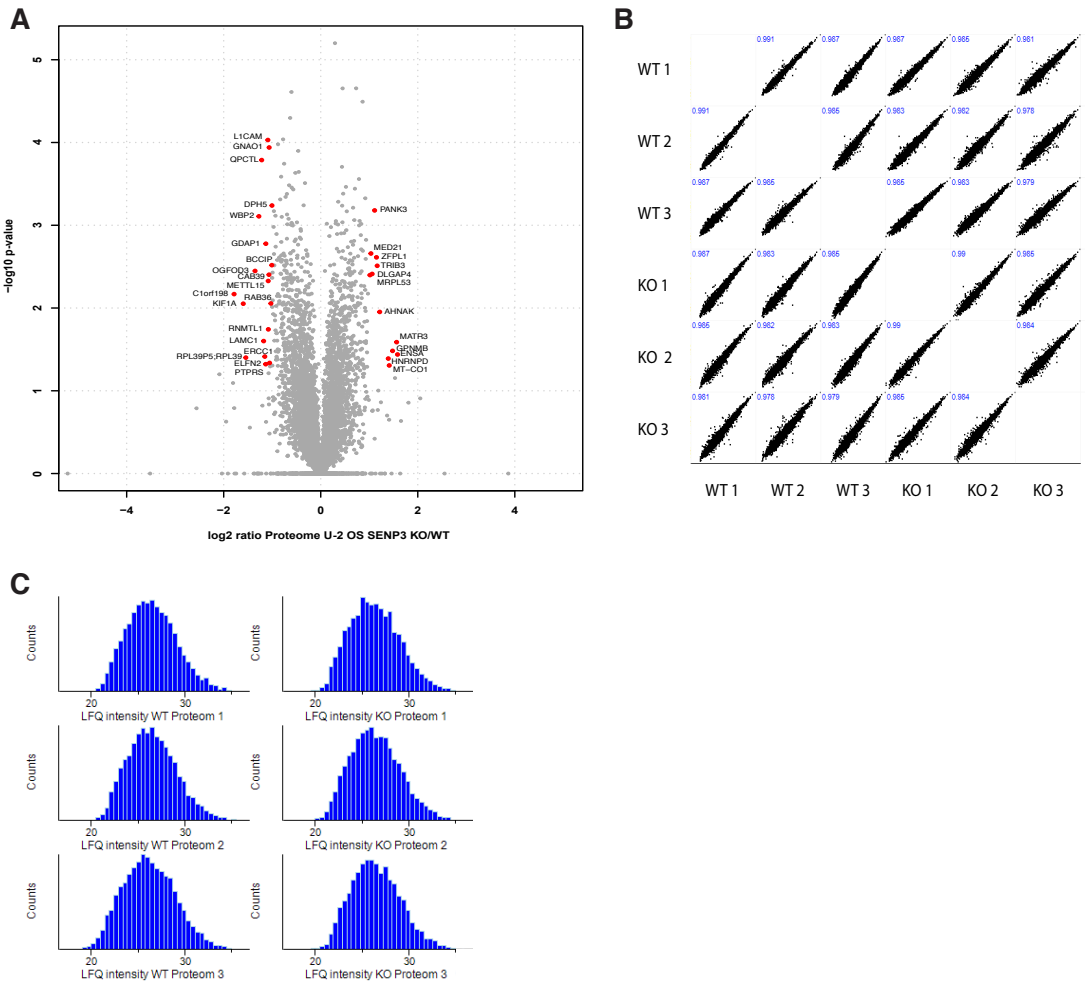

Supplemental Figure 8: Whole cell proteome analysis of U-2 OS WT and SENP3 KO cells. (A) Volcano plot summarizing significantly regulated proteins in U-2 OS SENP3 KO versus WT cells. Proteins

with a p-value < 0.05 and an absolute log2 ratio > 1 are considered as significantly regulated. **(B)** Multiscatter plot analysis of all proteins in WT or KO cells including Pearson correlation coefficient depicts similarity of all replicates. **(C)** Histogram analysis shows the distribution of the LFQ intensities for all replicates to ensure a Gaussian distribution of measured intensities.

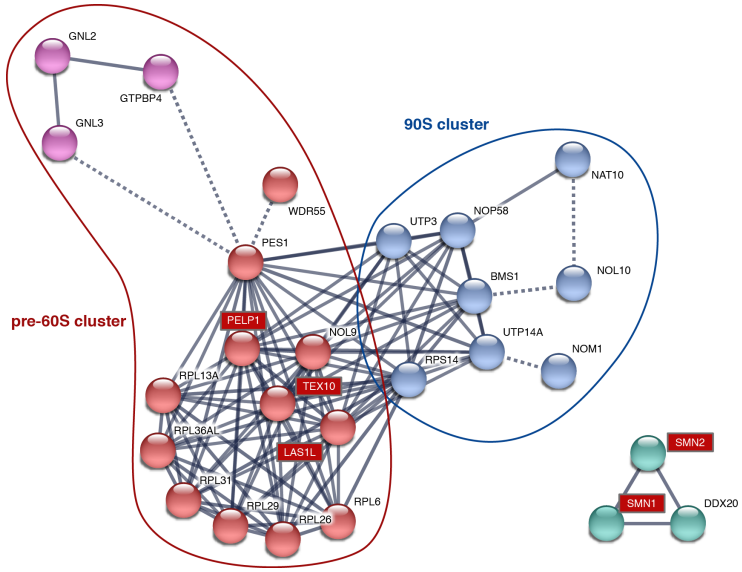

Supplemental Figure 9: Condensed core clusters of SENP3-regulated interactors and targets. Displayed are the core clusters from the integrated STRING network analysis of SENP3 interactors and target proteins from Figure 20.

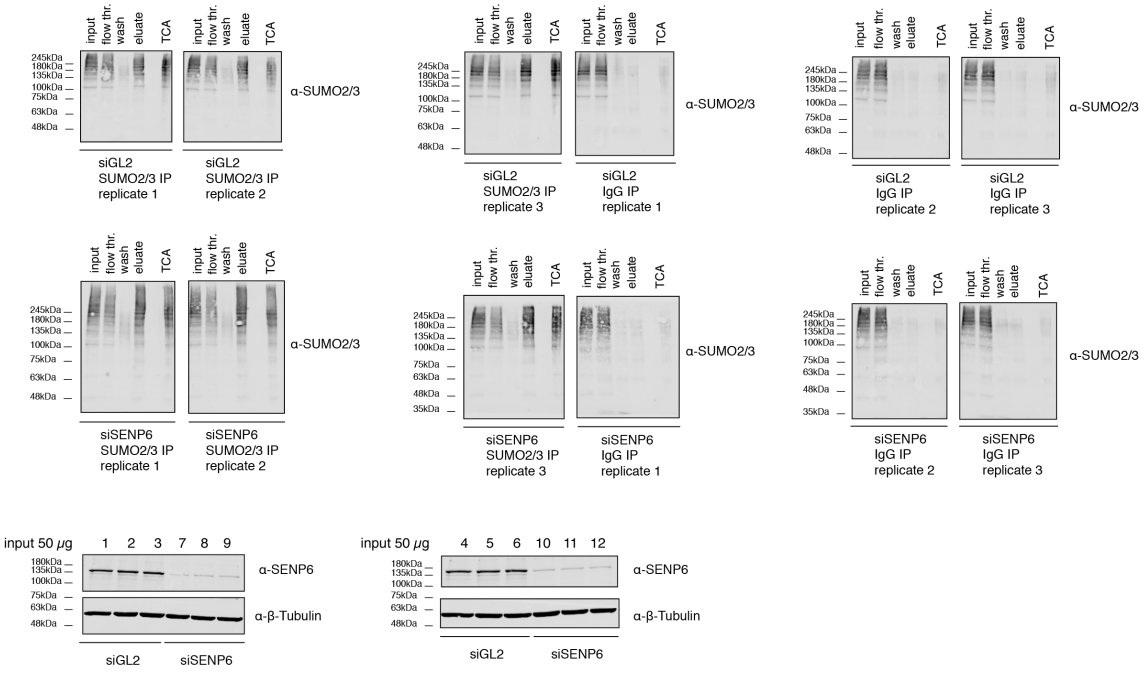

Supplemental Figure 10: Quality control of the SENP6 targetome IPs. To control for successful enrichment of SUMO2/3 conjugates in SENP6 depleted HeLa cells or control cells, samples were taken from different steps in the protocol. Input material, flow-through after IP, pre-elution wash step, a small aliquot of the eluted material and the final TCA-precipitated material were separated by SDS-PAGE and stained for SUMO2/3. Furthermore, all replicates were checked for proper SENP6 depletion by staining 50 µg input material against SENP6 or β-tubulin as loading control.

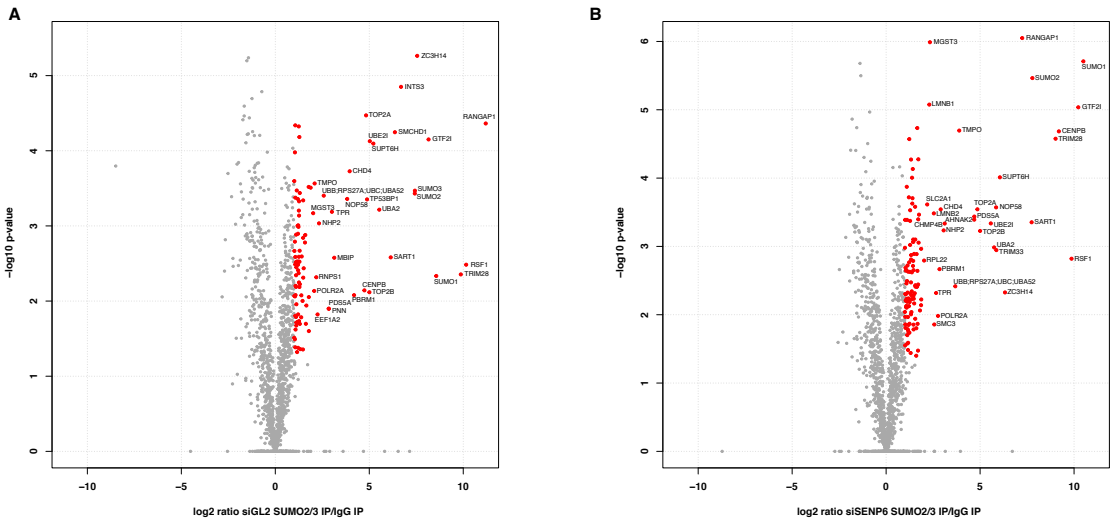

Supplemental Figure 11: Significantly enriched SUMO2/3 targets from control cells or SENP6 depleted cells. (A, B) Volcano plot summarizing the high-confident SUMO2/3 targets enriched over the IgG control IP from control cells (A) or siSENP6 treated cells (B). Proteins depicted as red dots fulfil the confidence criteria with a p-value < 0.05 and a log2 ratio > 1 in SUMO2/3 IP over IgG control.

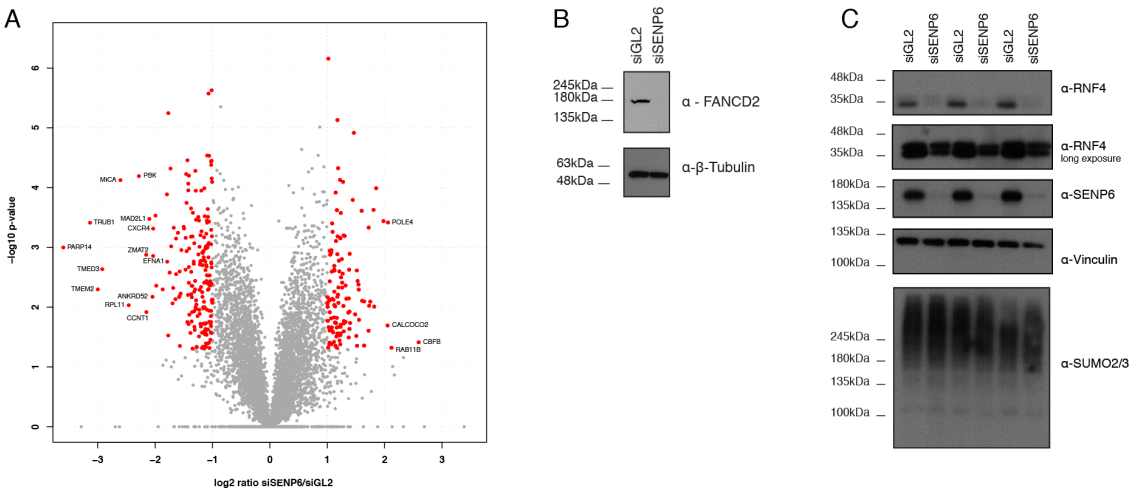

Supplemental Figure 12: Effects of SENP6 depletion on the whole cell proteome, on SENP6 targets and on RNF4 protein levels. (A) Whole cell proteome of SENP6 depleted HeLa cells in comparison to control cells is depicted in a volcano plot. Significantly changed proteins (p-value < 0.05 and absolute log2 ratio > 1) in siSENP6/siGL2 are marked as red dots. **(B)** Validation of the loss of FANCD2 under siSENP6. HeLa cells were depleted from SENP6 or control siRNA, lysed in Laemmli buffer and separated by SDS-PAGE. Staining was performed against FANCD2 and β-tubulin as loading control. **(C)** Input material in triplicates from SUMO2/3 IPs of SENP6-depleted HeLa cells or control cells was checked for RNF4 levels by staining against RNF4, SENP6, vinculin and SUMO2/3.

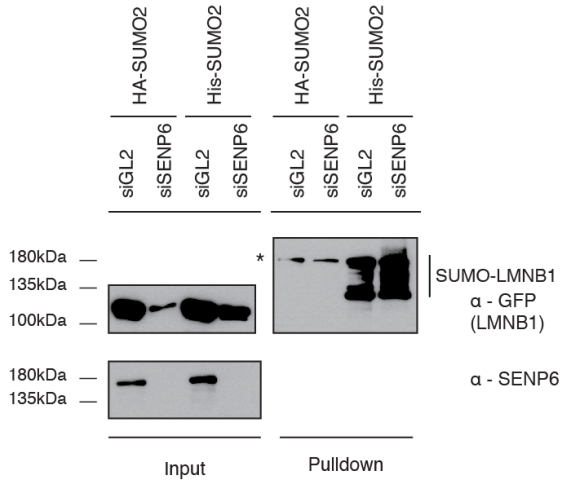

Supplemental Figure 13: HeLa cells depleted of SENP6 or control siRNA were introduced with His-SUMO2 or HA-SUMO in addition to GFP-LMNB1. After denaturing lysis, Ni-NTA pulldown of His-SUMO2 was performed, proteins were size-separated and stained against SENP6 to control for proper knockdown and against GFP-tag of LMNB1. Asterisk marks an unspecific band detected with the GFP antibody.

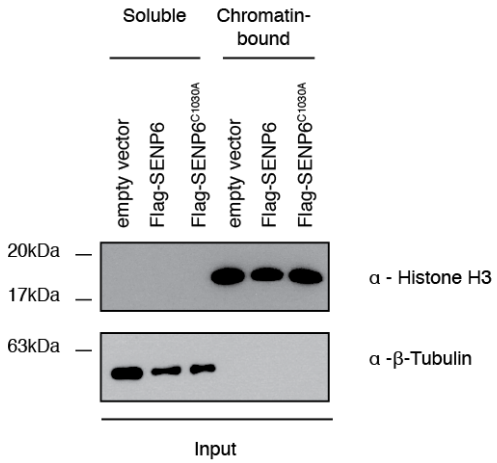

Supplemental Figure 14: Quality check of cellular fractionation in soluble and chromatin-bound fractions. Addition to Figure 26 A. Input material of cell lysates from Figure 26 A was probed against histone H3 or β-tubulin to ensure proper fractionation of the samples in soluble and chromatin-bound material without contamination.

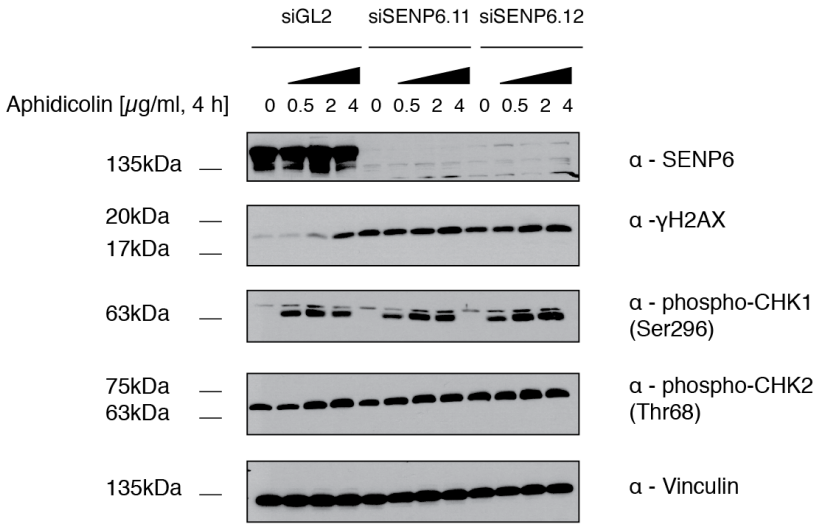

Supplemental Figure 15: Negative effects of SENP6 depletion on CHK1 activation. SENP6 was depleted from HeLa cells by using two different siRNAs. After treating cells with aphidicolin for 4 h with indicated concentrations, cell lysis was performed in Laemmli buffer, followed by separation of proteins by SDS-PAGE and transfer onto membranes. Staining was done with antibodies against SENP6, γ-H2AX, phospho-CHK1, phospho-CHK2 and vinculin serving as loading control.

9.2 Supplemental Table

Supplemental Table 1 contains gene names of SENP3 and SENP6 interactors and targets matching following criteria:

- SENP3 and SENP6 interactors: At least 2.5-fold enrichment over mock control and a p-value < 0.05
- SENP3 and SENP6 targets: At least 2-fold enrichment over IgG control and a p-value < 0.05 plus hits identified exclusively at least twice in siSENP6 or SENP3 KO cells.

SENP6 interactors	SENP6 targets	SENP3 interactors	SENP3 targets
AIFM1	AAAS	AHNAK	BAG2
AKAP10	ADNP	AKAP8	BCORL1
AKAP8L	AHCYL1	ARF1	BEND7
ANK3	AHCYL2	ARF3	BMS1
AP2M1	AHNAK2	ARHGEF2	BRE

ARAF	BCOR	BLM	CASP8AP2
ARHGEF2	CBX1	CAND2	CD3EAP
ATG2B	CCBL2	CCNT1	CHAMP1
ATM	CENPB	CDC7	CRYAB
ATP6V1E1	CENPC	CDK5RAP3	CUL3
BCAS2	CENPH	CDKN2AIP	DMAP1
BRCA2	CENPT	CEP170	EHMT1
C7orf50	CENPU	CHTF18	EPC1
CAD	CHMP4B	CKAP2	GBF1
CCNT1	CIRBP	CLPB	GON4L
CDC5L	CIZ1	CNNM3	GTF2IRD1
CDC7	COLGALT1	COIL	HMGCL
CDKN2AIP	COPS3	DDX10	INO80
CHCHD4	CTCF	DDX20	KMT2C
CKAP2	FANCI	DDX24	KMT2D
CRYBG3	FSBP	DDX46	LARS2
DCAF8	GDI1	DYM	LAS1L
DHCR7	GLYR1	DYNC1LI1	MKI67
DNA2	GNPDA1	EHD1	MRPS5
DNAJA3	GTPBP4	EMD	MYPOP
DYM	HNRNPUL1	ERBB2IP	NFRKB
ECT2	IRF2BP1	FANCD2	NOL10
EMD	LMNA	FASTKD2	NOL9
ERBB2IP	LMNA	FOXC1	NPAT
ESF1	LMNB1	G3BP2	NUMA1
EXOC2	LMNB2	GLB1	PELP1
FAM83H	LMO7	GNL2	RAB11FIP1
FANCA	MAGT1	GNL3	RAB11FIP2
FANCD2	MRPL18	GPRASP2	RIF1
FANCI	MVP	GTF3C5	RPL26
FASTKD5	MYOF	GTPBP4	RPL26L1
FOXK2	NBAS	HEATR6	RPL29

GEMIN2	NCAPH2	HIP1R	RPL31
GPRASP2	NCOR2	HLTF	RPL36AL
HAUS6	NEDD8	HP1BP3	RPL6
HEATR1	NUP133	INTS1	RREB1
HEATR6	NUP153	IRAK1	SERPINA12
HPS6	NUP98	IRS4	SLX4
HSPA6	PDS5A	KPNA1	SMN1
INTS1	PHF14	LAS1L	SMN2
INTS2	PIAS2	LUC7L2	TCF20
IQGAP3	PIAS3	MAGED2	TEX10
IRS4	PML	MAP1B	UBA6
MAGED1	POLR2A	MAP7	UBE2Z
NCAPG2	PPFIA1	MAP7D1	UTP3
NCAPH2	PRMT1	MELK	WDR55
NTPCR	PTPN1	MTPAP	ZNF106
NUP133	PYGL	MYBBP1A	ZNF292
NUP188	RAD21	NACA	ZNF462
NUP205	RANBP2	NAT10	ZNF512
OBSL1	SAE1	NOLC1	ZNF532
ORC3	SLC25A10	NOM1	ZNF592
PDS5B	SLC2A1	NOP58	ZNF644
PEF1	SLX4	NUMA1	
PGAM5	SMC1A	PCBP2	
PIK3C2A	SMC3	PELP1	
PRPF19	SMCHD1	PES1	
PSMA5	STAG1	PIK3C2A	
PUM1	STAG2	PKP2	
RAE1	STAT3	PLEC	
RARS2	SUCLA2	POP1	
RB1	SUN1	PPP1R12A	
RNF213	TERF2IP	PUM1	
SAMD1	TINF2	RARS2	

SEC16A	TMEM201	RAVER1
SETX	TMPO	RBM14
SLU7	TMPO	RBM39
SMN1	TOMM40	RPL13a
SMN2	TOPORS	RPL13A
SON	TP53BP1	RPS14
SRSF6	TPR	RRBP1
SYNRG	TRMT10C	RTKN
TCF25	UBB	SEC16A
TEX10	RPS27A	SENP3
THADA	UBC	SETD2
TIMM50	UBA52	SETDB1
TMEM33	ZHX1	SETX
TTC27	ZHX2	SLU7
TTI1	ZNF202	SMARCA5
TTK		SMN1
TUBB4A		SMN2
TUBB6		SNRNP70
TUBGCP2		SRRM1
TUBGCP5		SRRM2
VAPA		SUGP2
VPS51		TCF25
WDR48		TEX10
XPO6		TTI1
ZDBF2		UBE2K
		UTP14A
		VPS13A
		YTHDF2
		ZC3H18
		ZNF503
		ZRANB2

10 References

1. Allfrey VG, Mirsky AE. Structural modifications of histones and their possible role in the regulation of RNA synthesis. *Science*. 1964;144(3618):559.
2. Cuijpers SAG, Willemstein E, Vertegaal ACO. Converging SUMO and ubiquitin signaling: improved methodology identifies co-modified target proteins. *Mol Cell Proteomics*. 2017;16(12):2281-2295.
3. Hendriks IA, Lyon D, Young C, Jensen LJ, Vertegaal ACO, Nielsen ML. Site-specific mapping of the human SUMO proteome reveals co-modification with phosphorylation. *Nat Struct Mol Biol*. 2017;24(3):325-336.
4. Wiborg O, Pedersen MS, Wind ' A, Berglund LE, Marcker KA, Vuust J. The human ubiquitin multigene family: some genes contain multiple directly repeated ubiquitin coding sequences. *EMBO J*. 1985;4(3):755–759.
5. Redman KL, Rechsteiner M. Identification of the long ubiquitin extension as ribosomal protein S27a. *Nature*. 1989;338(6214):438-440.
6. Kraulis PJ, Gronenborn AM, Clore GM. Similarity of protein G and ubiquitin. *Science*. 1991;254(5031):581-582.
7. Lenkinski RE, Chen DM, Glickson JD, Goldstein G. Nuclear magnetic resonance studies of the denaturation of ubiquitin. *BBA - Protein Struct*. 1977;494(1):126-130.
8. Ciechanover A, Elias S, Heller H, Hershko A. 'Covalent affinity' purification of ubiquitin-activating enzyme. *J Biol Chem*. 1982;257(5):2537-2542.
9. Hershkos A, Heller H, Elias S, Ciechanover A. Components of Ubiquitin-Protein Ligase System. *J Biol Chem*. 1983;258(13):8206-8214.
10. Buetow L, Huang DT. Structural insights into the catalysis and regulation of E3 ubiquitin ligases. *Nat Rev Mol Cell Biol*. 2016;17:626–642.
11. Hershko A, Ciechanover A. The ubiquitin system. *Annu Rev Biochem*. 1998;67:425-479.

12. Chau V, Tobias JW, Bachmair A, et al. A multiubiquitin chain is confined to specific lysine in a targeted short-lived protein. *Science (80-)*. 1989;243(4898):1576-1583.
13. Husnjak K, Dikic I. Ubiquitin-binding proteins: decoders of ubiquitin-mediated cellular functions. *Annu Rev Biochem*. 2012;81:291-322.
14. Meyer HJ, Rape M. Enhanced protein degradation by branched ubiquitin chains. *Cell*. 2014;157(4):910-921.
15. McDowell GS, Philpott A. Non-canonical ubiquitylation: Mechanisms and consequences. *Int J Biochem Cell Biol*. 2013;45:1833-1842.
16. Hanpude P, Bhattacharya S, Dey AK, Maiti TK. Deubiquitinating enzymes in cellular signaling and disease regulation. *IUBMB Life*. 2015;67(7):544-555.
17. Owerbach D, McKay EM, Yeh ETH, Gabbay KH, Bohren KM. A proline-90 residue unique to SUMO-4 prevents maturation and sumoylation. *Biochem Biophys Res Commun*. 2005;337(2):517-520.
18. Kunz K, Piller T, Müller S. SUMO-specific proteases and isopeptidases of the SENP family at a glance. *J Cell Sci*. 2018;131(6).
19. Hay RT. SUMO: a history of modification. *Mol Cell*. 2005;18(1):1-12.
20. Rodriguez MS. SUMO-1 Conjugation in Vivo Requires Both a Consensus Modification Motif and Nuclear Targeting. *J Biol Chem*. 2000;276(16):12654-12659.
21. Hendriks IA, Vertegaal ACO. A comprehensive compilation of SUMO proteomics. *Nat Rev Mol Cell Biol*. 2016;17(9):581-595.
22. Matunis MJ, Wu J, Blobel G. SUMO-1 modification and its role in targeting the Ran GTPase-activating protein, RanGAP1, to the nuclear pore complex. *J Cell Biol*. 1998;140(3):499-509.
23. Mahajan R, Gerace L, Melchior F. Molecular characterization of the SUMO-1 modification of RanGAP1 and its role in nuclear envelope association. *J Cell Biol*. 1998;140(2):259-270.
24. Li SJ, Hochstrasser M. A new protease required for cell-cycle progression in yeast. *Nature*. 1999;398(6724):246-251.
25. Li SJ, Hochstrasser M. The yeast ULP2 (SMT4) gene encodes a novel

protease specific for the ubiquitin-like Smt3 protein. *Mol Cell Biol*. 2000;20(7):2367-2377.

26. Raman N, Nayak A, Muller S. mTOR Signaling Regulates Nucleolar Targeting of the SUMO-Specific Isopeptidase SENP3. *Mol Cell Biol*. 2014;34(24):4474-4484.
27. Hattersley N, Shen L, Jaffray EG, Hay RT. The SUMO protease SENP6 is a direct regulator of PML nuclear bodies. *Mol Biol Cell*. 2011;22(1):78-90.
28. Finkbeiner E, Haindl M, Raman N, Muller S. SUMO routes ribosome maturation. *Nucleus*. 2011;2(6):527-532.
29. Haindl M, Harasim T, Eick D, Muller S. The nucleolar SUMO-specific protease SENP3 reverses SUMO modification of nucleophosmin and is required for rRNA processing. *EMBO Rep*. 2008;9(3):273-279.
30. Finkbeiner E, Haindl M, Muller S. The SUMO system controls nucleolar partitioning of a novel mammalian ribosome biogenesis complex. *EMBO J*. 2011;30(6):1067-1078.
31. Ivanov A V, Peng H, Yurchenko V, et al. PHD domain-mediated E3 ligase activity directs intramolecular sumoylation of an adjacent bromodomain required for gene silencing. *Mol Cell*. 2007;28(5):823-837.
32. Garvin AJ, Densham RM, Blair-Reid SA, et al. The deSUMOylase SENP7 promotes chromatin relaxation for homologous recombination DNA repair. *EMBO Rep*. 2013;14(11):975-983.
33. Moldovan G-L, D'Andrea AD. How the Fanconi Anemia Pathway Guards the Genome. *Annu Rev Genet*. 2009;43(1):223-249.
34. Gibbs-Seymour I, Oka Y, Rajendra E, et al. Ubiquitin-SUMO circuitry controls activated fanconi anemia ID complex dosage in response to DNA damage. *Mol Cell*. 2015;57(1):150-164.
35. Mukhopadhyay D, Dasso M. The fate of metaphase kinetochores is weighed in the balance of SUMOylation during S phase. *Cell Cycle*. 2010;9(16):3214-3221.
36. Olsen J V., Vermeulen M, Santamaria A, et al. Quantitative phosphoproteomics revealswidespread full phosphorylation site occupancy during mitosis. *Sci Signal*. 2010;3(104):ra3.

37. Cimarosti H, Ashikaga E, Jaafari N, et al. Enhanced SUMOylation and SENP-1 protein levels following oxygen and glucose deprivation in neurones. *J Cereb Blood Flow Metab*. 2012;32(1):17-22.
38. Guo C, Hildick KL, Luo J, Dearden L, Wilkinson KA, Henley JM. SENP3-mediated deSUMOylation of dynamin-related protein 1 promotes cell death following ischaemia. *EMBO J*. 2013;32(11):1514-1528.
39. Huang C, Han Y, Wang Y, et al. SENP3 is responsible for HIF-1 transactivation under mild oxidative stress via p300 de-SUMOylation. *EMBO J*. 2009;28(18):2748-2762.
40. Yan S, Sun X, Xiang B, et al. Redox regulation of the stability of the SUMO protease SENP3 via interactions with CHIP and Hsp90. *EMBO J*. 2010;29(22):3773-3786.
41. Agbor TA, Cheong A, Comerford KM, et al. Small Ubiquitin-related Modifier (SUMO)-1 promotes glycolysis in hypoxia. *J Biol Chem*. 2011;286(6):4718-4726.
42. Halliwell B. Oxidative stress in cell culture: An under-appreciated problem? *FEBS Lett*. 2003;540(1-3):3-6.
43. Chandel NS, Maltepe E, Goldwasser E, Mathieu CE, Simon MC, Schumacker PT. Mitochondrial reactive oxygen species trigger hypoxia-induced transcription. *Proc Natl Acad Sci*. 2002;95(20):11715-11720.
44. Guzy RD, Hoyos B, Robin E, et al. Mitochondrial complex III is required for hypoxia-induced ROS production and cellular oxygen sensing. *Cell Metab*. 2005;1(6):401-408.
45. Halliwell B. Oxidative stress and cancer: have we moved forward? *Biochem J*. 2006;401(1):1-11.
46. Saitoh H, Hinchey J. Functional heterogeneity of small ubiquitin-related protein modifiers SUMO-1 versus SUMO-2/3. *J Biol Chem*. 2000;275(9):6252-6258.
47. Yang W, Sheng H, Warner DS, Paschen W. Transient global cerebral ischemia induces a massive increase in protein sumoylation. *J Cereb Blood Flow Metab*. 2008;28(2):269-279.
48. Bossis G, Melchior F. Regulation of SUMOylation by reversible oxidation

of SUMO conjugating enzymes. *Mol Cell*. 2006;21(3):349-357.

49. Xu Z, Lam LSM, Lam LH, Chau SF, Ng TB, Au SWN. Molecular basis of the redox regulation of SUMO proteases: a protective mechanism of intermolecular disulfide linkage against irreversible sulfhydryl oxidation. *FASEB J*. 2007;22(1):127-137.
50. Yang W, Thompson JW, Wang Z, et al. Analysis of oxygen/glucose-deprivation-induced changes in SUMO3 conjugation using SILAC-based quantitative proteomics. *J Proteome Res*. 2011;11(2):1108-1117.
51. Kunz K, Müller S, Mendler L. Assays of SUMO protease/isopeptidase activity and function in mammalian cells and tissues. *Methods Enzymol*. 2019;618:389-410.
52. Kunz K, Wagner K, Mendler L, Hölper S, Dehne N, Müller S. SUMO Signaling by Hypoxic Inactivation of SUMO-Specific Isopeptidases. *Cell Rep*. 2016;16(11):3075-3086.
53. Barysch S V, Dittner C, Flotho A, Becker J, Melchior F. Identification and analysis of endogenous SUMO1 and SUMO2/3 targets in mammalian cells and tissues using monoclonal antibodies. *Nat Protoc*. 2014;9(4):896-909.
54. Kato Y, Kawamoto T, Fujimoto K, Noshiro M. DEC1/STRA13/SHARP2 and DEC2/SHARP1 coordinate physiological processes, including circadian rhythms in response to environmental stimuli. *Curr Top Dev Biol*. 2014;110:339-372.
55. Hong Y, Xing X, Li S, et al. Sumoylation of DEC1 protein regulates its transcriptional activity and enhances its stability. *PLoS One*. 2011;6(8).
56. LaGory EL, Wu C, Taniguchi CM, et al. Suppression of PGC-1α Is Critical for Reprogramming Oxidative Metabolism in Renal Cell Carcinoma. *Cell Rep*. 2015;12(1):116-127.
57. Rojas-Fernandez A, Plechanovová A, Hattersley N, Jaffray E, Tatham MH, Hay RT. SUMO chain-induced dimerization activates RNF4. *Mol Cell*. 2014;53(6):880-892.
58. Mukhopadhyay D, Ayaydin F, Kolli N, et al. SUSP1 antagonizes formation of highly SUMO2/3-conjugated species. *J Cell Biol*. 2006;174(7):939-949.

59. Belgareh N, Rabut G, Baï SW, et al. An evolutionarily conserved NPC subcomplex, which redistributes in part to kinetochores in mammalian cells. *J Cell Biol*. 2001.

60. Chung SY, Kao CH, Villarroya F, et al. Bhlhe40 represses PGC-1α activity on metabolic gene promoters in myogenic cells. *Mol Cell Biol*. 2015;35(14):2518-2529.

61. Cai R, Yu T, Huang C, et al. SUMO-specific protease 1 regulates mitochondrial biogenesis through PGC-1α. *J Biol Chem*. 2012;287(53):44464-44470.

62. Leiherer A, Geiger K, Muendlein A, Drexel H. Hypoxia induces a HIF-1α dependent signaling cascade to make a complex metabolic switch in SGBS-adipocytes. *Mol Cell Endocrinol*. 2014;383(1-2):21-31.

63. Cheng J, Kang X, Zhang S, Yeh ETH. SUMO-Specific Protease 1 Is Essential for Stabilization of HIF1α during Hypoxia. *Cell*. 2007;131(3):584-595.

64. Cotto-Rios XM, Békés M, Chapman J, Ueberheide B, Huang TT. Deubiquitinases as a Signaling Target of Oxidative Stress. *Cell Rep*. 2012;2(6):1475-1484.

65. Kulathu Y, Garcia FJ, Mevissen TET, et al. Regulation of A20 and other OTU deubiquitinases by reversible oxidation. *Nat Commun*. 2013;4.

66. Murphy MP. Modulating mitochondrial intracellular location as a redox signal. *Sci Signal*. 2012;5(242):39.

67. Haindl M, Harasim T, Eick D, Muller S. The nucleolar SUMO-specific protease SENP3 reverses SUMO modification of nucleophosmin and is required for rRNA processing. *EMBO Rep*. 2008;9(3):273-279.

68. Panse VG, Kressler D, Pauli A, et al. Formation and nuclear export of preribosomes are functionally linked to the small-ubiquitin-related modifier pathway. *Traffic*. 2006;7(10):1311-1321.

69. Lam YW, Lamond AI, Mann M, Andersen JS. Analysis of Nucleolar Protein Dynamics Reveals the Nuclear Degradation of Ribosomal Proteins. *Curr Biol*. 2007;17(9):749-760.

70. Morris JR, Boutell C, Keppler M, et al. The SUMO modification pathway is

involved in the BRCA1 response to genotoxic stress. *Nature*. 2009;462(7275):886-890.

71. Bergink S, Jentsch S. Principles of ubiquitin and SUMO modifications in DNA repair. *Nature*. 2009;458:461-467.
72. Dou H, Huang C, Singh M, Carpenter PB, Yeh ETH. Regulation of DNA repair through deSUMOylation and SUMOylation of replication protein A complex. *Mol Cell*. 2010;39(3):333-345.
73. De Albuquerque CP, Liang J, Gaut NJ, Zhou H. Molecular circuitry of the SUMO (Small Ubiquitin-like Modifier) pathway in controlling sumoylation homeostasis and suppressing genome rearrangements. *J Biol Chem*. 2016;291(16):8825-8835.
74. Gibbs-Seymour I, Oka Y, Rajendra E, et al. Ubiquitin-SUMO circuitry controls activated fanconi anemia ID complex dosage in response to DNA damage. *Mol Cell*. 2015;57(1):150-164.
75. Xie J, Kim H, Moreau LA, et al. RNF4-mediated polyubiquitination regulates the Fanconi anemia/BRCA pathway. *J Clin Invest*. 2015;125(4):1523-1532.
76. Coleman KE, Huang TT. How SUMOylation fine-tunes the fanconi anemia DNA repair pathway. *Front Genet*. 2016;7(61):1-8.
77. Guervilly JH, Takedachi A, Naim V, et al. The SLX4 complex is a SUMO E3 ligase that impacts on replication stress outcome and genome stability. *Mol Cell*. 2015;57(1):123-137.
78. Guervilly JH, Gaillard PH. SLX4: multitasking to maintain genome stability. *Crit Rev Biochem Mol Biol*. 2018;53(5):475-514.
79. Mukhopadhyay D, Arnaoutov A, Dasso M. The SUMO protease SENP6 is essential for inner kinetochore assembly. *J Cell Biol*. 2010;188(5):681-692.
80. Køhler JB, Tammsalu T, Jørgensen MM, Steen N, Hay RT, Thon G. Targeting of SUMO substrates to a Cdc48-Ufd1-Npl4 segregase and STUbL pathway in fission yeast. *Nat Commun*. 2015;6.
81. Countryman P, Fan Y, Gorthi A, et al. Cohesin SA2 is a sequence-independent DNA-binding protein that recognizes DNA replication and

repair intermediates. *J Biol Chem*. 2018;293(3):1054-1069.

82. D'Ambrosio LM, Lavoie BD. Pds5 Prevents the PolySUMO-Dependent Separation of Sister Chromatids. *Curr Biol*. 2014;24(4):361-371.
83. Almedawar S, Colomina N, Bermúdez-López M, Pociño-Merino I, Torres-Rosell J. A SUMO-dependent step during establishment of sister chromatid cohesion. *Curr Biol*. 2012;22(17):1576-1581.
84. Wan L, Huang J. The PSO4 protein complex associates with replication protein a (RPA) and modulates the activation of ataxia telangiectasia-mutated and RAD3-related (ATR). *J Biol Chem*. 2014;289:6619-6626.
85. Maréchal A, Li JM, Ji XY, et al. PRP19 Transforms into a Sensor of RPA-ssDNA after DNA Damage and Drives ATR Activation via a Ubiquitin-Mediated Circuitry. *Mol Cell*. 2014;53(2):235-246.
86. Maréchal A, Zou L. DNA damage sensing by the ATM and ATR kinases. *Cold Spring Harb Perspect Biol*. 2013;5(9).
87. Munk S, Sigurðsson JO, Xiao Z, et al. Proteomics Reveals Global Regulation of Protein SUMOylation by ATM and ATR Kinases during Replication Stress. *Cell Rep*. 2017;21(2):546-558.
88. Wu C-S, Ouyang J, Mori E, et al. SUMOylation of ATRIP potentiates DNA damage signaling by boosting multiple protein interactions in the ATR pathway. *Genes Dev*. 2014;28(13):1472-1484.
89. Ullmann R., Chien C., Avantaggiati M., et al. An Acetylation Switch Regulates SUMO-Dependent Protein Interaction Networks. *Mol Cell.* 2012;46(8):759-770.

11 Acknowledgement

I would like to thank everyone, who contributed to the success of this work.

In the first place, my sincere appreciation and thanks go to my supervisor Prof. Dr. Stefan Müller for giving me the chance to do my PhD thesis in his lab and thereby not only becoming a member of the SUMO group but also grow as scientist. I'm deeply grateful for your guidance and support in experimental as well as personal questions. You always showed confidence in me and appreciated my work.

Further I thank the reviewers for the evaluation of this work and all members of the examining board for their valuable time spent on this thesis.

Also I would like to express my appreciation to my PhD advisory committee members Prof. Dr. Liliana Schaefer and Dr. med. habil. Dr. Nathalie Dehne for their helpful input and support on my project.

Thanks again to Nathalie and Dominik for an enjoyable collaboration on the first part of this project.

Furthermore, I thank all SFB815 members for nice lunch seminars, summer schools, discussions and importantly for sharing reagents and knowledge.

I am thankful to all current and former IBC II members not only for sharing materials and methods but also for creating a pleasant and stimulating atmosphere and for their input and suggestions during progress reports.
Special thanks goes to the MS team, first and foremost to Florian and Georg for their support in difficult questions concerning own projects and collaborations and for giving me (and Kristina) a free hand while processing our large-scale experiments.

My whole-hearted thank you goes to some actual and former IBC II and SUMO lab members who became friends and made the life outside IBC II enjoyable. Tanja, Nithya, Svenja, Suki, Alex, Jenny, Franzi, Sandra & Paolo, you are sadly missed. Special thanks go to Anne for being my first mentor in how to do experiments properly and supporting me in personal questions whenever it was needed. Soraya, I really appreciated your immense effort in teaching me all I know about mass spectrometry and making me confident in my way of working. Moreover, I'm deeply thankful for Meike becoming a familiar and reliable friend, especially in my last year. Thanks for keeping my motivation high and having a sympathetic ear for me.

Most important, to finish a PhD thesis, it needs an inspiring and motivating atmosphere. This was totally given in the SUMO lab where I was fully integrated from the beginning on. Therefore I would like to thank all SUMO lab members, including Hannah, Kristina, Jan, Paul and Luca. Thanks for the mutual support in daily lab routine, helpful discussions and advices, pleasant and premium-culinary breaks and being friends rather than competitors. A special and huge thank you deserves Kristina. Thanks for all support and effort you invested as my reliable "Co-Pipettor". It is a pleasure working with you.

Finally, I'm highly grateful for my family, my family-in-law and close friends who motivated and supported me in the last 5 years from every point of view. My deepest gratitude goes to Lukas for his everlasting support, love and patience with me.

12 Conferences and Posters

09/2015 EMBO Conference, Cavtat, Croatia: “Ubiquitin and ubiquitin-like modifiers: From molecular mechanisms to human diseases”

07/2016 Frankfurt Conference on Ubiquitin and Autophagy, Frankfurt am Main: “Quality control in life processes”

10/2016 7. UCT Science Day, Frankfurt am Main

Poster: “SUMO Signaling by Hypoxic Inactivation of SUMO Specific Isopeptidases“

Kathrin Kunz, Kristina Wagner, Luca Mendler, Soraya Hölper, Nathalie Dehne, Stefan Müller

10/2016 8. International Conference, Shanghai, China: „SUMO, Ubiquitin, UBL Proteins: Implications for human diseases“

Poster: “SUMO Signaling by Hypoxic Inactivation of SUMO Specific Isopeptidases“

Kathrin Kunz, Kristina Wagner, Luca Mendler, Soraya Hölper, Nathalie Dehne, Stefan Müller

Awarded with a poster prize

08/2018 11th International Conference on Ribosome Synthesis, Orford, Canada

Poster: „Integrating the SUMO isopeptidase SENP3 in the mammalian ribosome biogenesis network”

Kathrin Kunz*, Tanja Piller*, Kristina Wagner, Jan Keiten-Schmitz, Soraya Hölper and Stefan Müller

13 Schriftliche Erklärung

Ich erkläre hiermit ehrenwörtlich, dass ich die dem Fachbereich Medizin der Johann Wolfgang Goethe-Universität Frankfurt am Main zur Promotionsprüfung eingereichte Dissertation mit dem Titel

Deciphering regulation and substrate-specificity of SUMO-specific isopeptidases

im Institut für Biochemie II
unter Betreuung und Anleitung von Prof. Dr. Stefan Müller mit Unterstützung durch Kristina Wagner ohne sonstige Hilfe selbst durchgeführt und bei der Abfassung der Arbeit keine anderen als die in der Dissertation angeführten Hilfsmittel benutzt habe. Darüber hinaus versichere ich, nicht die Hilfe einer kommerziellen Promotionsvermittlung in Anspruch genommen zu haben.

Ich habe bisher an keiner in- oder ausländischen Universität ein Gesuch um Zulassung zur Promotion eingereicht. Die vorliegende Arbeit wurde bisher nicht als Dissertation eingereicht.

Vorliegende Ergebnisse der Arbeit wurden (oder werden) in folgendem Publikationsorgan veröffentlicht:

1) Kathrin Kunz, Kristina Wagner, Luca Mendler, Soraya Hölper, Nathalie Dehne, and Stefan Müller. SUMO Signaling by Hypoxic Inactivation of SUMO-Specific Isopeptidases. Cell Reports, 16, 3075-3086, 2016.

2) Kathrin Kunz, Tanja Piller and Stefan Müller. SUMO-specific proteases and isopeptidases of the SENP family at a glance. Journal of Cell Science, 131, 2018.

3) Kathrin Kunz, Stefan Müller and Luca Mendler, Assays of SUMO protease/isopeptidase activity and function in mammalian cells and tissues, Methods in Enzymology, 618, 389-410, 2019.

_____ _____

(Ort, Datum) (Unterschrift)

The experiments described in this work were, if not stated otherwise below, done by Kathrin Kunz between 2014 and 2018 in the Institute of Biochemistry II in Frankfurt under the supervision of Prof. Dr. Stefan Müller.

The first part of this work was already published in Cell Reports 2016 under the title: “SUMO Signaling by Hypoxic Inactivation of SUMO-Specific Isopeptidases” by Kunz K., Wagner K., Mendler L., Hölper S., Dehne N. and Müller S..

For the SENP3 part of this work, the U-2 OS SENP3 KO cell line was generated together with Jan Keiten-Schmitz. He also did the Western blot analysis shown in Supplemental Figure 12 C.

The SENP3 and SENP6 interactome analyses were performed by Tanja Piller during her master thesis (Figure 19 A and 24 C).

The SUMO2/3 IP-MS experiment under depletion of SENP6 in the last part of this work was done together with Kristina Wagner. The following experiments on SENP6 were done by Kristina Wagner with computational analyses and representation of the figures done by myself. These are in detail: Figure 24 A, B, 26, 27, 28 and Supplemental Figures 12 B, 13, 14 and 15.